Addis Ababa University

Addis Ababa Institute of Technology

School of Graduate Studies

Center for Renewable Energy

Functionality Test of DC Powered Induction Cook Stove Design

A Thesis Submitted to the School of Graduate Studies of Addis Ababa University in Partial Fulfillment of the Degree of Master of Science in Renewable Energy Technology

Prepared By: Meron Alemu Abate

Advisor: Dr. Mesfin Belayneh

Submission Date: September 2024

Addis Ababa, Ethiopia

Certification

I, the undersigned, certify that I read and at this moment recommend for the acceptance by Addis Ababa University, Addis Ababa Institute of Technology, Center of Renewable Energy a thesis entitled " Functionality Test of DC Powered Induction Cook Stove Design ". This certificate is used as a partial fulfillment of the requirement for the degree of Master of Science in Energy Technology.

Name and Signature of Advisor _____

Date _____

Declaration

I Meron Alemu Abate, declare that this thesis is the result of my work, and I have appropriately acknowledged all sources and materials utilized throughout this research. The submission of this thesis fulfills a partial requirement for the degree of Master of Science in Renewable Energy Technology at Addis Ababa University. I affirm with confidence that the research titled " Functionality Test of DC Powered Induction Cook Stove Design " is the result of my independent efforts and has not been previously submitted to any other academic institution to obtain a degree, diploma, or certificate.

Name: Meron Alemu Abate

Signature 

Date 9/10/2024

Addis Ababa University

Addis Ababa Institute of Technology

School of Graduate Studies

Center for Renewable Energy Technology

Functionality Test of DC Powered Induction Cook Stove Design

By: Meron Alemu Abate

Approved by the Board of Examiners:

Dr. Mesfin Belayneh	_____	_____
Advisor	**Signature**	**Date**
_____	_____	_____
External Examiner	**Signature**	**Date**
_____	_____	_____
Internal Examiner	**Signature**	**Date**
_____	_____	_____
Chairman	**Signature**	Date

Acknowledgment

I would like to acknowledge and give glory to God and the Virgin Mary, as I firmly believe that no work can endure without their divine will. I also wish to express my utmost respect and heartfelt gratitude to Assoc. Prof. Mesfin Belayneh (PhD) for his invaluable support and guidance throughout the development of this thesis. His encouragement to commence the laboratory tests sooner has been instrumental in the progress of this research.

I would also like to extend my deepest appreciation to the instructors at the Electrical and Computer Engineering Laboratory. Their expertise and guidance have been immensely valuable. I would like to offer a special thanks to Mr. Solomon for his exceptional support and assistance. I am truly grateful to have had his unwavering support throughout this endeavor.

Most importantly, I want to convey my profound love and gratitude to my family Alelaye, Wedye, Mahi, and Yeabye. Your love has been a constant source of inspiration for me, motivating me to overcome challenges and pursue my goals with determination. I am truly blessed to have such an incredible family. Thank you for being there for me every step of the way. I will forever cherish the memories we have created together.

Abstract

Solar energy is widely recognized as a clean, reliable, and promising power source for the future. This study is centered on conducting a functional evaluation of a DC-sourced induction cooking system. It analyzed household electric cooking demands and developed a DC-based system analogous to fulfilling these energy requirements. Induction heating was chosen for its efficiency compared to conventional electrical stoves available in the market, operating on the principle of electromagnetic induction. The magnetic field generated by the current flow induces heat in a resistive cooking pan. Tailored to Ethiopian urban cooking habits, a 500-watt induction stove design was crafted to meet the cooking needs of an average family of five, accounting for 3.5 hours of cooking per day. The PV system/DC source design comprised two parallel-connected 12V, 250W panels, and three parallel-connected 12V, 150Ah batteries, ensuring a reliable power supply to the induction cooker. Through the integration of Proteus software and laboratory simulations, the operationalization of an induction cooking system powered by a DC source was successfully demonstrated. This system utilized astable multivibrator and half-bridge topologies, with wireless electric conduction enabling LED lighting without direct contact. The variation in light intensity with height was attributed to voltage and current fluctuations caused by magnetic field variations. The addition of extra current, resulted in a buzzing noise due to magnetostriction. Experimental testing of the developed induction cook stove, using a small 24V panel and a voltage divider, exhibited similar output characteristics in terms of LED illumination and current flow, a maximum of 105 Vpp voltage was achieved at the cooking coil. Ansys simulations provided crucial insights into current flow direction, magnetic field density, field intensity, and their effects on the coil, mirror, and pan. Energy conduction was noted to be influenced by the current and frequency passing through the coil, while magnetic flux density impacted total energy transfer based on the distance between the pan and the coil. An examination of the interaction between the cookware and cooking coil was conducted for various values of operating currents (5A, 15A, and 30A) and frequencies (25kHz, 50kHz, and 75kHz). The magnetic field intensity was observed to be influenced by both the operating current and frequency. Notably, the pan exhibited quicker heating as the magnetic flux density increased. This study contributes to enhancing the understanding and implementation of DC-powered induction cooking systems, highlighting their potential for sustainable cooking solutions and promoting the adoption of clean energy practices.

Table of Contents

Table of Figures

Table of Tables

Nomenclatures

Cr.	Resonant Capacitor
F	Farad
IC	Induction Cooking
H	Henry, Inductance
J	Magnetic Polarization or Magnetization
kHz	Kilohertz
L	Inductance
Lr	Resonant Inductance
m	Meter
N	Number of Turns
Vpp	Voltage Peak to Peak
δ	Penetration Depth
Ø	Magnetic Flux density
ρ	Resistivity
μ	Permeability
Ω	Ohm
Ωm	Ohm Meter
f	Frequency
f_o	Operating frequency
f_{res}	Resonant frequency
ω	Angular frequency
ω_{res}	Resonant frequency

Acronyms

A	Ampere
AC	Alternating Current
AEDT	ANSYS Electronics Desktop
AH	Amperes-Hour
B	Magnetic Flux Density
CFD	Computational Fluid Dynamics
DC	Direct Current
DoD	Depth of Discharge
E	Induced Voltage
E-Cooking	Electronic Cooking
IC	Induction Cooking
IGBT	Insulated Gate Bipolar Transistor
Ix	Current density at x distance
H	Magnetic Field Intensity
H	Henry, Inductance
HH	Household
HBRC	Half Bridge Resonant Converter
I_p	Primary Current
I_s	Secondary Current
J	Magnetic Polarization or Magnetization
kHz	Kilohertz
LED	Light Emitting Diode
L	Inductance
N	Number of Turns
N_p	Primary winding
N_s	Secondary winding
P	Total power
PV	Photovoltaic
PWM	Pulse Width Modulation
QRC	Quasi-Resonant Converter

UPS	Uninterruptable Power Supply
V	Volts
V_p	Primary voltage
V_s	Secondary voltage
Vpp	Voltage Peak to Peak
ZCS	Zero Current Switching
ZVS	Zero Voltage Switching

Chapter one

1. Introduction

A solar cell, also known as a photovoltaic cell, is a device that converts solar energy into electricity through the photovoltaic effect [1]. Solar energy is converted into usable direct current (DC) electricity through an arrangement of solar panels. These solar cells can also be incorporated into various electronic devices, allowing them to operate independently using sunlight. Examples of such devices include solar cell phone chargers, solar bike lights, and solar camping lanterns, which people can utilize in their everyday activities [2]. Additionally, solar energy can serve as a reliable and plentiful power source for cooking appliances. Countries that possess a significant solar power generation capacity should contemplate adopting cooking systems that rely on solar energy. This approach would not only advance cooking practices but also promote energy conservation and facilitate the development of efficient cook stove designs [3].

1.1 Background

In developing countries like Ethiopia, the residential sector accounts for a significant portion of the country's total energy consumption. Most of the energy consumed in households is used for cooking [4]. Ethiopia's demand for electrical energy is steadily increasing due to rapid economic growth, shortages of firewood and biomass, and a large-scale electrification program underway in the country.

Globally, there are two common methods for electric stoves to function. The first method involves passing current through a resistive element, which produces ohmic heating. The thermal energy is then transferred to the pot or pan through thermal conduction. This method has lower efficiency, as only around 60% of the consumed power is utilized for heating the pot or its contents [1].

Another approach involves using induction to heat the cooking pot directly. In an induction stove, a powerful and variable magnetic field is created. When a pot made of a suitable conducting material is placed within this field, eddy currents are induced in the pot, resulting in the generation of ohmic heating directly within the pot [2]. As a result, the only energy loss occurs in powering the circuitry that controls the magnetic field of the stove. By employing induction heating, efficiencies of 90% or even higher can be attained [1].

Induction cooking involves the use of high-frequency electricity to heat electrically conductive materials without direct contact. This method relies on a power electronic converter circuit to generate the required high-frequency electricity. Induction cooking is renowned for its speedy heating, precise temperature control, cleanliness, energy efficiency, and repeatable performance [3]. It is widely recognized as one of the most efficient cooking technologies available. With induction cooking, up to 90% of the energy consumed is effectively transferred to the food being cooked, surpassing the efficiency of traditional electric systems (approximately 74%) and gas stoves (around 40%) [3].

Induction heating stands out as a highly efficient method of heating due to its unique approach to generating heat within the workpiece without direct contact. This sets it apart from conventional heating methods that rely on external heat sources like flames or heating elements [3]. The remarkable efficiency of induction heating has made it a prevalent choice across various industries and thermal processes, particularly in the realm of heating metals [4].

The extensive utilization of induction heating equipment and heaters spans a wide range of applications, including induction heat treatment, bonding, brazing, welding, forging, melting, and heat fitting solutions [5]. These systems are well-suited for any situation where there is a need for efficient, precise, and clean heating of electrically conductive materials. Mutual inductance serves as the underlying principle driving the operation of induction heating [5].

Induction cooking is often considered one of the most efficient technologies for stovetop cooking. It relies on the principle of magnetic induction, which excites eddy currents in ferromagnetic cookware when exposed to an oscillating magnetic field [6]. These induced currents dissipate heat through the Joule effect, directly generating heat for cooking in the cooking vessel. Consequently, less heat is lost through inefficient thermal conduction between the heating element and the cookware. A typical induction cooker consists of a switching power electronics circuit that delivers high-frequency current to a planar coil of wire embedded in the cooking surface. The cookware is magnetically coupled to the coil through the oscillating magnetic field, similar to the coupling between the primary and secondary coils of a transformer. Current flows through the cooking vessel due to its low resistance, resulting in power dissipation given by I^2R, where I is the current and R is the resistance of the cookware. The resistance of the vessel depends on the magnetic permeability (μ) and resistivity (ρ) of the cookware, as well as the excitation frequency [7].

Induction cookers have the flexibility to operate with various electric sources, including mains power from the grid or alternative renewable energy sources like solar power. They can also incorporate a combination of these sources. The objective of this research is to conduct a functionality design and test for a DC-sourced Induction cookstove. Thus, the research focuses on the design of components for an induction cook stove and the power system required to support the expected load for an average family size in Ethiopia. The study's results will provide valuable insights on the functionality and feasibility of operating induction stoves. This information will be beneficial for future designers, as it will guide their decision-making process. Additionally, the study will underscore the significance of both functionality and operation aspects when it comes to induction stoves. It will support the adoption of new cooking technologies that have high energy efficiency and are safe to perform. It enhances the Idea that DC-sourced clean cooking supports the off-grid population in the clean cooking implementation of the Nation.

1.2 Problem Statement

The use of electric cooking, known as cooking, has been a part of Ethiopian cooking practices since the 1970s. The government actively promoted cooking appliances, particularly electric injera stoves, to create demand for surplus power and reduce the environmental impact of biomass consumption. Surprisingly, despite the government's support and the low cost of electricity in Ethiopia, only 4.1% of households use electricity as their primary cooking fuel [6][7].

Currently, the majority of Ethiopia's population, which amounts to 96% of 115 million people (with 22% living in urban areas), still relies on polluting fuels for cooking, with firewood being the most commonly used fuel (82%) [36]. However, there has been a significant increase in the use of electricity for cooking in urban areas over the past decade. The electricity consumption of electric stoves during cooking depends on factors such as the power rating of the stove, voltage level, cooking duration, type of food being cooked, and the user's behavior and experience. Research conducted by the Ethiopian Energy Authority revealed that power demand for electric stoves, along with power loss, has increased from 75MW to 119MW between 2009 and 2019 [7].

The majority of stoves used in Ethiopia are locally produced and have low efficiencies, typically below 50%. As the demand for such stoves continues to rise due to population growth and increased adoption, power loss is expected to increase significantly in the coming years. One of the main obstacles to the widespread use of electric stoves in Ethiopia is the lack of readily

available and reliable electric power, especially in remote areas. Additionally, the predominant use of Alternating Current (AC) in electric stoves makes them unsuitable for off-grid connections with solar systems due to the high cost of inverters [6].

To address these challenges and reduce energy losses and costs associated with energy generation and usage, it is crucial to adopt more efficient cooking systems. This would not only benefit remote areas lacking electricity but also help harness renewable energy sources to improve the overall well-being of the population. Designing and manufacturing induction cookstoves is a necessary and valuable step in this direction. These stoves can serve as a starting point for further development and research in cooking technologies while creating awareness in the market and making the products more accessible.

1.3 Research objectives

1.3.1 General Research Objective

The primary objective of this study is to design, construct, and evaluate the functionality of a DC-powered induction cooking system. The study aims to conduct comprehensive functionality tests to assess the system's effectiveness, electromagnetic field effect, and heating effect on cooking pans with different operating currents and frequencies.

1.3.2 Specific Research Objectives

- Assess the e-cooking energy demand per household in Ethiopia
- Develop the conceptual design of the DC-powered induction cooking system.
- Test the DC-powered Induction system functionality by software simulation and laboratory physical implementation.

1.4 Scope of the study

The scope of the study is to design an Induction cook stove and test the circuit in the laboratory which operates by DC source. It aims to deliver a design that will help to reduce the power loss exhibited by less efficient electrical stoves used in Ethiopia. The study was conducted in October 2022. The experimental studies took place in the Electrical laboratories of the Addis Ababa Institute of Technology.

1.5 Research Questions

The research questions of the study are:

1. What are the advantages of induction cook stoves compared to other electrical stoves available in the market?

2. What are the fundamental components and operational principles of induction cookstoves?

3. How does electromagnetic induction enable the operation of induction cookstoves?

4. What is the energy demand for household cooking, specifically focusing on electric energy?

5. How can DC-sourced induction cook stoves be designed to meet the cooking demands of Ethiopian households?

1.6 Limitations

A significant limitation of this paper is its focus on lower voltage design, primarily due to the unavailability of ferrite core transformers capable of stepping up the generated output. Consequently, it was not possible to conduct an actual cooking efficiency test. Instead, the study examined wireless power transfer by utilizing LED lighting as a proxy, and the magnetic field was assessed by varying the height of the upper coil (which is an analogue for cooking pan) and observing the corresponding voltage waveform on an oscilloscope.

1.6 Organization of the Thesis

Chapter 2 provides a literature review which includes illustrating the background of the energy usage in the case study area, revealing previous works and energy modeling tools, and factors determining the parameters used for selecting the components of a circuit. Chapter 3 will present the methodology of the study. It discusses the data collection and research approach. Results of the designing tools on Proteus software, Ansys Electronics Desktop Student software 2023, and the laboratory implementations are discussed in Chapter 4. Primarily presenting the design and the simulation, and secondly, discussing the results of the software and hardware analysis for various types of scenarios. The conclusions of the study and recommendations for further research are presented in Chapter 5. Then the reference of the study and Annexes are presented consecutively.

Chapter Two

2. Literature review

2.1 Cook Stove

A stove is a device used for heating or cooking. Cookstoves have been used for centuries as a means of cooking and heating. One of the earliest known examples of a dedicated cookstove is the "mud stove" used in ancient China, which dates to around 1,000 BCE [8]. The Scandinavian stove that came later had a tall iron chimney with iron baffles inside to make the gases travel longer and extract more heat. [8]. In Europe, the development of enclosed cookstoves gained momentum during the medieval period. In the 18th and 19th centuries, advancements in iron-casting technology led to the production of more efficient and durable cookstoves [9].

The widespread adoption of cookstoves in households worldwide occurred during that period, coinciding with the Industrial Revolution. As urbanization increased and the demand for cooking appliances grew, various cookstoves, such as coal-burning stoves and later gas and electric stoves, became prevalent in homes [20] [41].

It's important to note that while traditional cookstoves have served as vital cooking tools for generations, they have also contributed to indoor air pollution, deforestation, and health issues in many parts of the world. Efforts are underway to develop cleaner, more efficient cookstove technologies to address these challenges. This research will concentrate on Electrical heating as a sustainable option. Electrical energy can produce heat with no soot or greenhouse emissions. It also enables precision heat control, which is not available with wood or fossil-fuel-burning stoves. Furthermore, it may be far more efficient than conventional techniques, with a much larger percentage of energy going towards heating the meal [38].

From Electric heating systems, solar energy will be used for this research to generate heat for cooking systems by Induction. Induction heating is a non-contact heating mechanism. It operates at a higher frequency of electricity to heat the electrically conductive materials [12]. The power electronic converter circuit is responsible for the high-frequency operation. It is heating that can be expressed as fast, precise, clean, energy-efficient, controllable, and repeatable [8].

Under the pot of the induction cooker is a coil of copper wire. When an alternating current flow through the coil, the magnetic field oscillates. This field causes a current to flow through the pot. Resistive heating occurs when an electric current is passed through a metal pot, warming the food. Even if the current is large, it can generate power at a low voltage. The electronics at the heart of such a system is the biggest design challenge, requiring a combination of power stages and digital control systems to solve thermal management problems [9].

Induction heating follows the electromagnetic laws. The overall system can be approximated by an electric transformer. The copper coil of the induction cooker works as a primary winding and the secondary coil will be represented by the bottom layer of the pot. The heat generated is due to the loading of the equivalent resistance of the losses in the pan, which in the transformer allegory, would be a load resistor on the secondary winding [11].

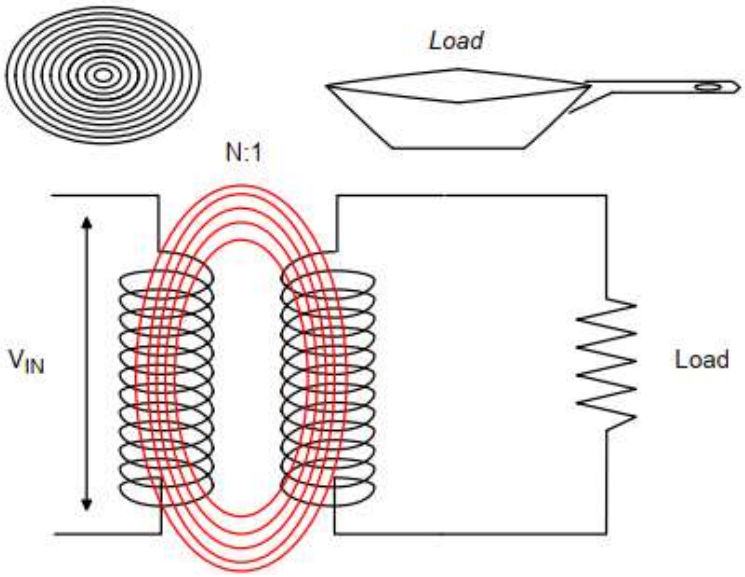

Figure 1 Equivalent of an Induction Cooking System [11]

2.2 Basic Physics of Induction Heating

2.2.1 The Fundamental Theory

Three basic factors affect induction heating. These are electromagnetic induction, the skin effect, and heat transfer. However, the fundamental theory of induction heating is based on transformer theory. Figure 2 (a) illustrates the simplest form of a transformer, where the secondary current "I_s "is directly proportional to the primary current "I according to the turn's ratio N where N equals

N_p/N_s. The primary and secondary copper losses are generally caused by the resistance of windings.

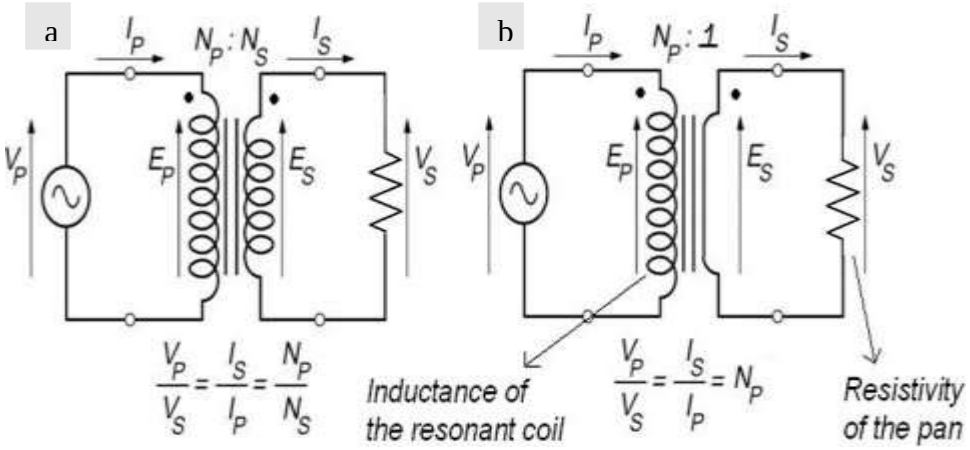

Figure 2 (a) Simplest form of a transformer (b) Secondary shorted transformer [11]

When N_s *(secondary winding)* is equal to one as the coil of the secondary circuit is turned only once, i.e., the secondary is short-circuited, there is a highly increased heat loss due to the increased load current as depicted in Figure 2 (b). This idea is the basic theory of induction heating.

The energy supplied from the power source is equal to the sum of losses of primary and secondary ignoring other circuit losses. For safety reasons, Insulation is used between the inductive heating coil. It can be ceramic glass with high insulation voltage as shown in picture [10].

As the main purpose of induction heating is to make the heat energy generated in the secondary maximum, the glass placed between the coil and the pan is designed to be as thin as possible while the secondary circuit, i.e., the pan in induction cooking, is made of a substance of low resistance and high permeability. Nonferrous metals decrease energy efficiency because of low permeability [15].

2.2.2 Electromagnetic Induction

When a high-frequency alternating current flows through a coil, a magnetic field is formed around the coil as stated by Ampere's Law.

$$\oint H \, dl = N \, I \qquad \text{Eq.1}$$

Where; *i* is the coil current, *dl* is the integration path, H is magnetic field intensity and N is the number of turns.

$$Ø = \mu H A \quad \text{Eq.2}$$

Where; *Ø* is the flux of the magnetic field through the area and A is the area of the field.

The flux induces a voltage as shown in Eq.3 (E) below the surface of the pan which produces the induced current as the secondary is short-circuited. The current-induced is called eddy current. Lenz Law determines the direction of the eddy currents. The generated flux by eddy currents is opposed to the original flux direction [11].

$$E = N\frac{Ø}{dt} \quad \text{Eq.3}$$

$$I = \frac{E}{R} \quad \text{Eq.4}$$

Where; E is the induced voltage, I the eddy current, and *R* is the resistivity of the secondary.

As a result, the electric energy caused by the eddy current is converted into heat energy as shown in Eq.5.

$$P = E^2 / R = I^2 R \quad \text{Eq.5}$$

Where; P is the total power, I the eddy current, and R is the resistance. The magnitude of the current is determined by the intensity of the magnetic field. Heat energy is inversely related to skin depth which will be described in the following section. For objects that have conductive properties like iron, additional energy of heat is generated because of magnetic hysteresis. But, hysteresis losses are ignored as it is much smaller than the energy generated by eddy currents [12].

2.2.3 Eddy Currents

Eddy currents are the primary mechanism by which heating occurs in induction stoves. The time-varying magnetic fields induce currents in the pot proportional to the magnetic field intensity. These currents cause ohmic losses on the pot due to the resistivity. The loss is a function of both the pot resistivity and the coil configuration and current [11].

The pot/coil combination can be modeled as a transformer as in Figure 3. The coil inductance is then the magnetizing inductance, and the eddy current loss can be modeled as a resistor Z_L on the secondary. However, the turns ratio and effective resistance are both non-linear functions of the

physical pot, its contents, the resonant frequency, and the magnetic field coupling between the coil and the pot.

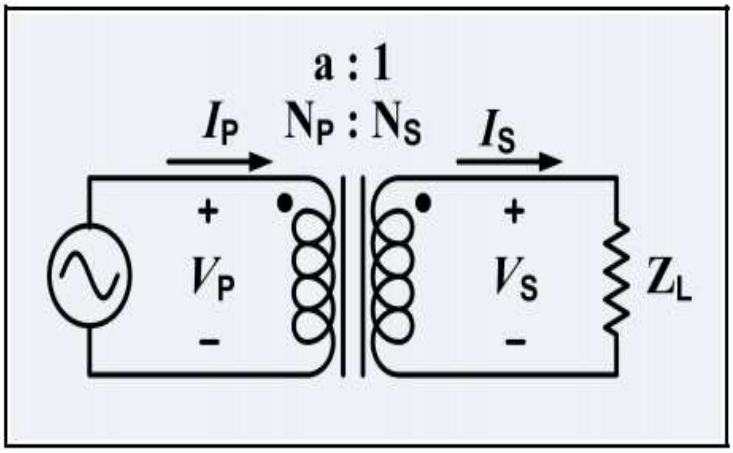

Figure 3 Model of Coil / Pot as a Transformer and Resistor [1]

2.2.4 Hysteresis Loss

Hysteresis loss is an additional loss mechanism in ferromagnetic materials, which involves the dissipation of heat. This loss can be understood as the energy required to flip the magnetic dipoles within the ferromagnetic material. In the context of an induction stove, hysteresis loss contributes a significant, although not dominant, portion of the heat generated [12].

2.2.5 Skin Effect

The skin effect is a phenomenon where currents with high frequency tend to flow predominantly on the conductors' surface. As the distance from the conductor's surface increases, the current density decreases exponentially [2]. The "skin depth" refers to the distance from the surface at which the current has attenuated to 1/e (approximately 36.8%) of the overall current. The formula governing the skin depth is shown below:

$$\delta = \sqrt{\frac{2\rho}{\omega \mu_r \mu_0}}.$$

Eq.6

Where.

δ: Penetration depth [m]

ρ: Resistivity [Ωm]

μ: Permeability [Vs/ (Am)]

ω: Frequency [Hz]

In induction heating, the skin effect plays a significant role in efficiently heating a pot. The increases in frequency will also cause the effective resistance of the pot to increase, following the square root of the frequency. It is important to note that non-magnetic materials, which have lower relative magnetic permeability, have much larger skin depths. As a result, non-magnetic materials are not favorable and will not be used for induction heating. Figure 4 illustrates the relationship between the skin depth and frequency for different materials [11].

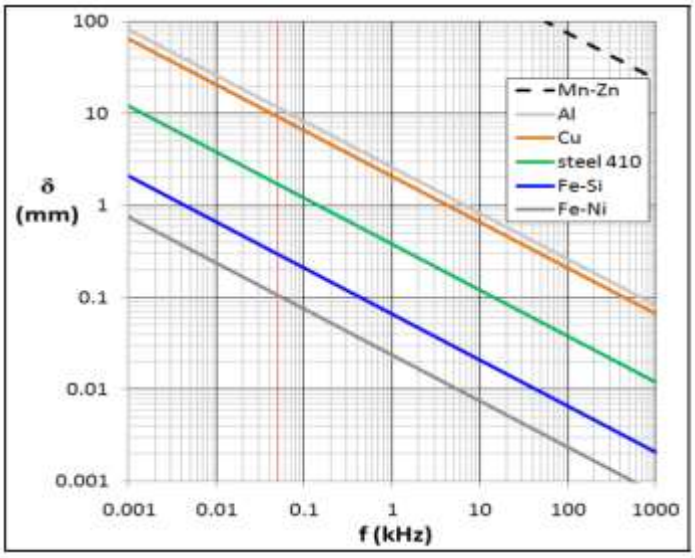

Figure 4 Graph of Skin Depth vs Frequency for Different Materials [1]

The coil of an induction cooker generates a magnetic field that induces a current beneath the pan surface. This induced current circulates on the surface by Lenz's Law. Due to the skin effect, which becomes prominent at the working frequency of induction cookers (around 20-30 kHz), the current density is highest at the edges or surface "skins" of the pan. The circulating eddy current itself generates its magnetic field. Since this magnetic field opposes the original flux, the current density is higher at the edges. When the frequency of the current within the coil increases, the induced current flowing along the surface of the pan becomes more pronounced [11].

As described by Equations 7 and 8, the density of the induced current decreases as it moves towards the center as stated in the skin effect. The conversion of electrical energy to heat energy is concentrated at the skin depth, which refers to the surface of the object, as depicted in Eq.7

$$Ix = Ioe^{\frac{r}{n}}$$ Eq.7

Where; i_x is the current density at distance x. It is the distance from the skin of the object and i_0 is the current density on the surface (x=0) and is a constant determined by the frequency (skin depth constant).

$$\delta = \sqrt{\frac{2\rho}{\mu\omega}}$$ Eq.8

In Eq.8, ρ is the resistivity of the pan surface (ohms meter), μ is the pan surface permeability (Henry/meter), and ω=2πf as f is the frequency of the current flowing through the pan surface (Hz).

Eq.7 shows that skin thickness is affected by the resistivity, permeability, and frequency of the applied current. Figure 5 is the distribution chart of current density concerning skin thickness "x". When x equals, the current drops down to e-1 i.e., 36% of its initial value.

2.2.6 Coil Design

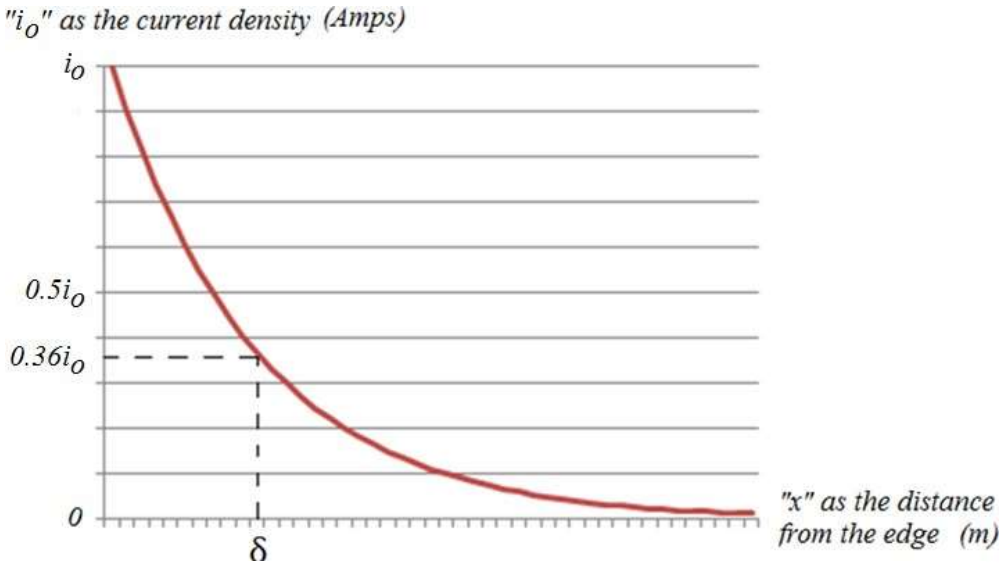

Figure 5 Current density vs skin thickness

The primary goal of an induction stove is to create a powerful magnetic field. The strength of this magnetic field relies on the coil's geometry and the number of ampere-turns within it. Ideally, a

flat "pancake" coil is commonly used for induction stoves [11], although a helical coil can also be effective.

The magnetic field's intensity is directly proportional to the number of ampere-turns. A number of turn increments is not always practical due to limitations in the converter's dynamics. For example, inductance is proportional to the square of the number of turns, which affects the resonant frequency. Consequently, when designing the coil, it is crucial to consider other system parameters to maintain optimal performance. Moreover, coils experience ohmic losses, particularly as a result of the skin effect. In induction heating, the objective is to heat the pot rather than the coil itself, so the skin effect reduces efficiency. Furthermore, increasing the number of turns in the coil leads to a longer conduction path, resulting in higher losses. This emphasizes the trade-off between coil design and efficiency when adding additional turns [48].

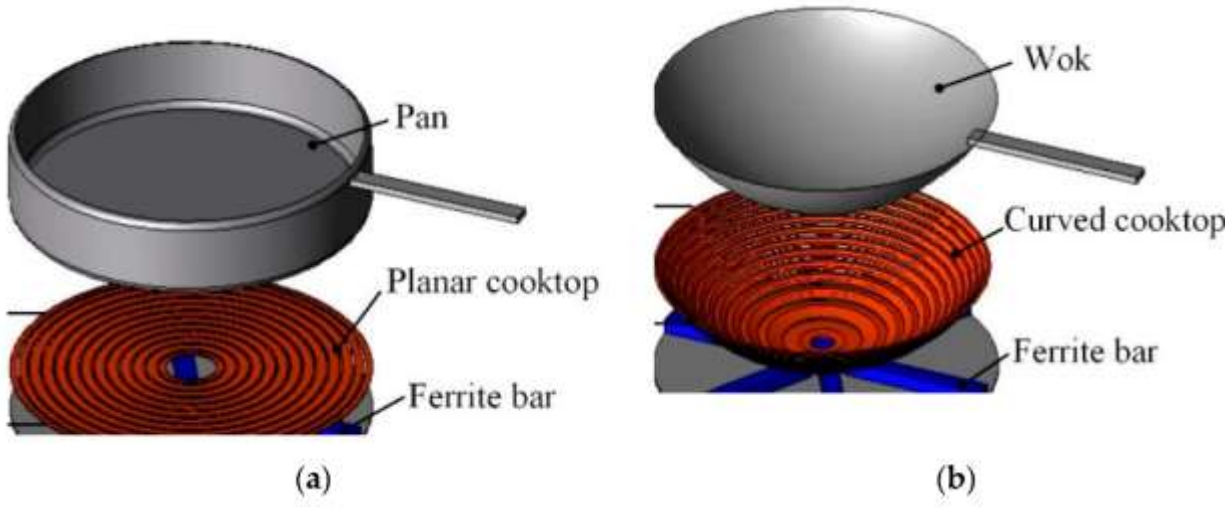

Figure 6 Examples of cooking coils of different shapes and sizes: (a) planar cooktop and (b) curved cooktop [50]

2.3 Types of cookstoves

As central heating became popular in the 20th century, traditional iron cooking stoves that burned wood or coal became uncomfortable due to excessive heat. They were replaced by steel ranges and electric/natural gas ovens. Today, there are various cooktop options like gas, electric, and induction, with different sizes and heating configurations. Clean cooking has gained attention for its health and environmental benefits, leading to a renewed focus on stove quality and performance. Electric stoves can be categorized into three main types based on the physical

configuration of their stove tops: iron hotplates, radiant coil, and ceramic. Additionally, stoves can also be classified according to technological advancements and methods of heat transfer [7].

2.3.1 Iron hot plates:

Iron hot plates were the initial technology for electric stoves, using coils to heat iron plates where pots were placed. They have lower energy efficiency, slower heating, and higher energy consumption. However, they are easier to clean and require good contact between the pot and the cooktop for effective cooking.

2.3.2 Radiant Coil stoves:

a. Open resistors type: These stoves have exposed heating elements that emit heat through radiation. They are affordable and commonly used.

b. Spiral hollow steel tube resistor types: Solid hot plate stoves feature a heating element inside a spiral-shaped tube. The steel spiral is heated to a red-hot temperature, providing increased heat transfer through conduction and radiation to the pan.

C. Ceramic cooktop (smooth-top) stoves:

i. Glass-ceramic: These cooktops heat quickly, have low thermal conductivity, and a smooth surface that is easy to clean. They are more expensive and take longer to cool down after use.

ii. Induction stoves: Made of glass ceramic, induction stoves utilize electromagnetic technology to heat the cooking pan. They offer precise temperature control, immediate response, and high energy efficiency. Only certain types of cookware, such as cast iron and certain types of glass, are suitable for induction cooking.

Iron hot plates	
Open resistor stoves	

Spiral hollow steel tube resistor types	
Glass-ceramic cooktops	
Induction stove	

Figure 7 Different cookstove type

2.4 Principle of Operation of Induction cook stoves

Electric stoves can feature single or multiple cooktops and are equipped with various control mechanisms. These controls can include fixed or rotary switches with different of positions, each engaging different combinations of electric resistances and providing varying heating power. Some electric stoves may also incorporate thermostats to regulate the power and control the overall heating effect of the elements.

Induction heating is a way of heating metals using electromagnetic induction. The generation of eddy currents and the resistance of the metal leads to Joule heating, as depicted in Figure 8. Additionally, there are losses due to the hysteresis of the magnetic material in the pan [13].

An IC typically consists of a copper coil through which a high-frequency alternating current (AC) is passed. The frequency of the AC is determined by the maximum switching frequency of the switch, which is typically an IGBT. Higher switching frequencies can reduce the inductance of the coil and the size of the resonant capacitor, resulting in cost savings for the unit [14].

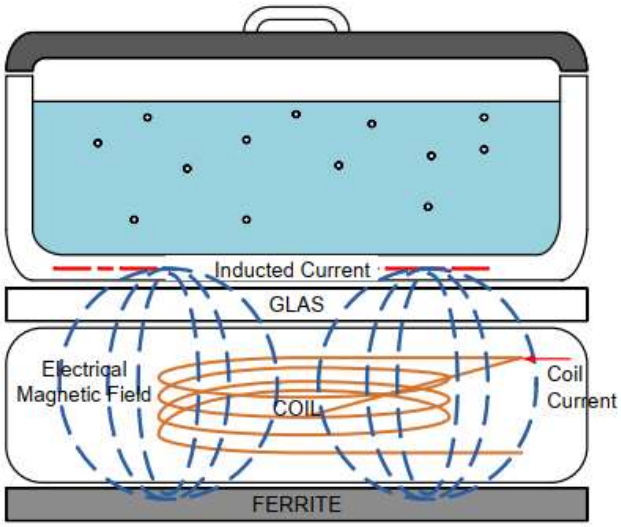

Figure 8 Scheme of an Induction Cooking [25]

2.5 Solar Energy for Induction Heating

Solar energy is a plentiful and environmentally friendly form of renewable energy that plays a crucial role in combating pollution and addressing resource scarcity. Among various renewable energy sources, photovoltaic (PV) systems that harness solar power are rapidly advancing. One significant advantage of PV technology is its simplicity, as it operates without any moving parts, making it highly durable with a long lifespan and minimal maintenance requirements. Solar power generation is increasingly recognized as an eco-friendly and sustainable alternative to fossil fuels and nuclear power, offering an efficient solution for generating electricity [15].

Solar energy is not only useful for electricity generation but also readily accessible for heat generation. Induction heaters have proven to be highly effective devices for utilizing solar energy in this regard. Solar energy and induction heating combination can be a productive solution. To achieve this, household induction heating applications often employ resonant converters with soft switching. These converters are favored due to their compact size and high efficiency. In a solar-based induction heating system, solar energy captured by a photovoltaic cell array serves as the

primary input. This energy is then converted into electricity through an inverter, enabling its utilization in induction heating applications.

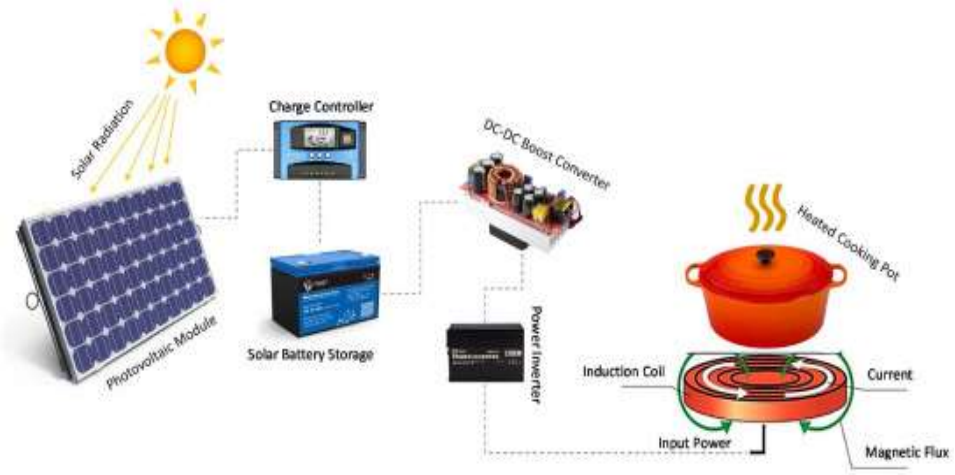

Figure 9 Custom solar-powered induction stove diagram [49]

In the figure above the solar induction cooker utilizes a solar panel to generate variable DC output. This DC voltage is converted into AC voltage using an inverter circuit and then fed into the induction cooking circuit. The AC voltage is rectified back to DC using a rectifier, and a filter is used to remove any pulsating DC from the rectifier output. The inverter is supplied with the DC voltage and pulses required for triggering the MOSFET, which acts as a switching device to generate the AC voltage [16].

The generated heat temperature is controlled by a PWM signal applied to the MOSFET's gate. When a pan is placed near the induction coil, an eddy current is induced in the cooking pan. This, in turn, produces heat energy on the surface of the pan. The heat dissipates through the pan's internal resistance. Consequently, it is the pan itself that gets heated, and this heat is used for cooking food [15].

2.6 Previous research on solar-powered induction cooker

In an MIT thesis, Weber (2015) has practically implemented a design of 500W to 1kW induction stove [5]. The designed stove has an input power of 24V DC and it uses a car battery, while also allowing integration with small-scale solar installations. However, there is no existing commercial stoves or academic research worked on a low-voltage DC source IC.

The study works on the design of a low voltage current-fed, full-bridge parallel resonant converter IS. The design consists of 3 major parts: the converter board, the control board, and the software. This stove is the first of it is kind and represents a new contribution to both the field of induction cooking and the field of clean cooking solutions for the developing world. This stove is a groundbreaking innovation in both induction cooking and clean cooking solutions for developing regions, making it a significant contribution to both fields. It is the first of its kind and introduces a new and valuable solution. The device's limitations included a basic coil design, low operational frequency, and a simple control system, among others. Enhancing these aspects of the design would greatly enhance the efficiency and functionality of the device [10].

A study conducted by the Myanmar Scientific and Technological Research Department showcased the design and simulation of an induction cooker powered by solar electricity. The cooker utilized a quasi-resonant topology [10]. The efficiency of a commercially available AC-based induction cooker was experimentally tested and found to be 85.56%. Similarly, the simulation of the functional circuit for the same cooker yielded an efficiency of 87%. Additionally, the design and simulation of a microcontroller-based DC induction cooker, with an output power range of 500 W to 1500 W, have been successfully completed. The average simulation efficiency for this cooker is measured to be 90.10%.

The study done by Shrestha (2018) show that IC using a battery (DC source) is possible [17]. A DC induction cooker powered by solar electricity, utilizing a quasi-resonant topology, has been designed and simulated. The simulation process involved the use of circuit simulators such as Multisim and Proteus. The simulated system is battery-operated, with a system voltage of 24 V DC, and relies on a microcontroller for control operations. It is designed to function with a 300 Ah battery and a 500 WP solar photovoltaic panel. The input power range of the system spans from 46.4 W to 1500 W, resulting in corresponding input currents ranging from 1.93 A to 62.5 A. The output power of the cooker falls within the range of 40.8 W to 1310 W, exhibiting an average efficiency of 90.10%. The performance parameters of the designed induction cooker demonstrate the technical feasibility of constructing such a system.

The performance parameters of the designed IC show that the simulated system can be technically implemented. They recommended the design be tested by using half and full bridge topologies for high power (more than 1Kw a below 2 Kw) systems at 24V. Also stated that the pan-coil modeling

will improve the design in addition to the appropriate size of a printed circuit board to further reduce the impact of parasitic capacitance by appropriate clearance between circuit components.

Maharjan (2016) conducted a study to examine the electrical and thermal performances of cooking appliances found in Kathmandu. The research findings revealed that the displayed power of induction and infrared cookers did not accurately reflect the actual power consumed. Additionally, the thermal performance of the induction heater and infrared heater was significantly better compared to the coil heater. It's important to note that this study specifically focused on AC-powered devices [18].

Thandar et al. (2008) have developed a power system specifically designed for an induction cooker, capable of operating at a 500W output and a frequency of 24 kHz [3]. The circuit employs a series resonant circuit. It's important to note that this study focuses solely on the power system in the context of AC, without considering DC.

Shakya (2014) conducted a study that explored various scenarios for replacing conventional energy resources with Renewable Energy Technologies (RETs) and examined different policy intervention scenarios. The study's findings suggest that implementing policy interventions can lead to a reduction of 14% in total final energy consumption within the residential sector [28]. The hardware realization of the design was not achieved with the use of available components in the market due to the component quality issues in low voltage and high current conditions for a given output power. However, if this design can be realized, solar PV-based cooking might be a prominent alternative technology of the nation in the future for achieving energy efficiency.

2.7 Energy efficiency of Electrical cook stoves

Different cook stove design elements have an impact on these efficiency factors. The shape of the cook stove and the heat transfer mechanisms are the two main factors that affect how efficiently heat is transferred. The performance of electrical cookstoves can be assessed through various factors and metrics. Here are some common methods used for evaluating the performance of electrical cook stoves energy efficiency, cooking time, heat distribution, temperature control, and power consumption. Safety features and durability of the material associated with user satisfaction also play a significant role in efficiency evaluation [7].

To examine the performance of an electrical cook stove, the following steps can be followed [19]:

1. Energy Efficiency Testing: Measure the input electrical energy and the output heat energy. Produced by the cook stove. The higher the efficiency the better the performance.

2. Cooking Time Evaluation: Compare the cooking times for different recipes and food items using the cook stove. Shorter cooking times indicates better performance.

3. Heat Distribution Analysis: Use temperature sensors or infrared cameras to measure and map the heat distribution across the cooking surface. Ensure the heat is evenly distributed without any significant hot or cold spots that could affect cooking quality.

4. Temperature Control Assessment: Evaluate the stove's temperature control capabilities by measuring how accurately it maintains and adjusts cooking temperatures. Use a calibrated thermometer or temperature probe to verify if the stove achieves and maintains the desired temperature levels.

5. Power Consumption Measurement: Monitor the electrical power consumed by the cook stove during different cooking scenarios. Measure the power usage in kilowatt-hours (kWh) and compare it with similar models or industry standards to assess its efficiency and operating costs.

Standardized tests for stove performance involve trade-offs, as highly controlled conditions with reduced variability are better for detecting small changes but may not represent actual cooking. Controlled tests are suitable for comparing technical aspects and pre-field evaluations, while field-based tests provide a better indication of real-world performance during actual use [20].

2.7.1 Observed Gap

The research conducted on locally manufactured electrical cooking stoves reveals that a lack of research and innovation in product improvement, as well as inadequate awareness regarding proper product use, result in low energy and cooking efficiencies. This leads to significant heat loss during operation. The previous version of the locally manufactured electrical cook stove featured a single switch, causing energy losses for pots of both small and large diameters. The study examined various factors such as energy consumption, costs, cooking time, thermal energy losses, and heat transfer behaviors to address these concerns [21].

Ethiopian Energy Authority has formulated a document on locally manufactured electric stoves for energy efficiency standards and labeling purposes. Their insights about local stoves are

summarized below. The major limitations based on the Ethiopian Energy Authority study about locally manufactured electric stoves are The absence of heat insulation, the lack of heat intensity control mechanisms and switching to control heat level, open and exposed heating elements, and dread of contact for users, frequent burning of the heating element due to spillage and poor quality, the increased gap between cookware base and the heating element, wear of clay plate and fast aging of framework and sub-optimal/poor and inefficient design and workmanship [7].

Quality of materials-related concerns include; the presence of up to three quality levels for the materials (resistance, switches, connectors, and plugs). Many of the components are of low quality. Some resistance melts away simply and upon spillage and further damages the clay plate. Thus, there shall be a standard for resistors supplied to producers. Circuit breakers in residential households do not protect against the high current occurring from over-voltage and voltage spikes and stove resistances burn often. Low quality of clay plate materials and hence cracks and breaking occur during use. The wiring of the resistance in the clay is also challenging [7].

Designing and manufacturing efficient induction cook stoves is important as it will, reduce the aggregated energy demand for cooking nationally, and save energy to the consumer (user) and the nation. enhance national economic efficiency by reducing energy bills, strengthening market competition among producers, encouraging research and innovation, assisting the country in meeting climate change goals and averting regional pollution, reducing deforestation in search of firewood and bio-mass fuel, mitigating land degradation and environmental pollution due to the production of clay plates, mitigate the burden on the rural women engaged in the production of clay plates [52].

The ambitious plan by the government to increase electricity access from the current 45% to 100% by 2025 offers further considerations and opportunities for e-Cooking going forward thus the induction stoves implementation will contribute to the conservation of energy and the environment. According to the BARHAP tool by WHO, if 40% of Ethiopia's grid-connected charcoal users (equivalent to 4.2 million people, with 0.9 million being households) were to switch to e-cooking, several positive outcomes could be achieved [6]. Based on figure 10 this includes avoiding 903 DALYs (Disability-Adjusted Life Years) per year, reducing CO2eq emissions by 2.2 million tonnes per year, decreasing unsustainable wood harvest by 0.4 million tonnes per year, saving 132 million hours of women's time annually (equivalent to 147 hours per household per

year), and achieving a payback period of 14 months for e-cooking appliances (with an upfront cost of $100 per household and $90 per household per year in fuel energy cost savings). Additionally, this transition would stimulate a demand for 517 GWh (gigawatt-hours) of electricity. The National Electrification Program 2.0, introduced in 2019, aims to achieve universal electrification by the year 2025. This will be accomplished through a combination of grid connections, accounting for 65% of the target, and off-grid connections, making up the remaining 35%. The program envisions further progress, targeting 96% grid access and 4% off-grid access by the year 2030 [53].

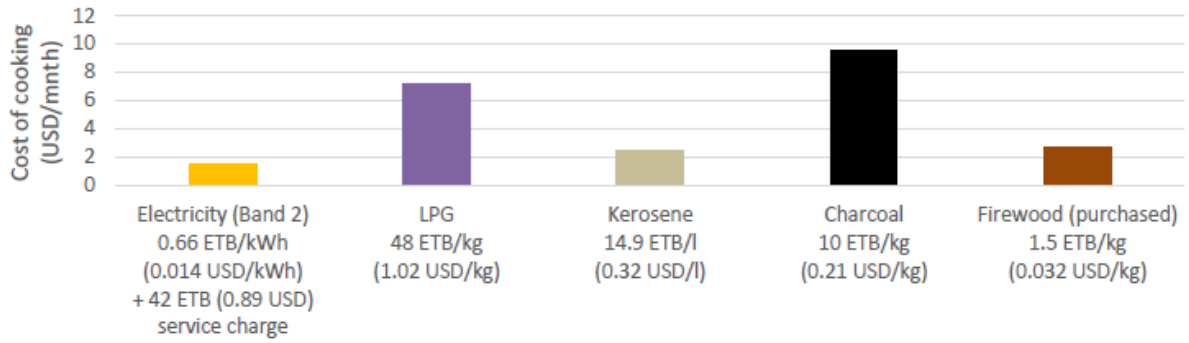

Figure 10 Cost comparison of different cooking fuels based on international averages for cooking energy demand from ESMAP (2020) and local electricity/fuel prices obtained during this market analysis [22]

2.8 Induction Cookstove designs

Commercial IC products were examined to determine the popular topologies. The popular are discussed below;

2.8.1 Some of the commercial designs

A. Fabiano Stove: The Fabiano stove is an affordable induction stove available in India, operating at a voltage of 220V. It utilizes a quasi-resonant topology, employing a single power device and operating at a frequency of 27 kHz.

B. Phillips Stove: In India, there is another affordable induction stove available for purchase that utilizes a quasi-resonant topology. This stove features a single IGBT (Insulated Gate Bipolar Transistor) and operates at a switching frequency of 30 kHz.

C. CookTek Stove: In the American market, there is an industrial model of induction stove available for sale. This stove is designed for high-power applications and adopts a resonant half-

bridge configuration, utilizing four power devices (with two devices in parallel for each leg of the bridge). It operates at a frequency of 25 kHz, making it suitable for industrial use.

Commercial stoves currently available in the market face certain drawbacks, particularly when considering their use in developing regions. While achieving high efficiencies of around 90% is feasible, many commercial offerings fall short and do not even reach 80% efficiency. This deficiency can be attributed to their design origins in countries with readily available and affordable mains power [12].

Furthermore, the existing commercial stoves lack built-in mechanisms to handle situations such as brownouts or blackouts. In regions where, reliable electricity supply is limited, relying on an induction stove becomes problematic. Families residing in such areas would struggle to cook their meals regularly due to the stove's inability to function during power disruptions. It becomes apparent that the commercial stoves are excessively designed for the typical users in developing regions.

2.8.2 Inverter topologies

The solar panel's direct voltage and current need to be converted into alternating current using an inverter. The inverter utilizes capacitors and inductors in different configurations to achieve a sinusoidal output waveform. Resonant converters, which consist of resonant L-C networks with capacitors, inductors, and resistance, are used for this purpose. During operation, energy is stored in the inductor and transferred to the capacitor, resulting in a sinusoidal waveform through resonance. However, some energy is lost due to resistance during this process [13][15].

Resonant converters are classified into various types, including Series Resonant Inverters, Parallel Resonant Inverters, Class E Resonant Converters, and more. These converters are designed for energy-saving systems operating at high frequencies, with semiconductor power components switching at zero voltage (ZVS) or zero current (ZCS) [22].

In induction heating applications like induction cooking, different converter topologies are used to generate the required time-varying magnetic field. Series resonant converters and series quasi-resonant converters are commonly employed in induction cooking [3]. Modulation strategies are employed to control the output power by adjusting the switching frequency or duty cycle. The choice of power converter topology depends on specific requirements such as cost, hardware

complexity, and control complexity. In a collection resonant converter, a series resonant tank is driven by a voltage-fed bridge that switches at the tank's resonant frequency [10]. This induces large resonant currents, heating the cookware. Soft-switching techniques ensure efficient operation. The driving bridge can be either a half-bridge with two power devices or a full bridge with four devices [7][19].

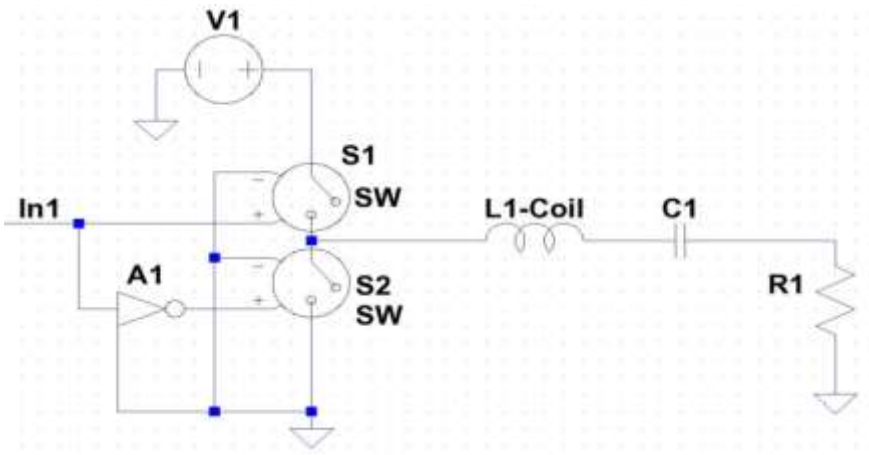

Figure 11 Schematic of the Fabiano brand stove with Quasi-Resonant Topology[14]

The overall design comprises three primary components: the converter board, the control board, and the controlling software. The converter board consists of several elements like gate drivers, a resonant tank, power components, and feedback circuitry. On the control board, you will find a microcontroller along with various I/O and signal conditioning components. The software running on the control board is responsible for managing the logic that controls the switches on the converter board. Regarding the topology, both modern and traditional approaches have unique features, which will be elaborated further in the following sections [14].

A. Conventional Topology used in Induction Heating:

This is the common approach, illustrated in Figure 12, where the battery serves as the main power source [10]. Induction cooking systems primarily operate on AC supply. If an IC is to be powered by a battery system, a high-frequency DC/AC inverter is required to convert the 12V battery power into a 230V AC system. The depicted figure represents the common approach commonly used by Induction cookstove designs. In this system, an internal conversion occurs using a rectifier to convert AC into DC supply. This conversion takes place specifically during the power delivery process of the resonant converter [1] [15] [26].

The conversion process involving the external inverter and the internal conversion within the system results in an efficiency that is less than 100%. The redundant operations of these blocks \significantly impact the efficiency of the overall system.

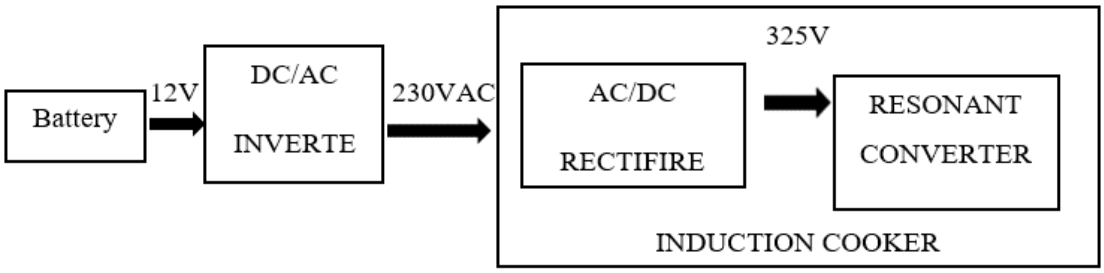

Figure 12 Convectional Topology [26]

B. Modern Topology

Figure 13 represents the modern approach we employ in our solar-powered induction cooking system. The realm of DC-powered IC systems is still new, and its growth potential has not yet peaked. One of the notable advantages of using this approach is that the auxiliary circuit consumes very little current, while the main resonant converter handles the majority of the current from the battery. This significantly boosts the efficiency of this topology [1][15][19].

However, a key limitation of this circuit is its straightforward coil design. Unlike the previous design, it lacks the complexity of a control system with direct fabrication and no complications.

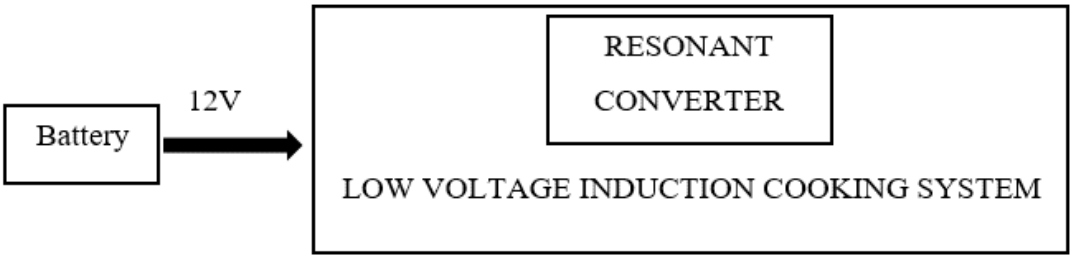

Figure 13 Modern Topology [26]

2.10 Resonant Converter for Induction Cooking

In power electronics, it is customary to employ traditional PWM (Pulse Width Modulation) power converters that operate in a switched mode. Typically, these converters employ a hard-switching mode, as shown in the Figure below, where the switches transition between high current and high voltage states. The term 'hard switching' refers to the difficult switching behavior exhibited by power electronic devices. During the switch-on and switch-off processes, these devices have to endure simultaneous high voltage and current, leading to elevated power switching losses and increased stress on the devices [44].

To mitigate voltage transients and switching losses in these circuits, snubbers are typically employed. Snubbers help reduce voltage transients at electronic devices, as well as minimize the switching losses in these devices. The switching losses are directly proportional to the switching frequency, thereby imposing limitations on the maximum switching frequency of the power converters [26].

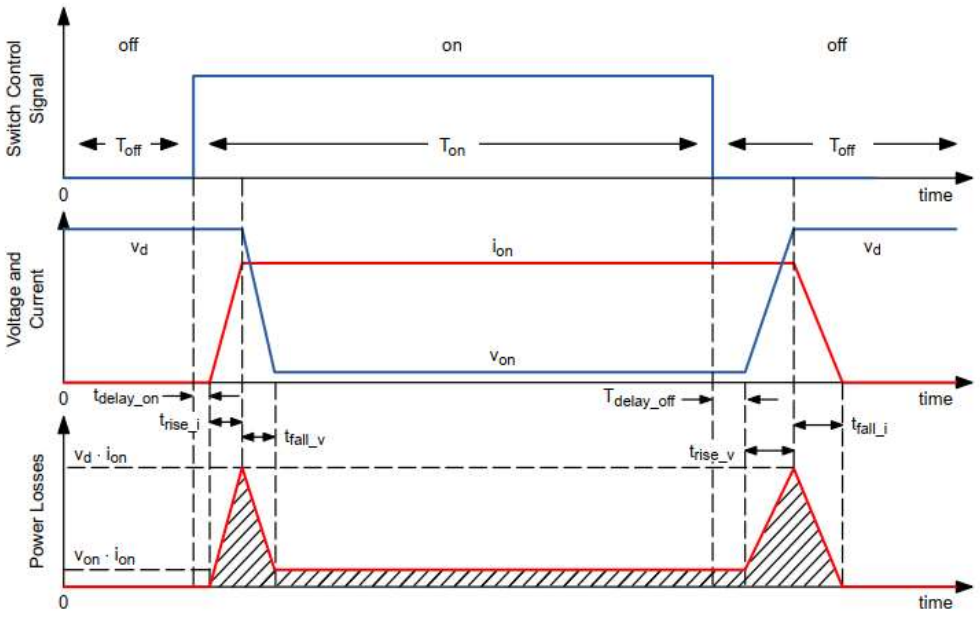

Figure 14 Power Losses in a Conventional SMPS Converter [26]

In power electronics, it is common to use traditional PWM power converters operating in switched mode. Conventionally, the switches transition from high current to high voltage, as shown in Figure 14, in what is known as hard switching mode. The term 'hard switching' refers to the challenging switching behavior of power electronic devices. During the switch-on and switch-off

processes, the power devices have to withstand high voltage and current simultaneously, resulting in high power switching losses and stress [22] [44].

To mitigate voltage transients and switching losses in these circuits, snubbers are typically employed. Snubbers are added to reduce voltage transients and minimize the switching losses in the power devices. The magnitude of switching losses is directly proportional to the switching frequency, which imposes limitations on the maximum switching frequency of the power converters [26].

Figure 15 illustrates the different switching regions in power electronics, including hard-switched conditions, snubber-assisted commutation, and soft-switching. In hard switching, during both turn-on and turn-off processes, the power devices face simultaneous high voltage and current, resulting in increased switching losses and stress. To mitigate this, dissipative passive snubbers are often incorporated into power circuits to reduce the rate of change of voltage (dv/dt) and suppress voltage spikes on the power devices [27] [26].

The reduction of switching losses and continuous improvement of power switches have enabled resonant converters to operate at switching frequencies approaching 100 kHz for IGBT switches. This allows for reduced sizes of magnetic and capacitive components and increased power density of the converters. As shown in the diagram below soft switching has a lower area and it will reduce the switching loss and high-frequency noise of the power electronic device [14].

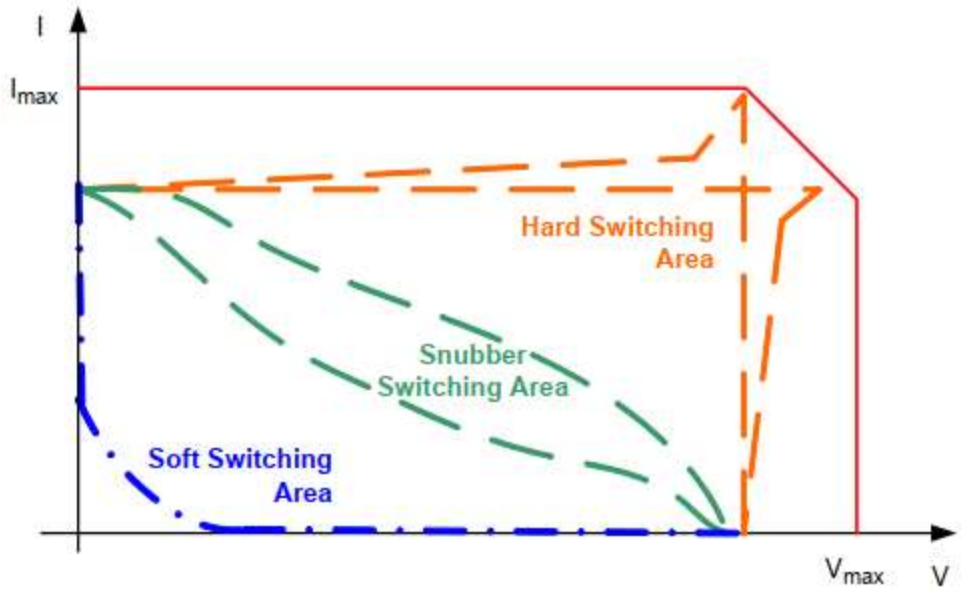

Figure 15 Switching Area [14] [54]

2.11 Most common topologies

The figures provided illustrate various topologies used in induction heating. Figures 16(a) and (b) showcase the full-bridge, half-bridge, and single-switch inverter topologies. Figure 16(c) demonstrates Zero Voltage Switching (ZVS), while Figure 16(d) depicts Zero Current Switching (ZCS) operation [11] [28] [29].

To control the output power in induction heating, modulation techniques are commonly employed. These techniques involve adjusting either the switching frequency or the duty cycle to achieve the desired power output [12]. Each power converter topology offers unique performance characteristics and comes with specific requirements in terms of costs, hardware, and control complexity. Extensive literature exists documenting these systems, including the design criteria for their essential parameters.

The most widely used topologies for induction heating are the Half-Bridge (HB) series-resonant converter and the Single-Switch Quasi-Resonant (QR) converter. The Resonant Half-Bridge topology is particularly popular for four-burner cooktops and has gained significant popularity in the European market.

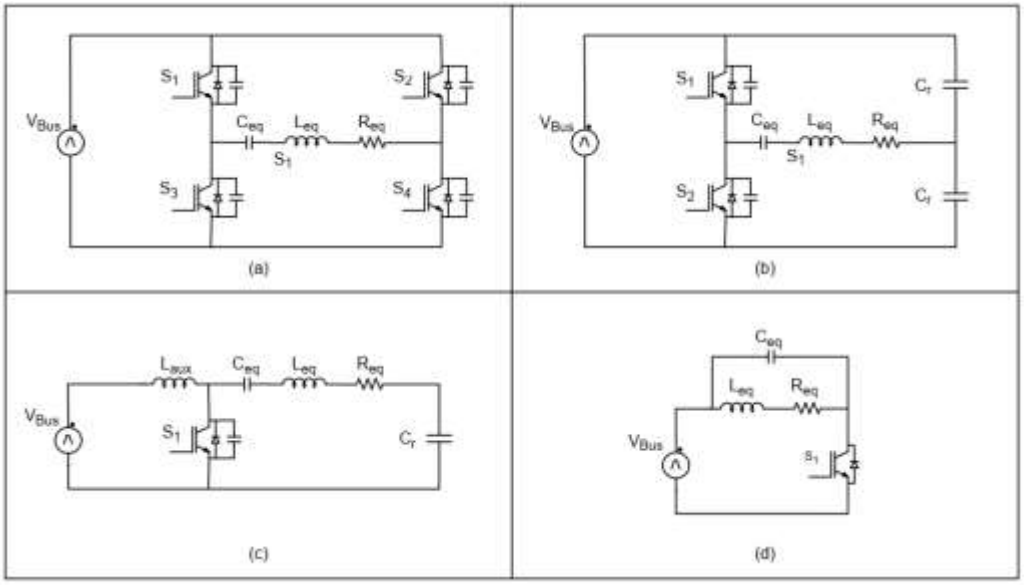

Figure 16 Samples of the Topologies Presented in Literature in the Last Decades [26]

2.11.1 Half Bridge Topology

The Resonant Half-Bridge inverter, depicted in Figure b below, is widely utilized as the preferred topology in induction cookers that have high-power and multiple burner systems. It is favored for its simplicity, cost-effectiveness, and its ability to meet the electrical requirements of its components. This particular topology is commonly found in European markets. In this configuration, the load consists of the resonant tank, which comprises the inductive coil, resonant capacitors, and the equivalent resistance of the pan [28] [31].

The coupling between the induction coil and the pan can be represented by a series connection of an inductor and a resistor, based on the analogy of a transformer. This coupling is determined by the values of Lr (inductance) and R load (resistance). These values are primarily influenced by the switching frequency applied to the switches, the material of the pan, temperature, and the degree of coupling between the inductor and the pan [26] [27].

The Resonant Half-Bridge topology belongs to the family of resonant converters. It resembles a standard half-bridge configuration, where the bus capacitance (resonant capacitors) is chosen to resonate with the coil at a specific frequency called the resonant frequency. The power stage consists of two switches with antiparallel diodes, two capacitors, and a coil [27].

For calculation purposes, the circuit can be simplified as demonstrated in Figure 17, where two capacitors are connected in parallel, unlike the configuration shown in the previous figure.

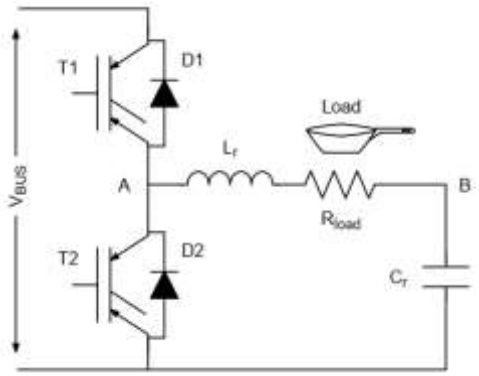

Figure 17 Equivalent Circuit for a Resonant [26]

Figure 18 depicts the equivalent series resonant circuit, which represents the resonant half-bridge configuration. In this circuit, the impedance can be described as follows:

$$\text{Z series} = \text{j}\omega\text{L} + \frac{1}{\text{j}\omega\text{C}} + R \qquad \text{Eq. 9}$$

$$\omega = 2\,\pi\,\text{f} \qquad \text{Eq. 10}$$

Where "jωL" represents the impedance of the inductor, "1/jωC" represents the impedance of the capacitor, "R" represents the impedance of the resistor, where R is the resistance.

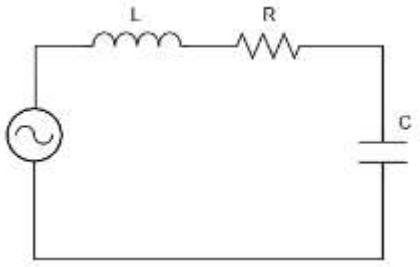

Figure 18 Equivalent Series Resonant Circuits

Figure 19 illustrates the impedance of the circuit denoted as Z series when analyzed from the perspective of the generator. The angular frequency is represented by ω in the equation. At the resonant frequency ω_0, the reactance of the inductor is equal and opposite to the reactance of the capacitor, resulting in the minimum value of the equation.

Another essential parameter to consider in a resonant circuit is the quality factor (Q). Q is a dimensionless parameter that quantifies the ratio of the circuit impedance to the losses in the

circuit. A higher Q value indicates a lower rate of energy loss in comparison to the stored energy in the resonator. As a result, the oscillations in the circuit decay at a slower rate over time.

$$Q = \frac{Zo}{R} \quad \text{Eq.11}$$

Where, Q is the dimension parameter, Zo is the impedance and R is the resistance.

A higher Q value indicates a circuit with lower losses and sharper resonance, while a lower Q value corresponds to a circuit with higher losses and broader resonance. The quality factor is an essential parameter for characterizing the performance and behavior of resonant circuits in various applications. Z_0 is the impedance at the resonance frequency.

$$f_{res} = \frac{1}{2*\pi*\sqrt{Lr*Cr}} \quad \text{Eq.12}$$

$$\omega_{res} = \frac{1}{\sqrt{Lr*Cr}} \quad \text{Eq.13}$$

$$Z_0 = \sqrt{\frac{Lr}{Cr}} \quad \text{Eq.14}$$

$$Q_L = \frac{Z0}{r\ pot} \quad \text{Eq.15}$$

$$\varphi = a\tan\left(\frac{\frac{Lr}{Cr}}{r\ pot}\right) \quad \text{Eq.16}$$

The resonant frequency, denoted as f_{res}, is the frequency at which the circuit exhibits resonance. The inductance of the coil is represented by Lr, while Cr refers to the combined value of the parallel resonant capacitances. The phase difference between the current and voltage in the circuit is indicated by φ.

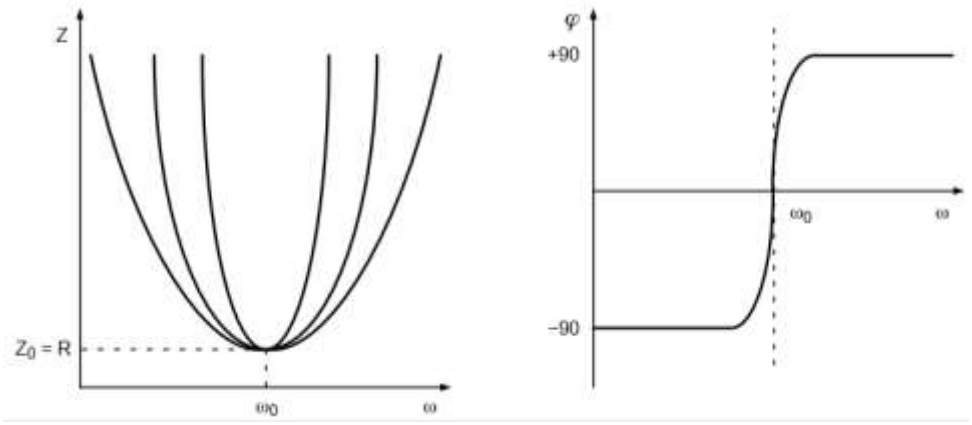

Figure 19 Impedance Module and Phase of the Equivalent Half-Bridge Resonant Circuit [26]

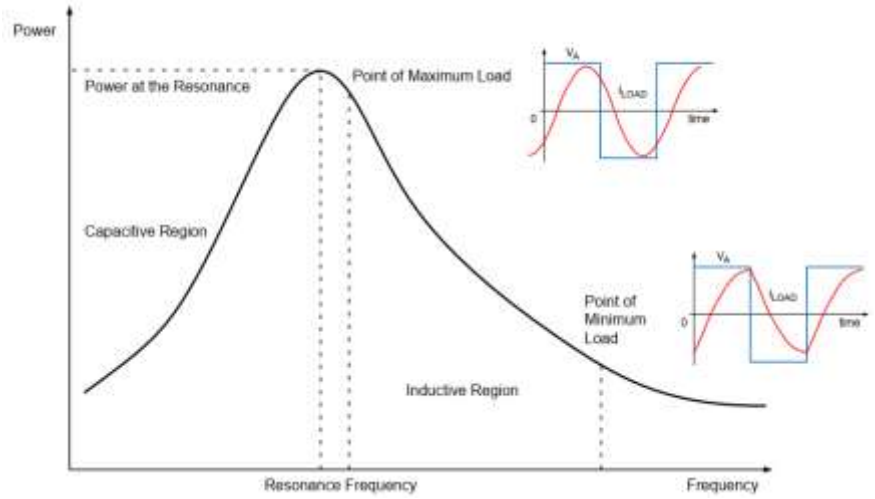

Figure 20 Output Power vs. Switching Frequency for Maximum Load and Minimum Load [26]

Below resonance, above resonance, and at the resonance frequency are the three operational modes of the circuit. These modes are characterized by a capacitive load when the frequency (f) is less than the resonance frequency (f_{res}), an inductive load when f is greater than f_{res}, and a purely resistive load when f equals f_{res}. The figure 20 illustrates these modes.

When designing a resonant half-bridge for induction heating applications, it is crucial to ensure that the overall system operates within the inductive load region and the range of the resonant frequency. This is because operating in the capacitive load region can result in three significant detrimental effects during turn-on: reverse recovery of the antiparallel diode of the opposite switch, discharge of the transistor output capacitance, and the Miller capacitance effect. These effects have the potential to cause damage to the device [11] [26].

2.11.2 Operating Principle of the Half-Bridge

Figure 21 provides an overview of the waveforms in an induction cooker, including voltage (upper graph, blue waveform) and current (upper graph, red waveform) in the resonant circuit, as well as the gate signals (lower graph, blue waveform for gate T_1 and red waveform for T_2) for the two switches. These waveforms demonstrate the operation near the resonance frequency, where the switching frequency matches the resonant frequency. This mode optimizes power delivery to the load, maximizing efficiency [3].

When operating below maximum power levels, the switching frequency increases, causing the waveforms to deviate from a sinusoidal shape. This occurs when the burner is not in boost mode. Figure 22 illustrates the waveforms for both switches at a switching frequency above the resonant frequency. The normal operation can be divided into four intervals: t_0-t_1, t_1-t_2, t_2-t_3, and t_3-t_4. Figure 24 focuses on the current in one switch, and the conduction sequence of the semiconductor devices is D_1-T_1-D_2-T_2. Let's examine the interval t_0-t_1 (Figure 23). Before t_0, the current flows through T_2. When T_2 is turned off, D_1 conducts while the gate of T_1 remains off to prevent cross-conduction. The interval during which neither the gate of T_1 nor T_2 is active is called the dead time. At t_0, the gate of T_1 is activated, but the current still flows through D_1. At t_1, the current undergoes a transition from negative to positive and begins to flow through T_1. The reverse recovery current of the diode flows through the opposing IGBT without causing additional losses in the resonant half-bridge devices. During turn-on, losses in the devices are minimal, whereas turn-off incurs significant losses due to the overlap between high current and high voltage. At t_2, T_1 turns off while the current remains high, resulting in an overlap with the voltage waveform and causing turn-off losses in the device. Additionally, the Miller effect is present, leading to an increase in the transistor's input gate charge, reducing the turn-off speed, and increasing losses. The intervals t_2-t_3 and t_3-t_4 follow a similar pattern to the previous intervals, but now T_2 and D_2 become the active devices [3] [19][26].

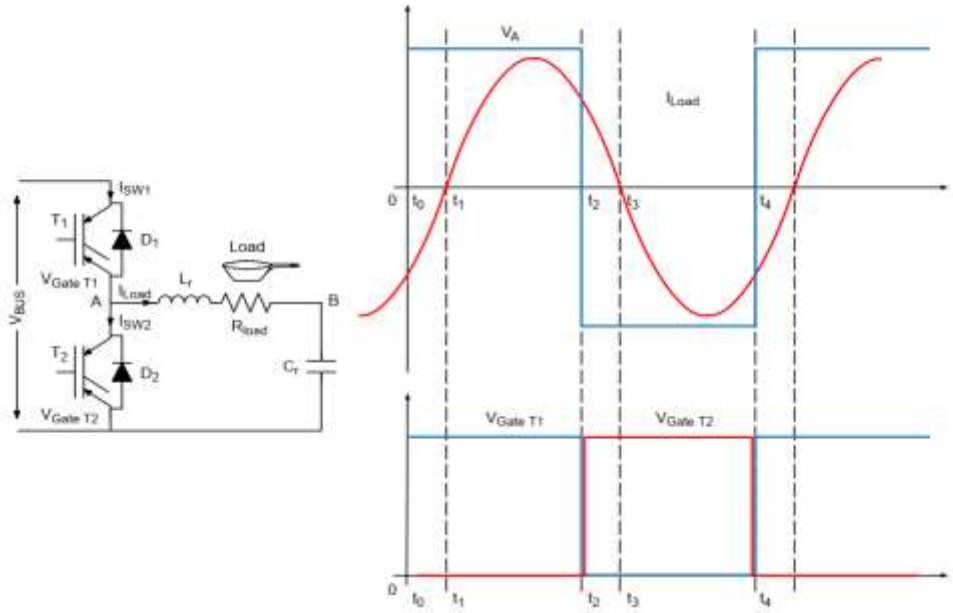

Figure 21 Resonant HB Waveforms [26]

Upper Graph: Load Current (Red) and Voltage at the Central Point A (Blue),

Lower Graph: Gate Voltage for the Higher Side IGBT (Blue) and the Lower Side IGBT (Red)

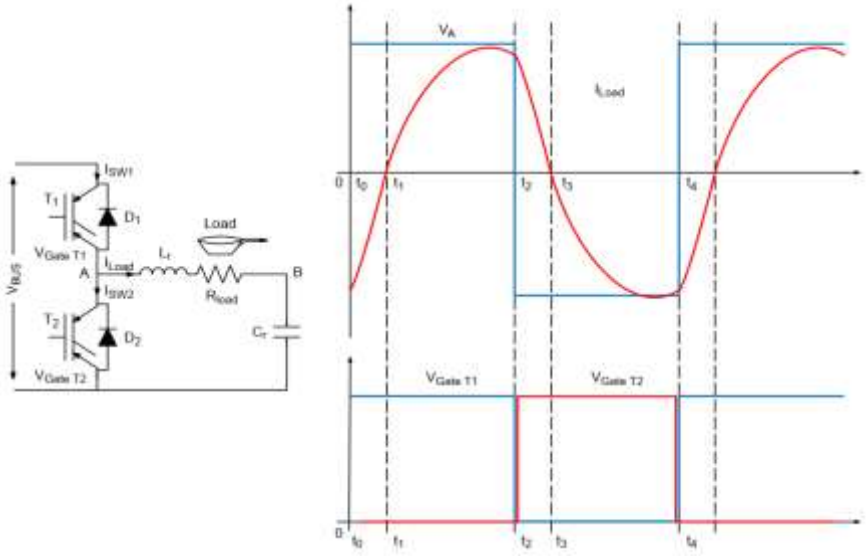

Figure 22 Resonant HB Waveforms for a Switching Frequency > Resonant Frequency [26]

Upper Graph: Load Current (Red) and Voltage at the Central Point A (Blue).

Lower Graph: Gate Voltage for the Higher Side IGBT (Blue) and the Lower Side IGBT (Red)

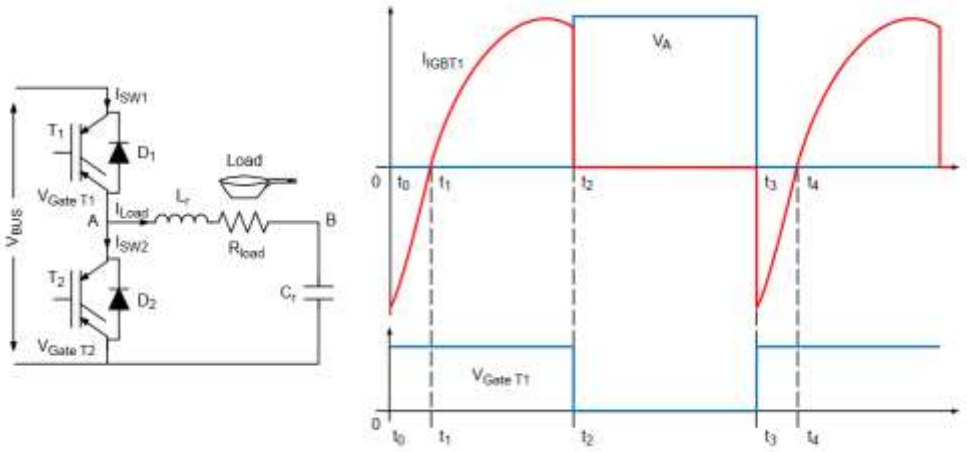

Figure 23 Resonant HB Waveforms for the High Side IGBT T1 [26]

Switching Frequency > Resonant Frequency.

Upper Graph: IGBT1 Current (Red) and Voltage Collector Emitter IGBT1 (Blue).

Lower Graph: Gate Voltage for the Higher Side IGBT (Blue)

Advantages and disadvantages of HBRS for IC

Advantages of the HBSR topology; offering excellent power-conversion efficiency through soft-switching operation, particularly without PWM control. It is easily controllable by adjusting the switching frequency or utilizing a PWM approach. The topology demonstrates high efficiency across all output power levels and allows for the use of 600 V/650 V IGBTs, which provide a favorable trade-off between conduction and switching losses compared to higher voltage operations. Furthermore, switches do not restrict the output power. The main disadvantages of the half-bridge (HB) configuration in relation to the quasi-resonant topology are associated with its increased number of switches, more complex design, higher cost, and larger space requirements [57]. The HB series resonant (HBSR) topology is primarily employed in induction cooking appliances that have multiple cooking zones or when the desired output power per inverter exceeds 2.5 kW. However, due to its higher cost compared to the quasi-resonant topology, the utilization of the half-bridge configuration is primarily limited to high-end models. Some stoves use the other topology. Quasi-resonant (QR) converters [32] are widely utilized as AC power supplies in various applications, including induction heating cooktops and microwave inverters for magnetron power [30]. These converters are particularly attractive for household appliances due to their simple configuration, typically consisting of just one switch (usually an IGBT) and one resonant capacitor

[31]. QR converters strike a good balance between cost and energy conversion efficiency, making them popular for single-burner countertop units in the Asian market [33].

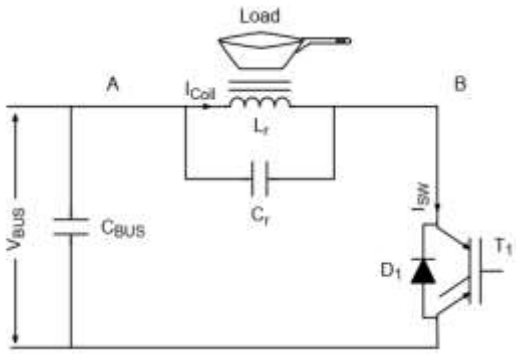

Figure 24 Impedance Module and Phase of the Equivalent HB Resonant Circuit [26]

2.12 Capacitors, Inductors and Transformers in IC

2.12.1 Capacitor

Capacitors are essential components in induction cooking appliances as they are used in the resonant tank circuit of the power converter. The resonant capacitor stores and releases energy, creating an oscillating current that generates a high-frequency magnetic field. Heating is induced due to the eddy currents in the cookware. Capacitors, such as film capacitors and ceramic capacitors, are commonly used in induction cooking appliances due to their high-frequency performance and energy storage capabilities. Film capacitors offer stable capacitance and low losses, while ceramic capacitors are compact and suitable for lower capacitance values. The choice of capacitors depends on design requirements, operating conditions, and cost considerations [1][2].

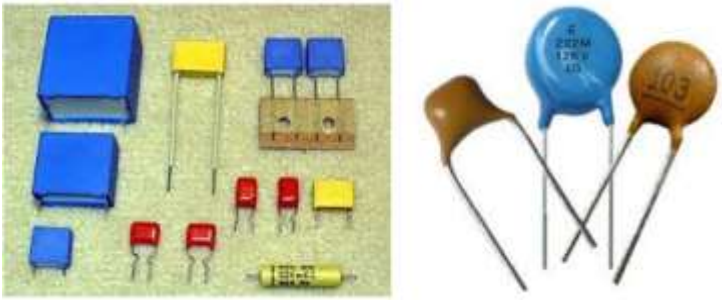

Figure 25 Film and Ceramic Capacitors

2.12.2 Inductor

An inductor is a passive component commonly used in power electronic circuits. Its primary function is to store energy. It stores it in the form of magnetic energy when electrical current flows

through it. One important characteristic of an inductor is its ability to impede any changes in the current flowing through it. Inductors are available in a wide range of values, typically from 1 µH (10^-6 H) to 20 H. Many inductors are constructed with a magnetic core made of materials such as iron or ferrite. This magnetic core enhances the magnetic field and consequently increases the inductance of the component. In the context of induction cooking, inductors are utilized in the form of copper wire coils to generate a high-frequency magnetic field. When an AC pass through these inductors, a rapidly changing magnetic field is created. When ferromagnetic cookware is placed on the cooking surface, the magnetic field induces eddy currents within the base of the cookware. These eddy currents generate resistance, resulting in the heating of the cookware. The heat is then transferred to the food. Inductors in induction cooktops are designed to facilitate efficient and uniform heating. Power electronics are employed to control the heating process, enabling fast and responsive cooking while minimizing energy waste when compared to traditional cooking methods [1].

Figure 26 Inductors used for IC

Figure 27 High Frequency Transformers

2.12.3 Transformers

A transformer is an electrical device that transfers electrical energy between different circuits using electromagnetic induction. It consists of coils of wire, called windings, wrapped around a magnetic core. When an AC passes through the primary winding, it creates a changing magnetic field, which induces a voltage in the secondary winding. Induction cookstoves rely on inductors, not transformers, to generate the high-frequency magnetic field necessary for induction heating. Induction coils, also known as inductors, create a magnetic field when high-frequency AC passes through them. This magnetic field induces eddy currents in the cookware, resulting in heat

generation. Transformers, on the other hand, are primarily used for voltage conversion and are not directly involved in the induction heating process of cookstoves. While transformers may be present in the electrical system of an induction cookstove for voltage regulation or isolation, their main role is not specific to induction heating an example of them is shown on figure 27 [8] [31].

The choice of ferrite cores in induction cookstoves is based on their ability to provide efficient magnetic coupling and concentrate the magnetic field generated by the inductor. By using ferrite cores, energy losses are minimized, and the overall performance of the induction heating process is improved [44].

Chapter Three

3. Methodology

3.1 Introduction

The cooking energy demand profile for Ethiopian household cooking and the design procedures for induction cook stove design powered by solar power are discussed in this section. The study has three basic interdependent steps. Namely; the energy demand assessment for household cooking energy consumption, then the system circuit is developed. Finally, the hardware implementation was conducted. The overall system was evaluated.

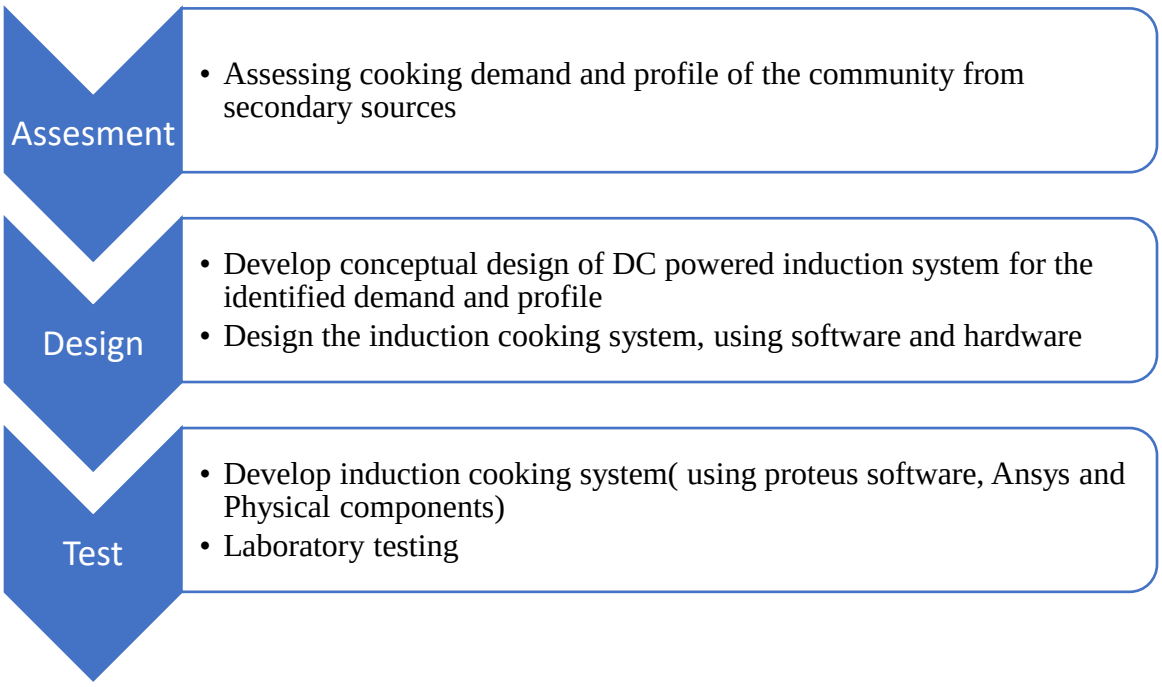

Figure 28 Overall system steps (own development,2023)

3.2 Data Types Used for the Study

For the study, qualitative and quantitative data were used. Secondary data from government research publications and academic research are used for the estimation of household cooking energy consumption and cooking profile. For the design primary data obtained from laboratory tests are used to bind, compare, and evaluate existing research. Each finding is examined and discussed relative to scientific approaches and evaluated to the expected outcomes.

3.3 Cooking Energy Demand Assessment

The assessment was done from secondary sources. The studies were conducted to assess the frequency of cooking, the power consumption, the duration of cooking, and the impact of HH cooking on the power demand in Ethiopia. The following tables are compiled for this study from secondary sources addressed;

a. Family size and cooking hour

The table indicates that for a family of three, five, and ten persons, the daily cooking time was estimated to be 2.9 to 3.3 hours, 3.6 to 4.2 hours, and 4.9 to 5.4 hours respectively.

	Family Size			
No	Meal combination	Three persons	Five persons	Ten persons
1	Tea+ wheat kinche, cracked ater alcha +misir wot and gommen wot	2.9	3.6	4.9
2	Coffee + kolo(barley with chickpeas), meat wot and misir wot	3.4	5.0	5.1
3	Tea + ambasha, misir wot + atkilt wot (mixed vegetable) and nifro (wheat & peas)	3.3	4.2	5.4

Table 1Sample meal combinations and estimated daily time differing family sizes in Injera staple food area [7]

The data provided by the EEU offers a close estimation of the number of electric stoves, as it is based on actual electric energy consumption. Therefore, it serves as a reliable basis for estimating the number of electric stoves in the country.

b. Installed power demand

From secondary sources used for the study and the local electric consumption of cookstoves, it has been determined that the average power demand for the most common electric stove with a diameter of 22cm is 1.4 kW per stove.

No	common stove (diameter 22 cm)	Average Power demand per cook stove (Kw)
1	Single cooktop	1.4
2	Double cooktop	2.8

Table 2 Installed power demand of local electric stoves at the national level in 2009[7]

For the functionality test, Induction cooktops are commonly used for cooking, with power ratings ranging from 500W to 1500W. However, it is important to note that using induction cooktops at power levels exceeding 1200W increases the likelihood of burning food. For the design being discussed, an optimal operating power of 500W is preferred for the induction cooktop. The subsequent sections will delve into the design and optimization of the system.

For the study, a family size of five was assumed and an average of 3.5 hours of cooking time per day was considered. This includes 0.5 hours for breakfast, 1 hour for lunch, and 2 hours for dinner.

The estimated minimum energy consumption for a family of such size is calculated to be 1.2 KW x 3.5 hours/day x 30 days/month = 126 kWh per month.

3.3.1 Design and Sizing of PV System

Appropriate design and sizing are crucial for ensuring good operation, optimal performance, safety, and longevity of a solar PV system. The sizing principles differ for grid-connected systems without energy storage and stand-alone systems with energy storage, as they have different design and functional requirements [37]. Both systems;

a. Grid-Connected Systems; These systems provide supplementary power to facility loads, and the failure of the PV system does not result in a loss of loads.
b. Stand-Alone Systems; These systems are designed for specific loads and work independently to other sources. Stand-alone systems are being chosen for this research to provide energy alternatives that reduce energy wastage and enhance stove operating efficiency.

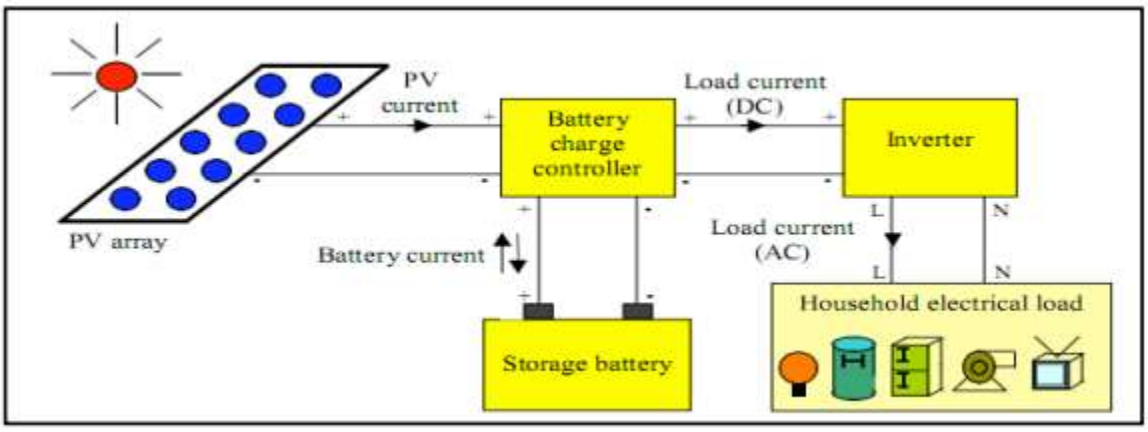

Figure 29 Standalone PV System

For the study to test the functionality of the induction stove, I used a DC power supply which was analogous to the designed solar PV system for the required load. A stand-alone system was employed.

The designed system takes the input of 500 Watts from the PV panel. At night times it can draw energy from the battery storage. In my design, a 12 Volt solar panel is considered.

As discussed in previous sections, 3.5 hours of operation is expected on average family size for household cooking. The energy in watt hours is given by:

E = P×H = 500×3.5 = 1,750 Wh

The battery is required to deliver 1,750 Wh of energy daily. This much energy must be supplied from the Solar PV panel. Regarding this system, $500W_P$ of solar panels will be used.

The battery capacity in the Ampere Hour is given by the following equation [10],

$$C = \left(\frac{\mathrm{E}}{\mathrm{Bv}*\mathrm{DOD}*\eta\mathrm{B}}\right) * (nA) \qquad \text{Eq.17}$$

Where,

Bv = Battery Voltage

E = Energy in Wh

DOD = Depth of Discharge

ηB = Battery Efficiency

nA = Autonomy days

We have BV =12V, E= 1,750 Wh, DOD = 0.8, ηB = 0.8, and nA is days using equation Eq.17 can be calculated as follows;

$$C = \left(\frac{1750\ Wh}{12\ h*0.8*0.8}\right) * (2) = 455.73\ Ah$$

In practice, batteries are typically available in standard capacities, so you would need to choose a battery capacity that is equal to or greater than 455.76 Ah. Common battery capacities include 100 Ah, 200 Ah, 400 Ah, and so on.

The Ah (ampere-hour) capacity of the batteries remains the same when connected in series. When batteries are connected in parallel, the Ah capacity adds up. For example, if three 12V, 150Ah batteries are connected in parallel, the total capacity would be:

Total Capacity = 150Ah + 150Ah + 150Ah = 450Ah

So, in parallel connection, the Ah capacity increases, and the Voltage will remain 12V.

For this study, C (battery capacity) comes out to be 455.73 Ah. The nearest value is 450 Ah. As 12V, 450 Ah these values are not available on the market. Thus, three 12V, 150 Ah batteries in parallel connection can be used to make a 12V, 450Ah battery system.

The system used in the study is shown in the figure below. It consists of a solar PV panel and, a charge controller based on the calculated values of PV Size and Battery Size:

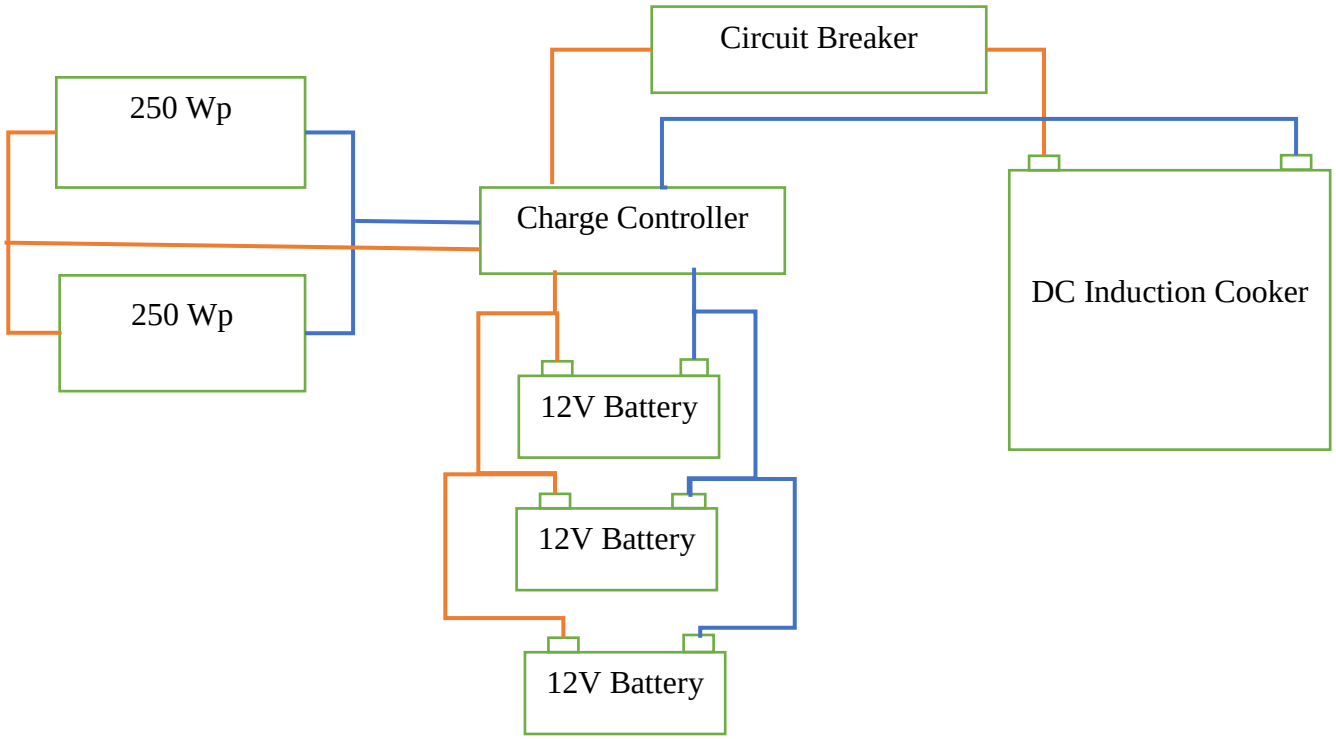

Figure 30 Solar PV system design for IC cooking

3.4 Inverter Design

The block diagram illustrates the key components of a DC-to-AC converter or Inverter.

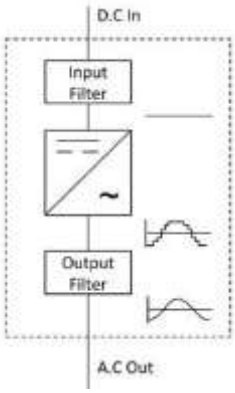

Figure 31 DC-to-AC Converters or Inverter

Inverters are advanced tools that allow the transformation of direct current (DC) electricity into alternating current (AC) electricity, enabling the use of AC-based equipment in systems originally designed for DC power. This ability enables more flexibility and harmony between various kinds of electrical devices.

Various electronic circuits can produce AC (Alternating Current) from DC (Direct Current). Some commonly used circuits are inverters, Oscillators, Multivibrator Circuits, and H-Bridge Circuits. The specific choice of circuit depends on the desired waveform, power requirements, and application needs.

3.4.1 Astable Multivibrator

Astable Multivibrator circuits, which fall under the category of regenerative switching circuits, are widely employed as relaxation oscillators due to their simplicity, reliability, ease of construction, and ability to generate a consistent square wave output. Thus, it was used for the study based on its two states and ability to operate at high frequency.

The Astable Multivibrator is made up of two switching transistors, a feedback network, and two capacitors that introduce time delays. Unlike other circuits, it doesn't have stable output states and doesn't require external triggering. The basic circuit of the Astable Multivibrator uses two transistors connected in a way that creates a square wave output. These transistors, whether NPN or PNP, are biased to work in their linear region and act as Common Emitter Amplifiers with positive feedback.

This configuration allows for oscillation when a certain condition is met. One transistor conducts fully (saturation) while the other turns off completely (cut-off), resulting in strong mutual

amplification between the two. The conduction is transferred from one transistor to the other through the discharge of a capacitor via a resistor, as shown in the diagram.

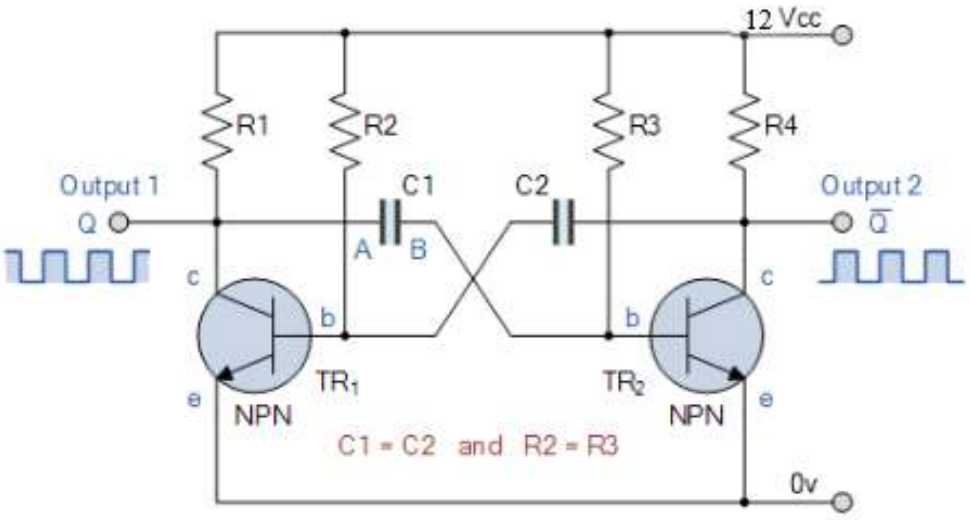

Figure 32 Astable Multivibrator

Initially, transistor TR1 is off, and its collector voltage is rising towards the supply voltage (Vcc). Transistor TR2 is turning on, and capacitor C1's plate A is also rising towards Vcc since it is connected to TR1's collector. Plate B of capacitor C1 is connected to TR2's base, which is at 0.6V because TR2 is conducting. So, there is a potential difference of +11.4V across the plates of C1 (from point A to point B). When TR2 is fully on, capacitor C2 starts charging through resistor R2 towards Vcc. When the voltage across C2 exceeds 0.6V, it biases TR1 into conduction and saturation. When TR1 switches on, plate A of C1 immediately falls to 0.6V, causing an equal and immediate fall in voltage on plate B. Plate B now becomes -11.4V, which turns TR2 off. Now, TR2 is in the cut-off, and capacitor C1 charges in the opposite direction through resistor R3, connected to Vcc. This causes the base of TR2 to move positively towards Vcc with a specific time constant.

Once the base voltage of TR2 reaches 0.6V, TR2 turns fully on, starting the process again with C2 charging and TR1 entering the second unstable state. The circuit alternates between these two unstable states, with TR1 and TR2 switching on and off at a rate determined by the RC values.

The output waveform has an amplitude similar to the supply voltage (Vcc) and appears as a square wave with slightly rounded corners due to the current charging the capacitors.

This alternating process continues as long as the supply voltage is present. If the two-time constants produced by C2 x R2 and C1 x R3 in the base circuits are the same, the mark-to-space ratio (t1/t2) will be equal to one-to-one making the output waveform symmetrical in shape. By varying the capacitors, C1, C2, or the resistors, R2, R3 the mark-to-space ratio and therefore the frequency can be altered.

$T = t_1 + t_2$ Eq.18

$t_1 = 0.693\ R_3C_1$ Eq.19

$t_2 = 0.693\ R_2C_2$ Eq.20

Where R is in Ω's and C in Farads.

By adjusting the time constant of a single RC network, we can change the ratio and frequency of the output waveform. However, if we want to change the output frequency while keeping the ratio between the high and low states the same, we need to modify both RC time constants simultaneously.

If the values of capacitor C1 and C2 are equal (C1 = C2), and the values of base resistors R2 and R3 are also equal (R2 = R3), then we can determine the total duration of one cycle of the multivibrator for a symmetrical output waveform.

3.4.2 Frequency of Oscillation

$$f = \frac{1}{T}$$ Eq. 21

Where; R represents resistance in ohms (Ω), C represents capacitance in farads (F), T represents time in seconds, and *f* represents frequency in hertz (Hz), the Astable Multivibrator has a parameter called the "Pulse Repetition Frequency." This frequency determines how often the multivibrator generates short square wave output waveforms from each transistor.

Depending on the time constant of the RC network, the Astable Multivibrator can produce either two very short square wave output waveforms from each transistor or a longer rectangular-shaped output waveform. This output waveform can be symmetrical or non-symmetrical, depending on the characteristics of the RC network.

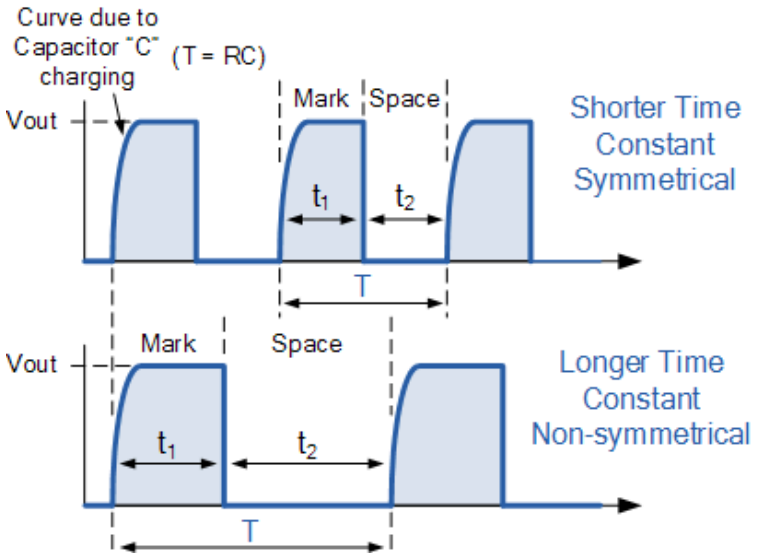

Figure 33 Frequency of Astable Multivibrator

3.4.3 IGBT vs. FET

IGBTs are the preferred switching devices due to their ability to handle high currents, high voltages, and block reverse conduction. However, these devices have limitations in terms of their maximum operating frequency, typically restricted to the kHz range, and tend to have higher conduction losses at low voltages compared to FETs.

In induction cookers, MOSFETs are often avoided because they cannot withstand the extreme voltages and currents associated with series resonant designs. Nevertheless, MOSFETs offer advantages such as higher switching speeds and lower conduction losses at low currents. It is important to note that MOSFETs cannot block reverse conduction, but in my design, I have implemented voltage and current limitations, with voltages below 100V and currents below 5A.

This design diverges significantly from series resonant converters, which often require components capable of withstanding hundreds of volts and hundreds of amps. To prevent current backflow, Zener diodes have been employed. Specifically, a PN2222a IGBT is utilized to generate a 50kHz square wave from a 12V direct solar panel. Subsequently, an IRF740 is employed to convert this signal into a higher frequency for driving the magnetic field around the pancake coil. Given a fixed switching frequency and a predetermined capacitor size, the inductor dimensions are entirely constrained and chosen using the half-bridge formula.

3.4.4 Inverter (Half Bridge) Components calculation

Induction cooking systems typically operate at high frequencies, ranging from a few kilohertz (kHz) to several tens of kilohertz (kHz). The choice of switching frequency and resonant frequency is crucial for achieving efficient magnetic field generation and optimal performance.

In general, the switching frequency is selected to be higher than the resonant frequency in an induction cooking system. Here's why:

1.Switching Frequency: The switching frequency determines how quickly the power switches (transistors or IGBTs) in the circuit turn on and off. A higher switching frequency allows for faster power delivery and more precise control of the power delivered to the induction coil. It also helps reduce energy losses and improve overall system efficiency.

2. Resonant Frequency: The resonant frequency is the natural frequency at which the LC circuit formed by the induction coil (L) and the capacitor (C) connected in parallel resonates. Resonance occurs when the inductive and capacitive components of the circuit are in balance, resulting in efficient energy transfer and magnetic field generation.

To achieve better magnetic field generation and efficient energy transfer, the switching frequency is typically set higher than the resonant frequency. This approach allows the system to take advantage of the resonant behavior and efficiently transfer energy to the induction coil.

Ideally, the resonant frequency and switching frequency should be as close as possible to maximize the efficiency and effectiveness of the system. A smaller difference between these frequencies allows for better energy transfer, more stable magnetic field generation, and improved heating performance.

In practice, the acceptable difference between the resonant frequency and switching frequency can vary, but it is generally recommended to keep it within a few kilohertz (kHz) or less. A commonly used guideline is to aim for a difference of around 1-5 kHz. However, this can vary depending on the specific design and requirements of the induction cooking system.

For this study, 3 kHz difference is selected.

$$f_r = f_o - 3kHz \quad \text{Eq.22}$$

where; Operating frequency (f_o) is 50kHz and resonant frequency (f_r)

3.4.5 Heating Coil Selection

When designing a domestic induction system, it is important to consider the type of wire used in the inductor to minimize self-losses. Various copper wire profiles have been employed for domestic inductors over time, including foils or tapes [35]-[36], round wires [37], and multi-stranded wires. Multi-stranded wires are further classified into litz wires, constructed with careful strand-transposition patterns and having tens of strands [38]-[39], and twisted wires, which involve simply twisted or bunched strands and can comprise thousands of fine strands [41]-[42].

A schematic representation in the figure below illustrates the comparative cost of an inductor wound with each type of wire.

Currently, litz wires are widely utilized due to their favorable cost-performance ratio. Additionally, the number of strands and the diameter of the cable can be customized to optimize η_{ind} (inductor efficiency) at a specific operating frequency [31].

The efficiency of the heating system, η_{ind} is the ratio of the power transferred to the load, P_l to the total power supplied, P_t, that is

$$\eta_{ind} = \left(\frac{Pl}{Pt}\right) = \left(\frac{Pl}{pl+pw}\right) \qquad \text{Eq.23}$$

Where;

P_w represents the power dissipated in the windings, which causes a non-desirable warming up of the inductor. Therefore, two ways could be followed to improve η_{ind}: improving P_l; on the other hand, reducing P_w with an adequate yarn design.

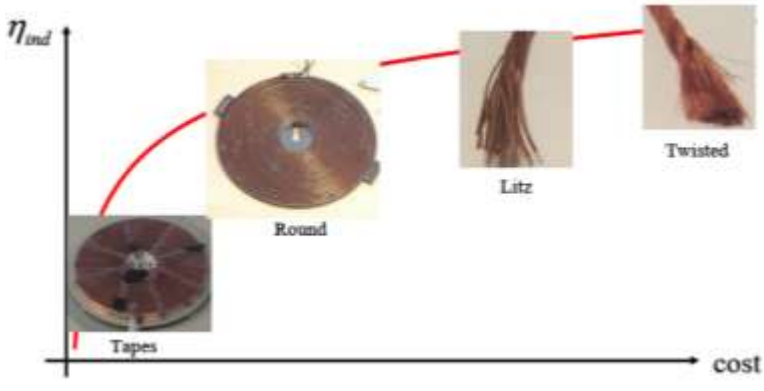

Figure 34 Schematic cost-efficiency representation for an inductor wound with [37]

Litz Copper Wire offers advantages over Solid Copper Wire for induction cooking applications. It has lower resistance, reduced inductance, improved skin depth, and similar magnetic field generation capabilities. These characteristics contribute to more efficient heating, faster response times, improved control of the magnetic field, and overall enhanced performance in induction cooking systems

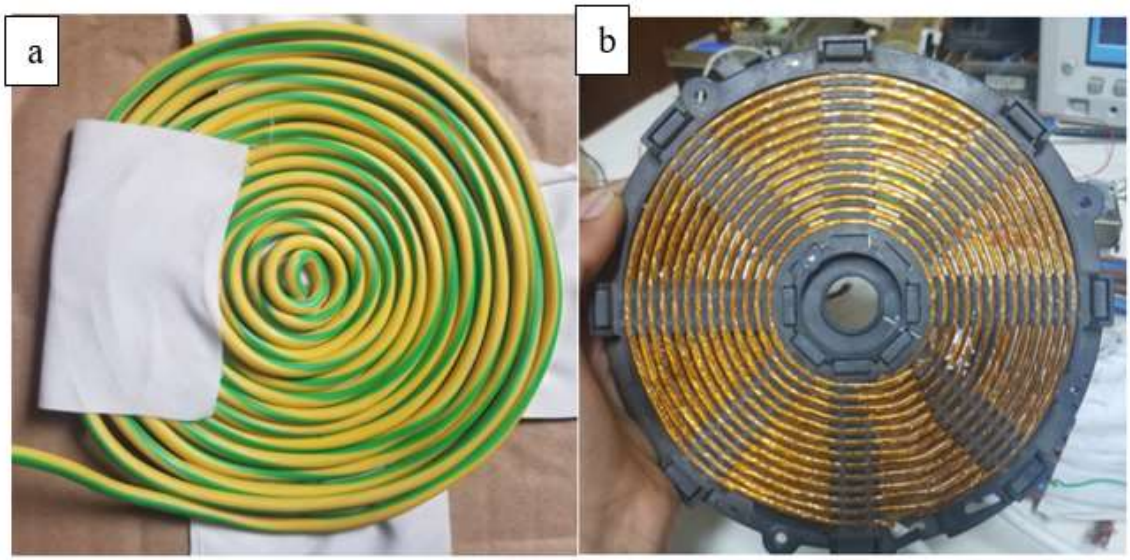

Figure 35 a. Solid copper wire b. Twisted copper wire (captured by Meron)

For the study, a pancake coil of 9 turn with 3mm diameter wire which was made of 50 strands was used as a pan and for comparison with a standard copper induction cooking litz wire. The former has 6 cm diameter and the cooking coil has a 12cm diameter.

Comprising the astable multivariate, inverter topology ang cooking coil a step by step design was as follows;

For a family size of five and an average of 3.5 hours of cooking time per day was considered. Including 0.5 hours for breakfast, 1 hour for lunch, and 2 hours for dinner.

The minimum energy consumption for a family of such size is 1.2 KW x 3.5 hours/day x 30 days/month = 126 kWh per month.

A battery capacity of 450 Ah was used. Thus, three 12V, 150 Ah batteries in parallel connection can be used for a 12V, 450Ah battery system.

In place of solar PV panels, this study used a DC power generator for the laboratory experiments. It can generate a maximum of 30 volts. The input current can vary based on the load connected to the circuit. The device makes the experiments to be safe, and controllable and helps to examine the various output characteristics of the design for different input and load values.

Typical induction cookers operate at switching frequencies between 25 kHz and 50 kHz. For this thesis, 50 kHz is chosen to generate the maximum magnetic field around the working coil.

The input Voltage is 12 V DC and the expected output frequency of the square wave output at both collectors of the IGBT is 50 kHz. Then the period will be, $= \frac{1}{50\ \mathrm{khz}} = 2 * 10^{-5}\ s$

By reciprocating the equation of frequency, a period, since both the mark and space are equal (50% Duty cycle);

$t_1 = t_2 = \frac{T}{2}$, the result will be 10^{-5} seconds

To get the values for the R_2, R_3, C_1 and C_2 based on the characteristics of the astable multivibrator. They must be balanced.

Thus, $R_2 = R_3 = R$ and $C_1 = C_2 = C$

$t_1 = t_2 = 0.693 * R * C$

The value of R is chosen to be 10K ohm. It is selected with a high ohmic value to reduce the size of the capacitor. The capacitor will be,

$$C = \frac{10^{-5}\ sec}{0.693 * 10{,}000\ \mathrm{ohm}} = 1.44\ \mathrm{nF}$$

For R_1 and R_4 a value of 470 Ohm is assigned.

Name	Value
R_1	470 Ω
R_2	10 KΩ
R_3	10 K Ω
R_4	470 Ω
C_1	1.44 nF

C_2	1.44 nF
IGBT	PN2222

Table 3 Components of Astable multivibrator

For the selection of Operating frequency (f_o) is 50kHz, thus the resonant frequency (f_r) becomes;

$f_r = f_o$ - 3kHz = 50kHz - 3kHz

fr = 47 kHz

It is important to note that the specific requirements and constraints of your induction cook stove design, such as power levels, size, cost, and targeted efficiency, will influence the choice between ZCS and ZVS.

Calculating the L and C values;

Since the cooking coil used for the laboratory experiment has 110uH the same inductance value is considered in the simulation.

Lr = 110μH

$f_{res} = \frac{1}{2*\pi*\sqrt{Lr*Cr}}$ and $\omega_{res} = \frac{1}{\sqrt{Lr*Cr}}$

f_{res} = 47kHz, L=110uH

$Cr = \frac{1}{(2\pi f r^2)L} = \frac{1}{(2\pi*47khz)^2 110\mu H}$

Cr= 1.043 x 10^{-7}, F = 104.3nH

Thus, L= 110μH and C= 104.3nF

In summary, Litz Copper Wire offers advantages over Solid Copper Wire for induction cooking applications. It has lower resistance, reduced inductance, improved skin depth, and similar magnetic field generation capabilities. These characteristics contribute to more efficient heating, faster response times, improved control of the magnetic field, and overall enhanced performance in induction cooking systems.

3.4.6 Conceptual System Integration

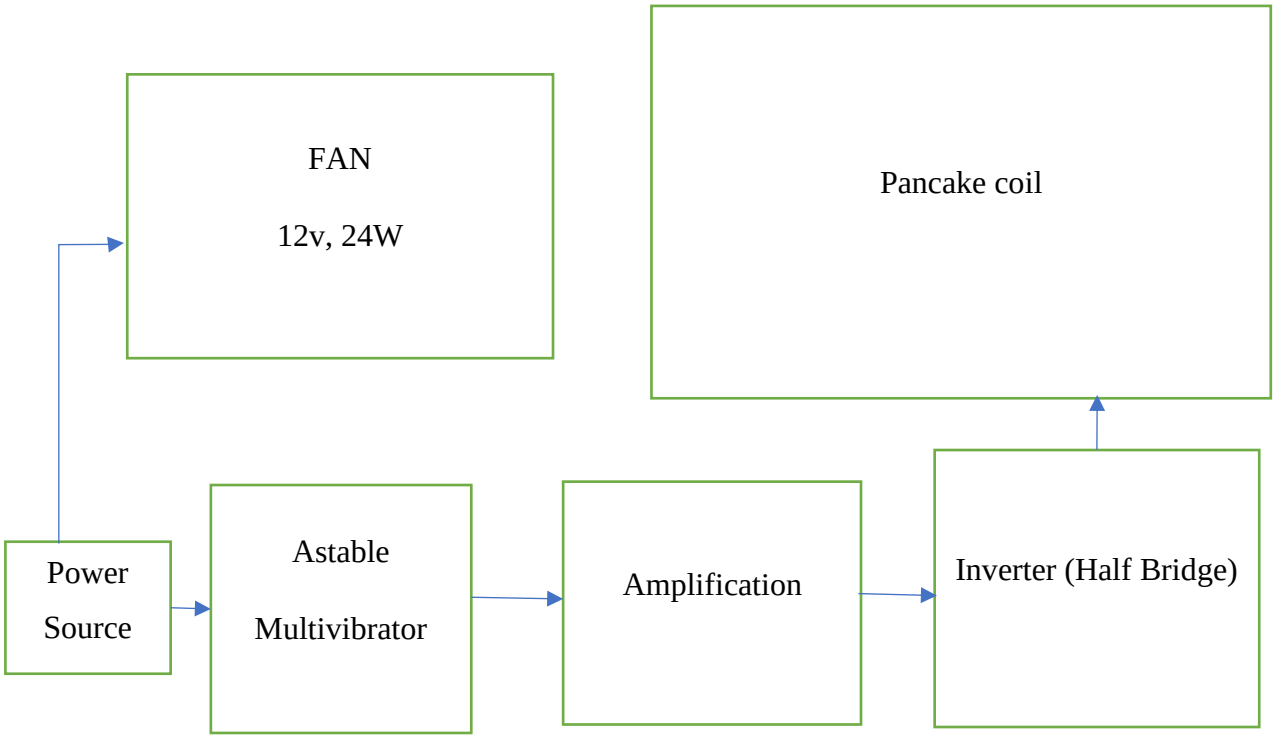

Figure 36 Conceptual system design (own development)

The system design illustrates the power flow from the source to the load, where the power source energizes various electronic components within the circuit. It powers both the fan and the astable multivibrator, as well as the inverter and the amplification part of the transformer.

To begin, the fan operates with a 12V DC source, capable of delivering 2.4 watts of power. In parallel, the panel supplies voltage to the multivibrator. The multivibrator generates a high-frequency square wave, which is then amplified using a ferrite transformer. The amplified signal is subsequently fed into the half-bridge inverter. In this configuration, the inductor within the half-bridge functions as the primary winding of a transformer, while the iron bar placed atop acts as a representation of a pan.

Overall, this system design effectively demonstrates the power flow and the specific roles of each component, enabling the conversion of power from the source to the load while incorporating the necessary amplification and inverter mechanisms.

3.5 Circuits design on proteus software

Using the calculated values obtained in from basing the operating principles of the half bridge on section 2.11.1 and multivibrator operation at section 3.4.1 the following circuits were designed on Proteus 8 software.

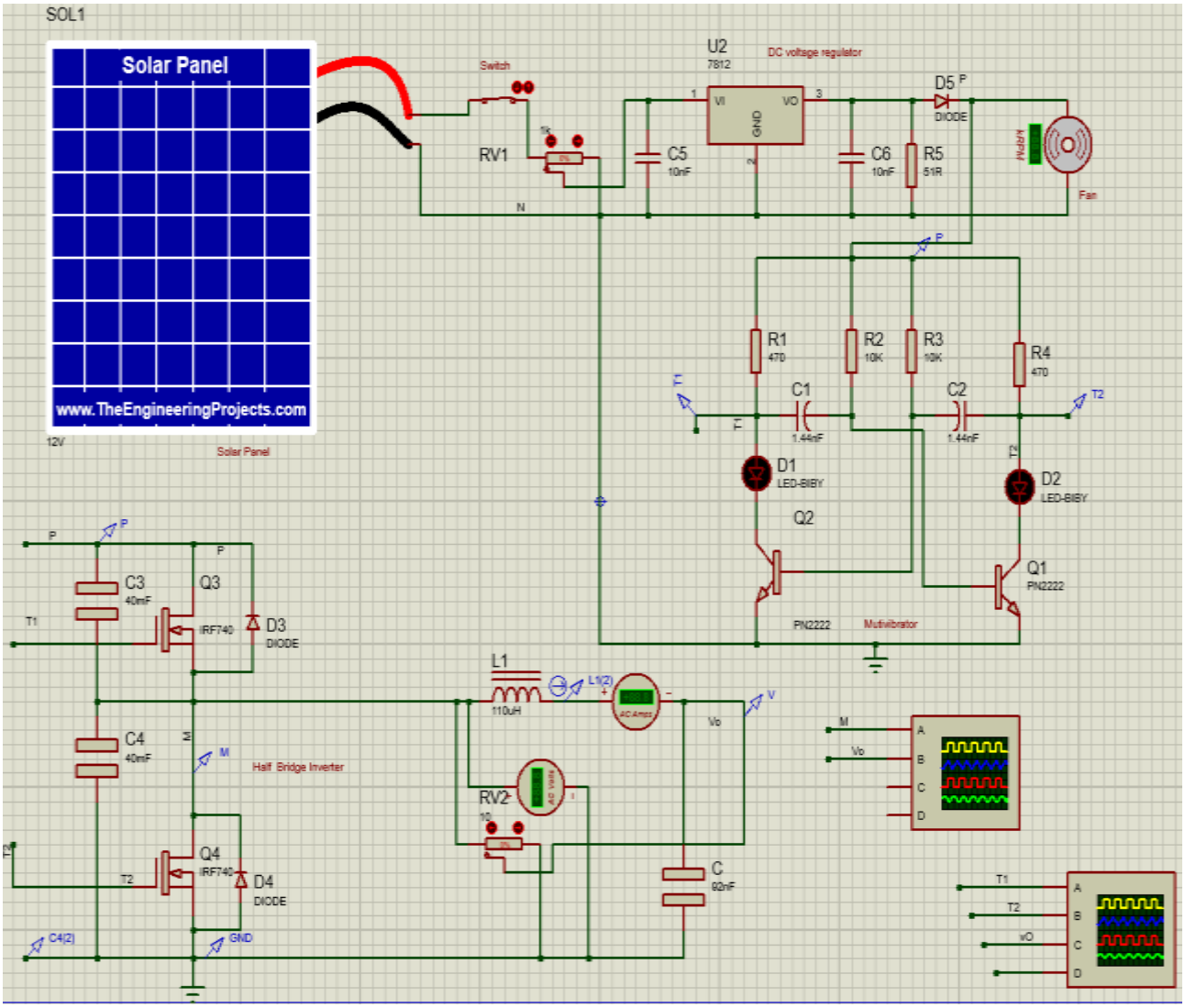

Figure 37 The system design at Proteus software (own design 2023)

A 12V solar PV is used to derive the circuit. A 2.4-watt DC is used for regulating the temperature of the electronic components as the high-frequency operation on the MOSFET and transistor induces heat. They are attached to a heat sink to maintain their temperature.

A switch is attached to the PV source to control the current flow and the diode next to the switch is placed to prevent a backflow of current and maintain the unidirectional flow of the circuit.

On the half bridge circuit C3 and C4 values were obtained by using variable capacitors. Their values were altered until a suitable waveform on the output was obtained.

3.6 Laboratory circuit development and testing

The laboratory setup for the physical implementation was established in the Electrical Lab within the AAiT compound. The experiment utilized various materials and equipment, including a functional signal generator, DC power supply, multimeter, AC power supply, oscilloscope, and PV panel. The main electrical components employed in the study encompassed resistors, capacitors, diodes, inductors, DC fans, LEDs, conductive wire, potentiometers, MOSFETs, variable resistors and capacitors, transformers, and push buttons.

For The laboratory experiments DC power supply was used as a solar PV source. The signal generator is used to generate different waveforms and supply them to the circuit whenever needed. The Oscilloscope for signal waveform observation, frequency, and voltage reading.

The primary objective of the study was to design a specific circuit through a step-by-step development and testing process. Initially, the solar PV system was designed to accommodate the load. Subsequently, the circuit components for the system were designed, followed by a systematic testing procedure.

The circuits were developed and tested using Proteus software, and the resulting outputs were recorded. The accompanying sections include pictorial diagrams and detailed results for reference. Overall, the study employed a comprehensive laboratory setup, utilizing a range of electrical equipment and components to design and test the target circuit. The progression from designing the solar PV system to developing and testing the circuit components was carried out systematically, with the aid of simulation software and careful documentation of the physical components.

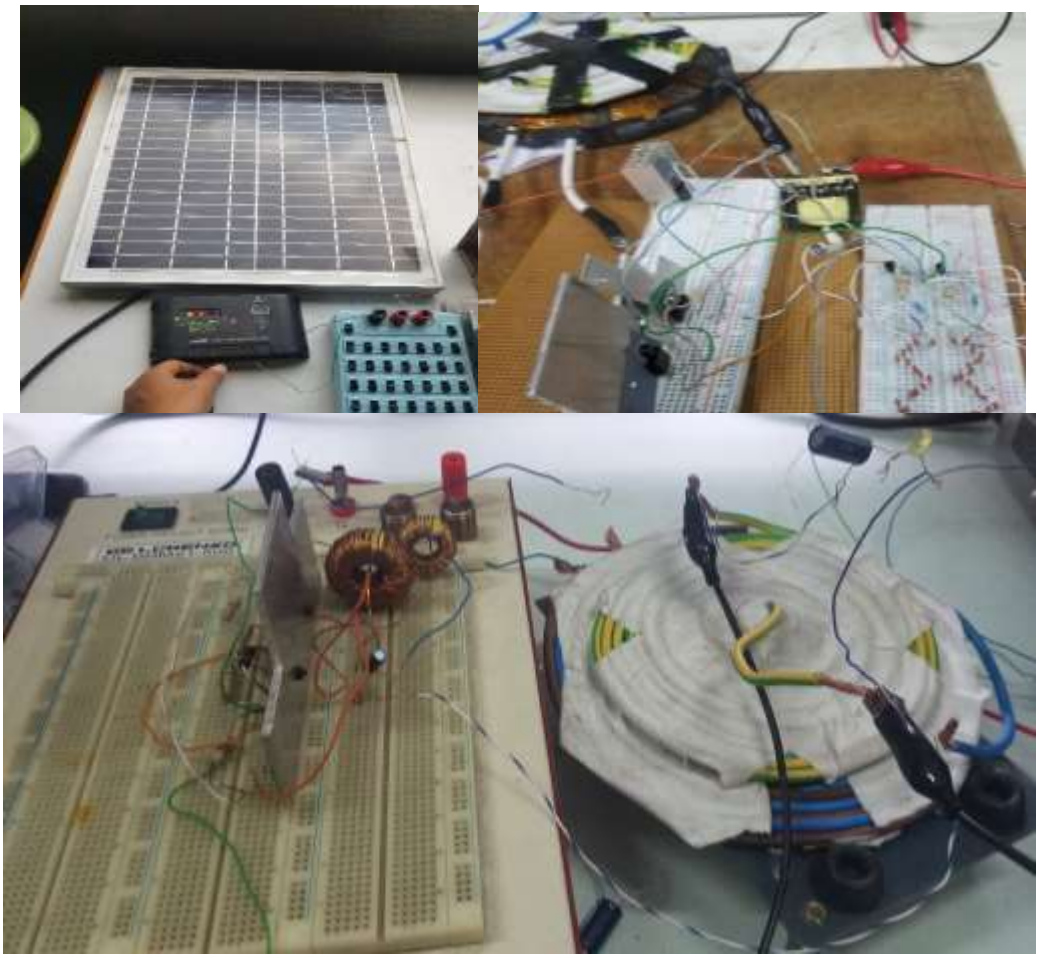

Figure 38 Circuits at Laboratory (own development 2023)

3.7 Cooking coil and Cooking pan 3D design and simulation by AEDT

ANSYS Electronics Desktop Student is an educational software tool that enables students to design, simulate, and analyze electronic circuits and electromagnetic systems. It has applications in circuit design, signal integrity analysis, electromagnetic field simulation, RF and microwave design, electromechanical systems, and thermal analysis. It provides a comprehensive set of simulation capabilities to help students gain hands-on experience and solve engineering challenges in various industries.

AEDT is used to observe the magnetic field effect of the cooking coil on the cooking pan. A mirror with a thickness of 0.25mm was placed between the two conductive components to resemble the real-world scenario to prevent damage to the coil and any leakage from the pan and for ease of cleaning. The ohmic loss, inductance, and capacitance of the two objects were assessed at different

Current and frequency values. The 3D model of the system dimension and the diagram is presented below;

The cooking pan has a thickness of 0.25mm and the coil has 10 turns and 7cm diameter. The building material of the pan is cast iron, the cooking coil is from stranded copper wire, and the insulator is made of mirror. The selected colors for the 3D models are; silver for a pan, the cooking copper coil in brown, and the mirror in gray. A region or domain for ANSYS Electronic Desktop for simulation to specify and define the physical space or area where the simulation will take place. This is particularly important in electronic simulations because it allows us to accurately model and analyze the behavior of the electronic components within a specific region or geometry. The box shown in the picture below is used as a domain for the system.

The coil size is selected based on the induction cook stove used in the laboratory assessment. The size of the mirror and pan are influenced by the AEDT mesh limits of the software. ANSYS Student license is limited to 512K cells/nodes for a CFD model. A full license has no such limitation. As I had the free license I was forced to reduce the size. During the laboratory assessment, the selection of the coil size for the induction cook stove was based on certain considerations. Similarly, the size of the mirror and pan used in the assessment was influenced by the mesh limits of the AEDT software.

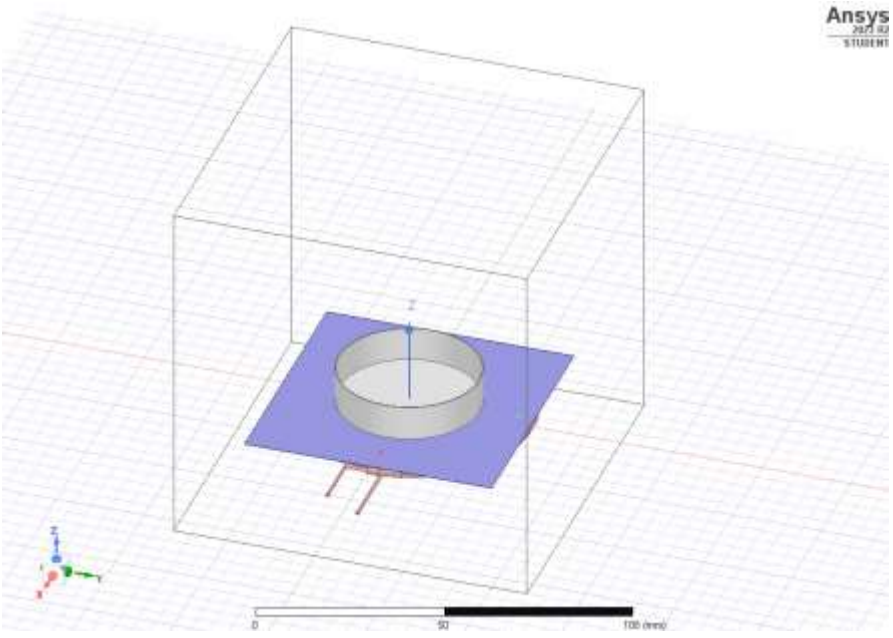

Figure 39 3D model of the system(own design 2023)

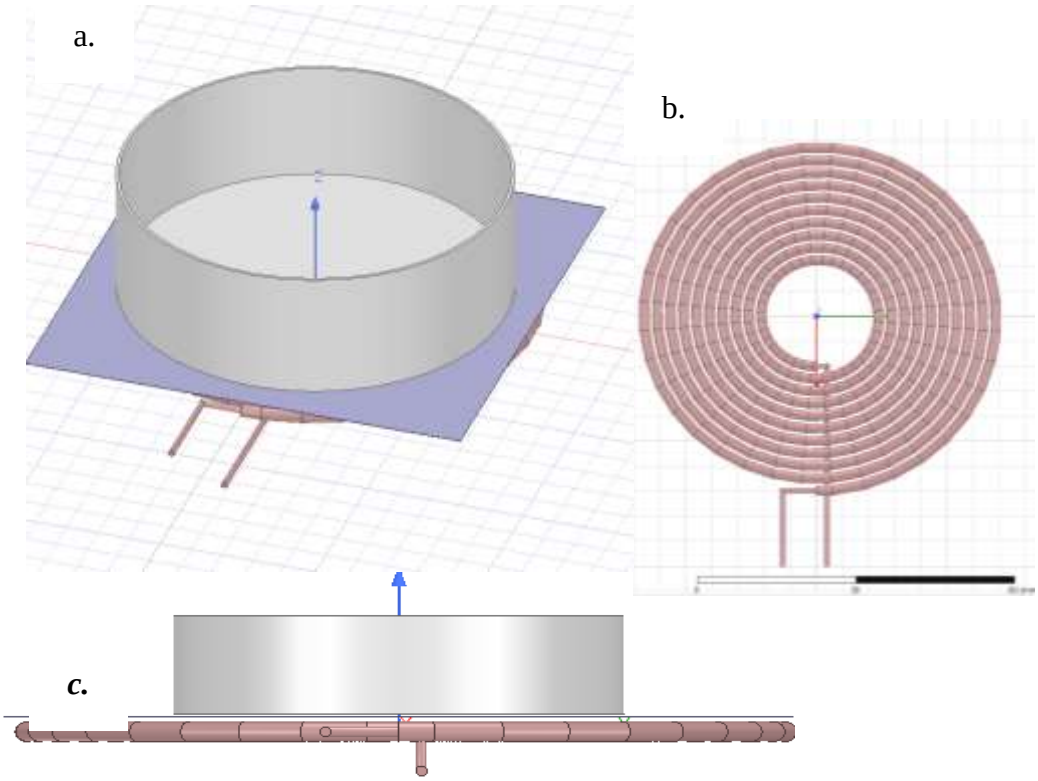

Figure 40 a. Isometric view of the system; b. The spiral coil; C. Front view of the design

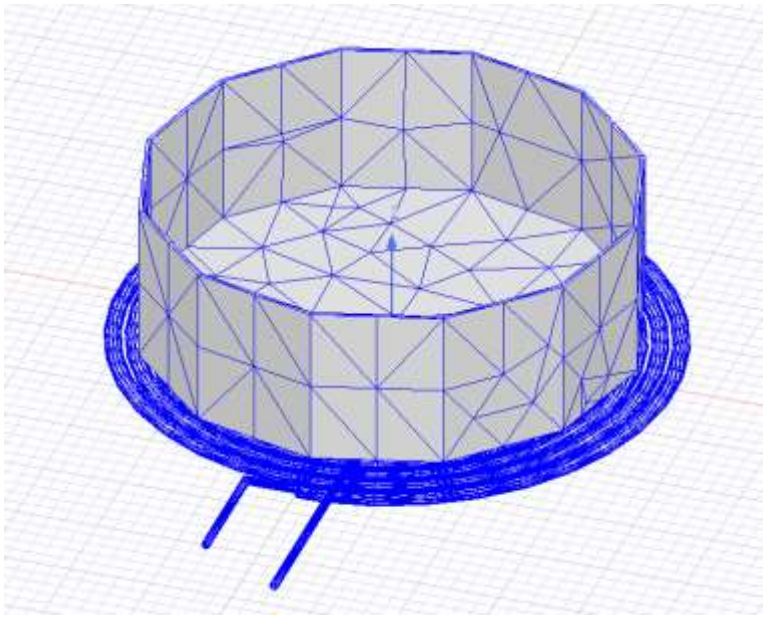

Figure 41 The mesh diagram of the 3Dmodel

	Pan	Coil (PolygonHelix1)	Mirror	Box
Volume	4728.096944mm^3	4491.738049mm^3	245mm^3	1000000mm^3
Area	13259.09179mm^2	9092.233387mm^2	9814mm^2	60000mm^2
No. of Lumps	1	1	1	1
No. of Shells	1	1	1	1
No. of Faces	5	371	6	6
No. of Loops	8	739	6	6
No. of Edges	4	371	12	12
No. of Co Edges	8	742	24	24
No. of Vertices		2	8	8

Table 4 Design specifications

It is worth noting that the ANSYS Student license has a limitation of 512K cells/nodes for a Computational Fluid Dynamics (CFD) model. This means that the complexity and size of the simulation are restricted by this limitation. In contrast, a full license does not have such limitations, allowing for more extensive and detailed simulations. Since the free license was used, it was compelled to reduce the size of the simulation to comply with the licensing restrictions. This size reduction was necessary to ensure that the simulation could be carried out within the limitations imposed by the license.

It is important to work within the constraints of the software license and adjust the simulation parameters accordingly. Despite the limitations, i was able to conduct a meaningful assessment by adapting the size to fit within the available computational resources provided by the free license. Regarding the mesh operation selection for the pan, cooking oil, and mirror the selection with length-based meshing was selected. For the box inside selection was chosen. The values were 16.9mm, 14 mm, 14 mm and 20 mm respectively.

Chapter Four

4. Results and Discussion

This chapter presents the conclusive results of all analyses conducted in this thesis and provides interpretations of the obtained results. The research aimed to evaluate the outcomes of each software and laboratory implementation. By configuring the circuits with the calculated electronic component values, they generated the output graphs discussed in the following sections.

4.1 Proteus simulation results

1. Transistors output, T1 and T2

The astable multivibrator works nicely and it generates the desired frequency for the design. However, the software is unable to show the high frequency thus the R and C values are reduced to assess the visual output and it resulted in the following graph output for T1. In Yellow and T2 in blue. Both will have opposite rise and fall times but have the same period and peak voltage.

This process is essential for the next step to switch on and off the MOSFET in half-bride circuits. The higher the frequency is the better the magnetic field. Voltage at T1 and Voltage at T2 have similar wave shapes with 180-degree phase shifts. When T1 is on T2 gets off and when T2 is on t1 is off. The voltage value yields a maximum of 11.2 Volts. Switching frequency = 50 kHz

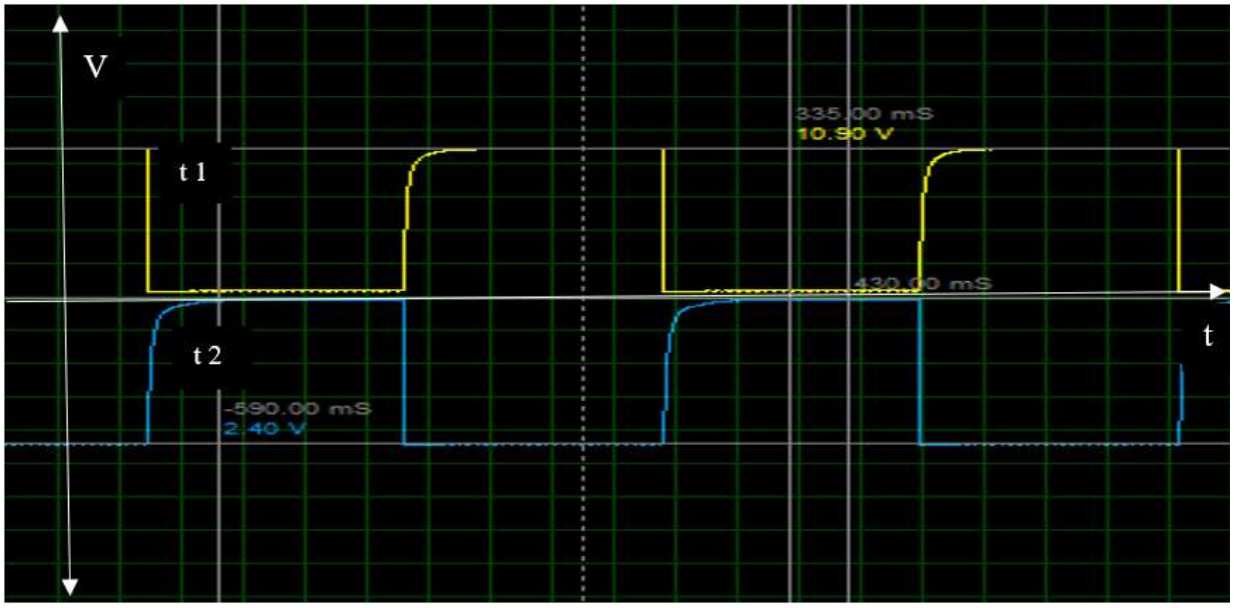

Figure 42 Output of T1 and T2

2. Amplification stage

Ferrite transformers are not available in the market. Thus, I was forced to reuse from other electronic devices and due to the fracture of the core in the process of recycling the desired value of voltage and current was unable to be obtained. However, by using an EE-33-38T transformer from UPS I get an output up to 105 Vpp (35 V) as shown in figure 45. It operates well but the design of the winding is for LED driving only due to low voltage and current rating.

Using a 12-0-12 Center tapped transformer a high voltage with very little current reading was obtained. The value was affected by the input voltage. By a 5V DC source maximum of 238V was reached but the current was too small and was unable to create the required magnetic field.

For amplification, many transformers are tested as well, but they fail to amplify due to the high-frequency operation of the system. I have checked 3 different step-down transformers for stepping-up purposes if they will help to amplify the developed circuit. However, the amplification was inconsistent and unreliable. Thus, the reason for not using non-ferrite core transformers was understood.

Ferrite core transformers are not available in the Ethiopian market thus I tried to find them from boards of UPS and other appliances. I got two and they got damaged during the dismantling, boiling, and drying processes. The safe one was EE-33 and I connected it to the half-bridge circuit to examine the impact on the cooking coil.

To get the expected amplification, I used the ferrite winding calculation EXCEL form and

EI33 size (unit: mm) of high-frequency transformer Specification:

Input: AC 110-120V/220-240V, 50 - 60Hz

Output: AC 3.0- 36V 100-2500mA

Power range 10W-10kw

During the design phase, the type of wire utilized for the primary and secondary windings of a transformer can be different. Usually, the primary winding is intended to withstand higher voltages and lower currents, and the secondary winding is intended for lower voltages and higher currents. The main purpose of the primary winding is to receive the input voltage and transfer energy to the

secondary winding. Typically, the wire used for winding is covered with insulation that has a higher voltage rating so that it can effectively withstand the potentially elevated voltages found in the primary circuit.

The role of the secondary winding, however, is to transmit the converted output voltage to the load. The wire used in the winding is specifically designed to handle higher levels of current, as the secondary winding typically carries more current than the primary winding. In this depiction, the main wire has a diameter of 0.5mm while the secondary coil has a diameter of 2mm.

Ferrite Transformer Turns Calculation

Npri = Vin * 10^8 / (4 * F * Bmax * Ae)

Bmax = Vin*10^8 / (4 * F * Npri * Ae)

Vin =	5.00	Volt	Bmax CHECKING			
F =	50.00	Khz	Npri =	2.00	Turn	
Ae =	0.79	Cm²	Bmax =	1592.36	G	
Bmax =	1592.36	G	Bmax from 1200 to 2000			
Npri =	2.00	Turn	Volt per 1 turn =	2.50	Volt	
WIRE						
Vout =	110.00	Volt	Nsec =	44.00	Turn	
Iout =	5.00	A	Sec Wire =	2.00	mm	
P =	550.00	W	Pri Wire =	0.50	mm	
Iin =	110.00	A	Current density =	5.00	A/mm²	
RESULT OF TRANSFORMER WINDING						
V in =	5.00	V	Npri =	2.00	Turn	
I in =	110.00	A	Nsec =	44.00	Turn	
V out =	110.00	V	P =	550.00	W	
I out =	5.00	A	Volt/Turn =	2.50	V/T	
F =	50.00	Khz	Diameter Wire Sec =	2.00	mm	
Ae =	0.79	Cm²	Diameter Wire Pri =	0.50	mm	
LIZT WIRE FROM WIRE YOU HAVE AT HOME						
Second	2.00	mm	Lizt wire	2	mm X	1
Pri	0.50	mm	Lizt wire	0.5	mm X	44

Figure 43 Ferrite core turns calculation (source: From Excel calculation template online)

From the result, the primary winding is made of 0.5mm diameter from 44 similar wires.

Wire D * Turn

Np = 0.5mm, 44 strands and 2 turn

Ns1= 2mm, Solid wire with 44 turns

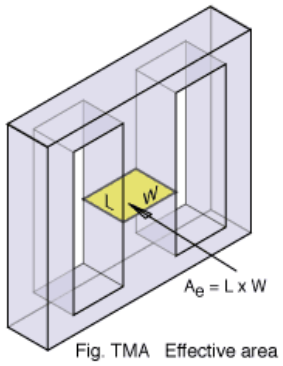

Figure 44 Effective area of the ferrite core

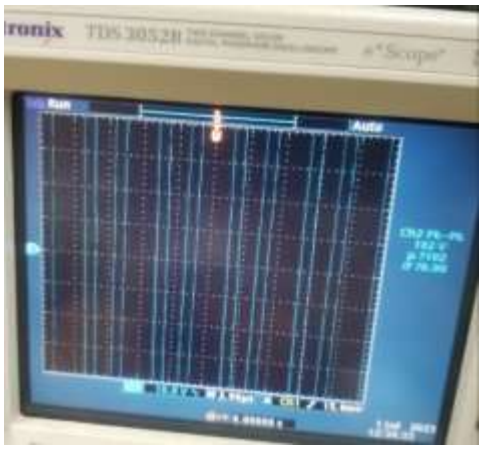

Figure 45 output using EE-33, 105 Vpp

The appropriate winding development will help to get the voltage and current values of the design would be met. To wind the first transformer, the copper wire was wrapped around the core, ensuring that the three parts of the transformer were properly isolated. To facilitate the removal of insulation and windings, the transformer was boiled. Afterward, the separated parts were cleaned and removed the winding and other components. For any remaining insulation, a hot gun was used for removal.

However, during the process, the core of the transformer developed cracks due to its age and temperature variations. As a result, it was unable to wind the copper wire as intended for the desired application. Consequently, the researcher did not attempt to remove the windings from the second transformer. Instead, its ability to function solely based on its existing winding was observed. For further testing was no suitable replacement for the transformer on the market.

The challenges with the first transformer highlight the importance of working with well-maintained equipment and considering the limitations of older components. Despite the setback, the assessment of the second transformer provided insights into its standalone performance.

The used transformer was designed for low-frequency application, but the ferrite structure has tolerated the high-frequency flow without any problem relative to the other tested center-tapped transformers.

Figure 46 Different transformers checked for the amplification

Figure 47 Ferrite transformer Dismantling

3. Half Bridge Inverter

The two outputs of the astable multivibrator was used to control the on/off characters of the MOSFET in the half-bridge at high frequency. The same DC value of 12 V was provided to the drain of the top MOSFET and the bottom connected to the negative terminal of the panel. The capacitor and the inductor oscillating at resonance to create a sine wave which as a frequency a bit lower than the switching frequency.

The half bridge inverter was expected to generate a sine wave or modified sine wave from the amplified input. The resonant frequency is 47 kHz and the operating frequency for the mosfet's is 50 kHz to be on the safe side to generate the magnetic field that will cause the flow of current in cooking pan. The cooking coil works as an inductor and the capacitor will be was resonating.It creates a flow of current on a wire which was placed on it without any connection. It lighted up an

LED as the result and the brightness of the LED reduced when the above coil winding with the LED moved from the bottom to some height.

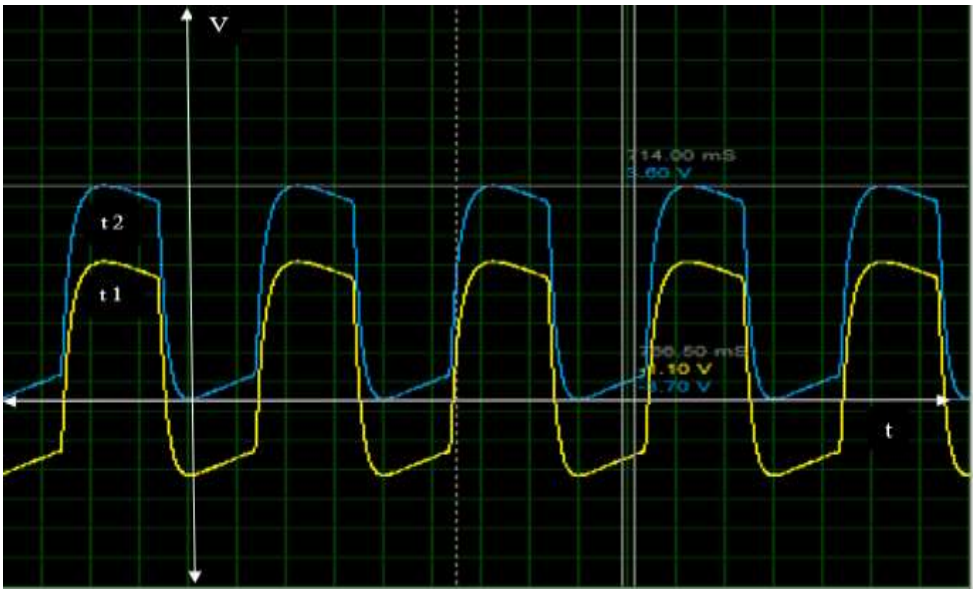

Figure 48 The output of Half bridge inverter

4.2 Laboratory Experiment Results

The waveforms that were generated from the same steps as the Proteus design are the following

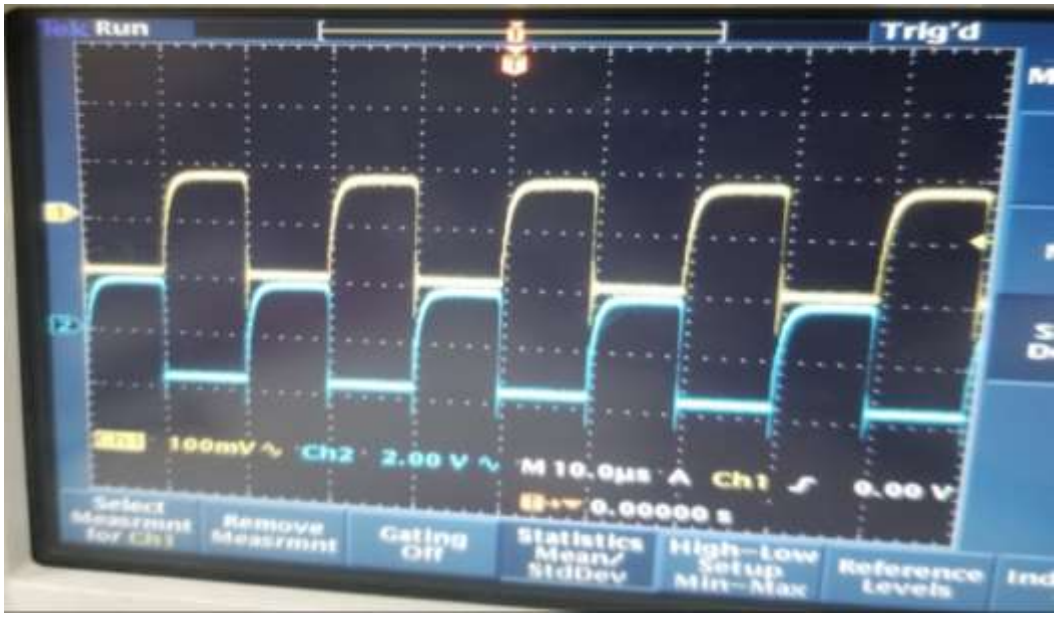

Figure 49 Astable multivibrator output

Figure 50 Half-Bridge Output

After getting the required sine wave from the system. A spiral coil connected with an LED in series with a capacitor was used to check the magnetic field availability in terms of wireless electric transfer. Different colored LEDs were checked on separate days. LEDs operate in a forward direction and they have different wavelength and operating voltage ranges. The red, green, or yellow LEDs have relatively low forward voltage ranging from 1.6-2.2V. However, blue and white LEDs can begin conducting from 2.5-4V and the typical forward voltage of a white LED is in the range of 3V to 5V. The circuit was able to light different colors of LEDs.

When the coil and led is placed immediately above the cooking coil. The LED is on with the maximum brightness and the brightness decreased for some centimeters above.	

It keeps the brightness even in the presence of a ceramic /mirror in between as the magnetic field is not affected by the insulation.	
The brightness is very dimmer 7-10cm gap and turns off after that. The increase in the working current and voltage will increase the total magnetic flux around the cooking coil.	
There is a slight light effect when some portion of the cooking coil gets in contact with the heating coil. But brightness/magnetic flux decreases sideways as well.	
When the cooking coil is fully removed from the heating coil, there will not be flux to create lightening and heating.	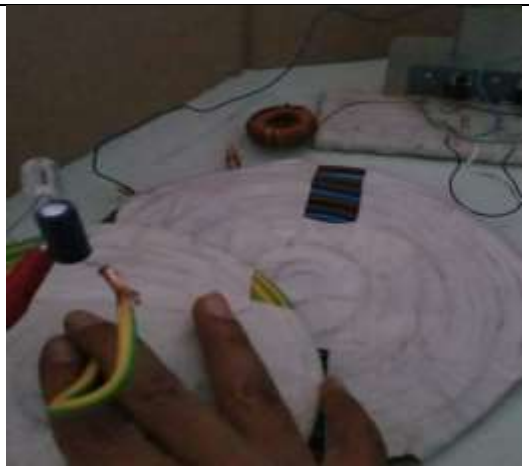

Figure 51 Magnetic Flux effect on the lighting bulb

Studies have shown that the human eye can perceive the flicker of LEDs at rates of up to 90 Hz, and anything above that is imperceptible to the human eye. Thus, the researcher was not able to see the blinking. It confirms that the frequency is much higher.

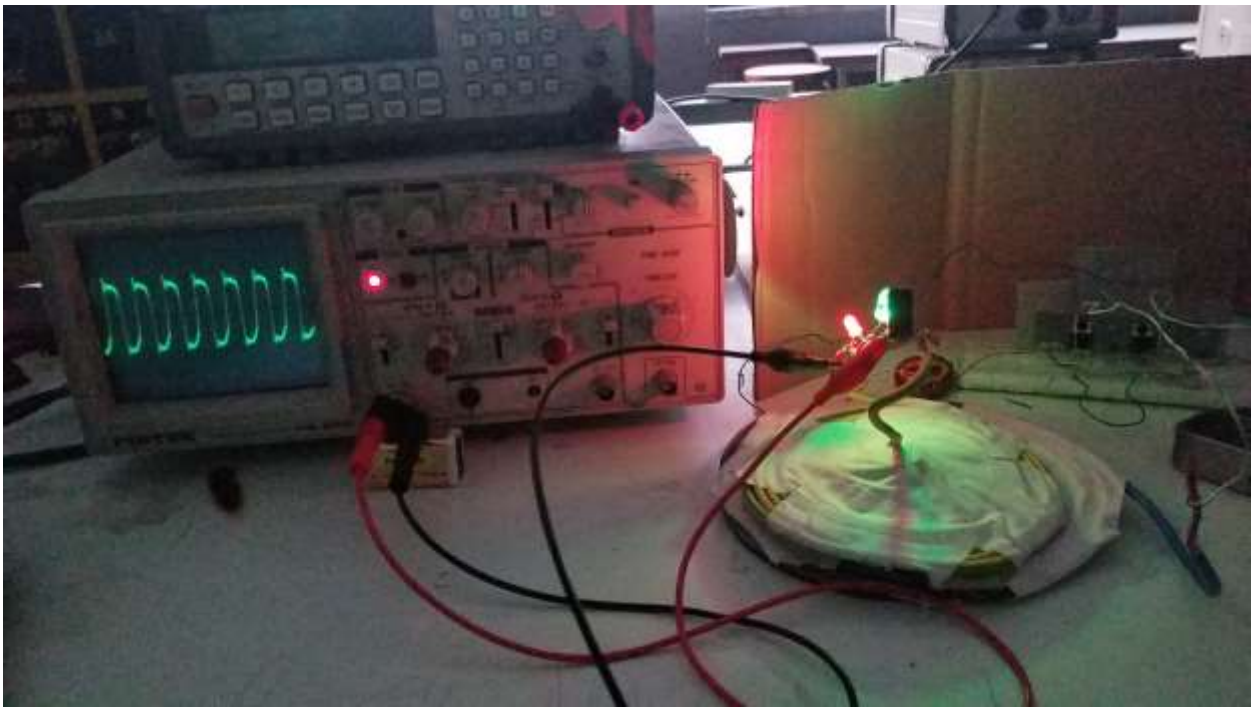

Figure 52 Wireless power transfer

4.3 Ansys Simulation results

In the context of electromagnetism and magnetic materials, H, B, and J are commonly used to represent different quantities:

H represents the intensity of the magnetic field or the field that magnetizes. The measurement is expressed in units of amperes per meter (A/m). The magnetomotive force (MMF) or the current passing through a coil winding that generates the magnetic field is associated with H.

The letter "B" symbolizes the magnetic flux density or magnetic induction. The unit of measurement for it is expressed in either Teslas (T) or Gauss (G). B refers to the true magnetic field present in a substance or in a vacuum. The strength of the magnetic field H is determined by the permeability of the material, which influences the relationship between B and H.

J represents the magnetic polarization or magnetization of a substance. The unit of measurement for it is A/m. This refers to the concentration of magnetic forces inside a substance, which can be caused by an outside magnetic field or by the inherent magnetic characteristics of the material.

The strength of the magnetic field exerted on a cooking pan during induction cooking can change based on different elements, such as the induction cooktop's structure and the type of cooking pan

being utilized. Nevertheless, the average magnetic flux density found in induction cooktops ranges between 0.1 and 1.5 tesla (T).

Induction cooktops generate a high-frequency alternating magnetic field, typically in the range of 20 kHz to a few hundred kilohertz. This magnetic field induces eddy currents in the bottom of the cooking pan, which in turn generate heat due to the resistance of the pan material.

The magnetic flux density required for efficient induction cooking depends on factors such as the size and thickness of the pan, the type of material used, and the desired heating performance. Manufacturers of induction cooktops generally design their products to provide magnetic fields within the optimal range for effective and efficient cooking.

The table below presents the results obtained from studying the impact of the cooking coil on the cooking pan by varying the current and frequency. Three different current values of 5, 15, and 30 Amps were tested, while the frequencies were varied at 25 kHz, 50 kHz, and 75 kHz.

Parameter		5A			15A			30A		
		25kHz	50kHz	75kHz	25kz	50kHz	75kHz	25kHz	50kHz	75kHz
Coil loss(W/m^3)		0.121466	0.121466	0.121466	1.09319	1.09319	1.09319	4.37278	4.37278	4.37278
Pan loss(W/m^3)		0.855628	1.1057	1.22812	7.70066	9.95134	11.0531	30.8026	39.8054	44.2124
H (A/m)	Max	4333.7	4313.8	4308	13001	12941	12923	26002	25883	25847.73
	Min	1.509	1.644	2.228	4.53	4.932	6.685	9.052	9.864	13.37
B (Tesla)	Max	0.06385	0.074569	0.088T	0.192	0.2237	0.263	0.3831	0.4472	0.526
	Min	0.142E-6	0.422	0.0T	0.00	0.00	0.0	0.8506E-7	2.259E-6	3.419E-6
Mag J (A/m^2)	Max	3.96E+7	3.96E+7	1.32E+7	3.96E+7	3.958E+7	3.958E+7	7.917E+7	7.917E+7	7.917E+7
	Min	5.22E+4	5.22E+4	1.51E+4	5.22E+4	3.13E+4	4.531E+4	1.044E+05	6.256+4	9.062+4

Table 5 Loss values, H, B, and Mag J values

To analyze the provided simulation results, let's break down the table and examine each parameter:

Coil loss (W/m^3): This parameter represents the power loss in the cooking coil per unit volume. The values are given for different currents (5A, 15A, and 30A) and frequencies (25 kHz, 50 kHz, and 75 kHz). It appears that the coil loss remains relatively constant across all current and frequency combinations, with a value of approximately 0.121466 W/m^3.

Frequency	25kHz	50kHz	75kHz
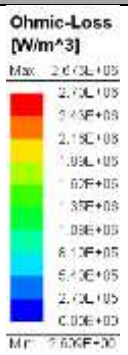 Coil and Pan losses	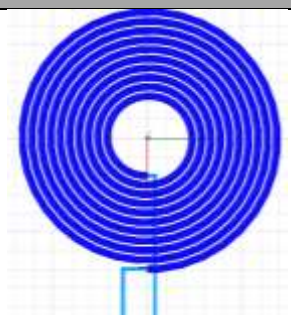	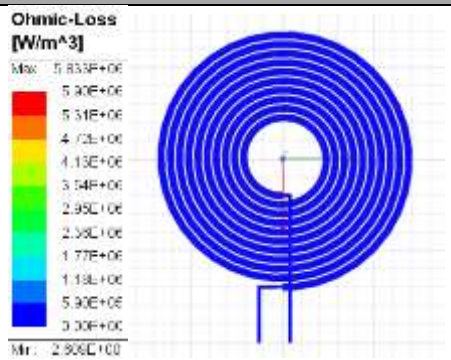	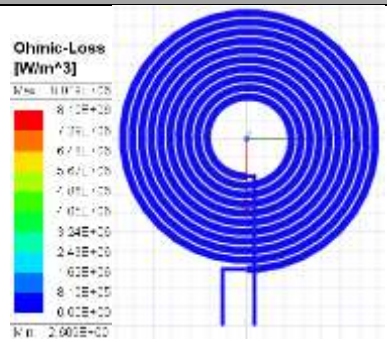
	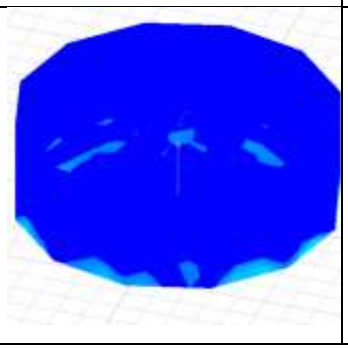	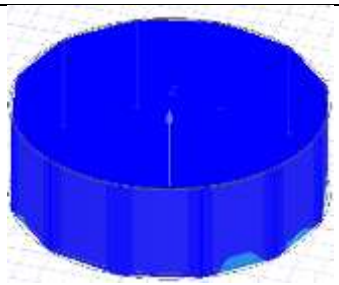	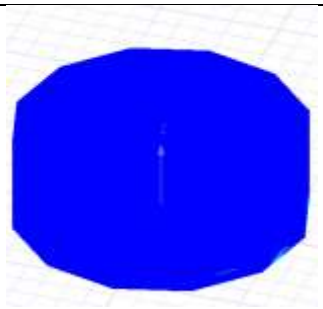

Figure 53 Coil and Pan losses

Pan loss (W/m^3): This parameter indicates the power loss in the cooking pan per unit volume. Similar to the coil loss, the values are provided for different currents and frequencies. As expected, the pan loss increases with higher currents and frequencies. For example, at 5A and 25 kHz, the pan loss is 0.855628 W/m^3, whereas at 30A and 75 kHz, it reaches 44.2124 W/m, figure above.

Frequency	25kHz	50kHz	75kHz
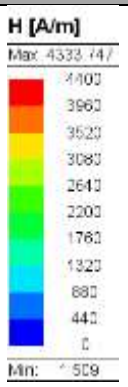	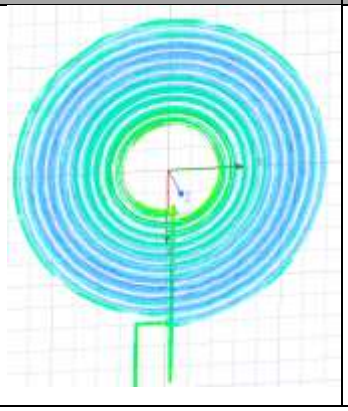	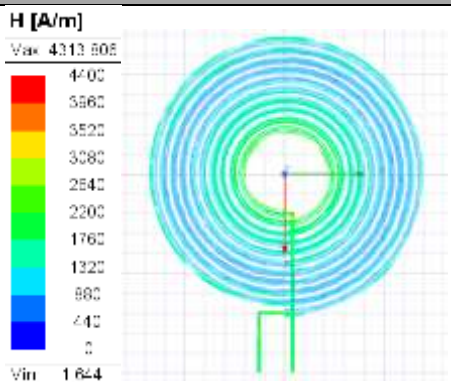	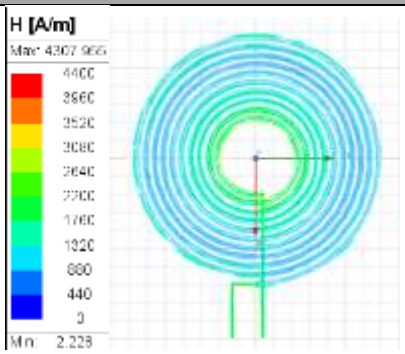

H for Coil and pan	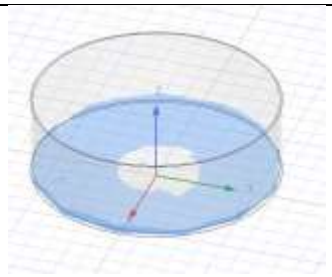	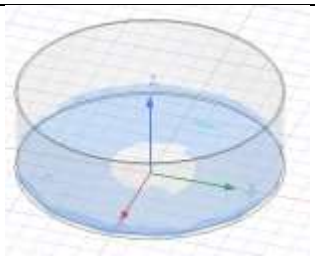	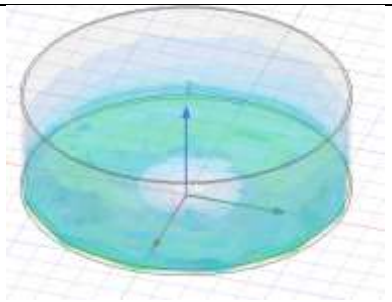

Figure 54 magnetic field strength

H (A/m): This parameter represents the maximum and minimum values of magnetic field strength (H) in amperes per meter. The maximum value ranges from approximately 4333.7 A/m to 26002 A/m, while the minimum value varies from 1.509 A/m to 13.37 A/m as shown in figure 54. The values depend on the current and frequency settings, with higher currents and frequencies generally resulting in higher magnetic field strengths.

B (Tesla): This parameter indicates the maximum and minimum values of magnetic flux density (B) in Tesla. The maximum value ranges from approximately 0.06385 T to 0.526 T, while the minimum value varies from 0.142 T to 3.419E-6 T. The magnetic flux density is influenced by the current and frequency settings, with higher currents and frequencies leading to higher values.

Frequency	25kHz	50kHz	75kHz
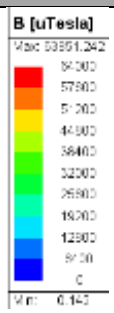	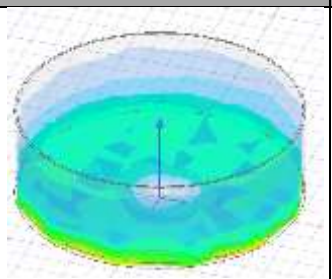	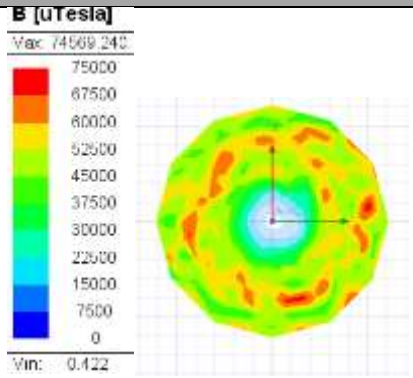	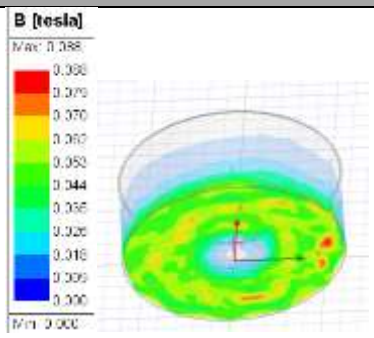

Magnetic flux density in the YZ plane	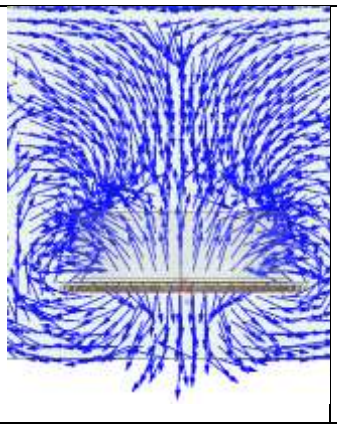	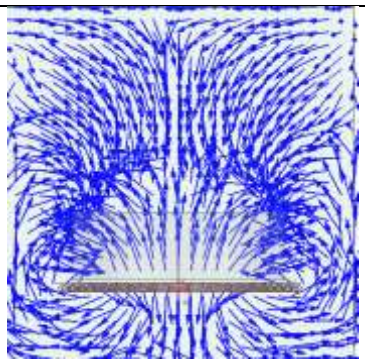	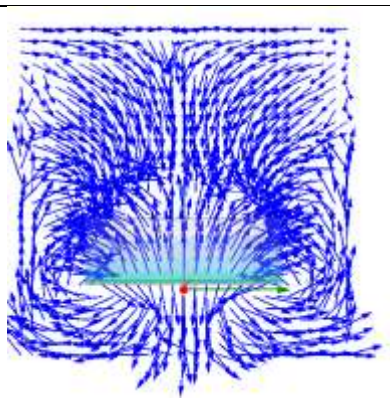

Figure 55 magnetic flux density (B)

Faster heating: Higher B values provide faster heating times, reducing cooking durations.

Enhanced cooking performance: With higher B values, the cookware can reach higher temperatures, enabling better searing and browning of food.

Improved responsiveness: Higher B values result in more responsive temperature control, allowing for precise adjustments during cooking.

On the opposite higher B values can lead to; Increased energy consumption: Higher B values may require more power, leading to increased energy consumption.

Heat concentration(as shown in figure 56): Higher B values can lead to localized hotspots in the cookware, which may require careful temperature management and stirring to avoid uneven cooking.

I(A) / f (kHz)	15A	30A
75k	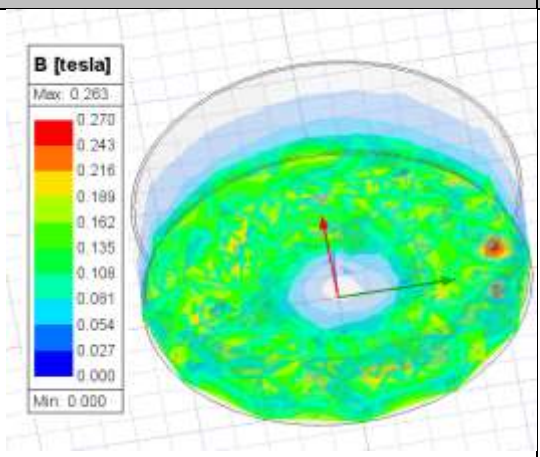	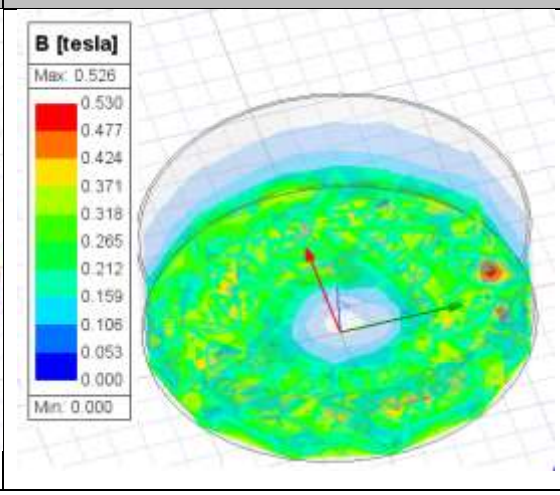

50kHz	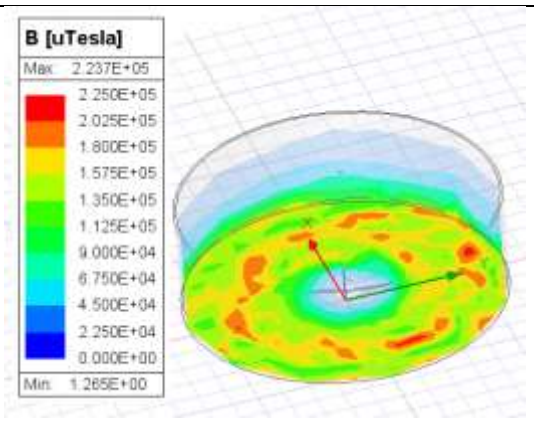	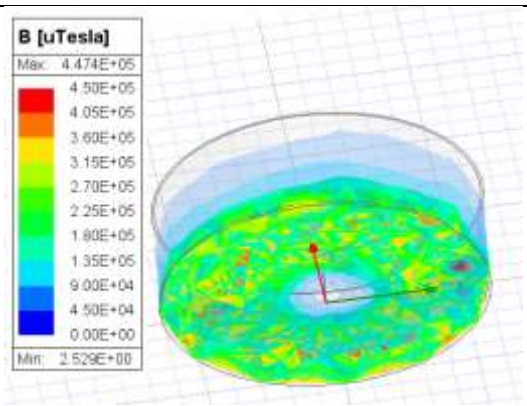
25kHz	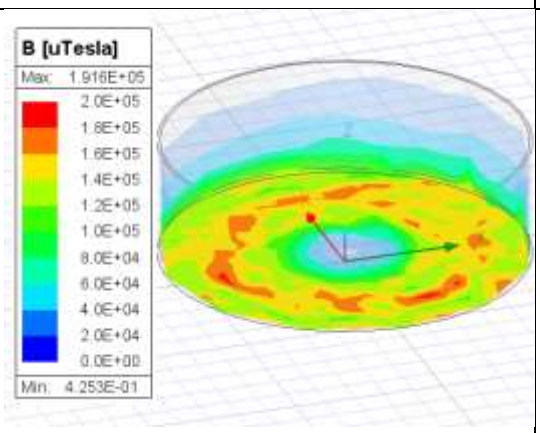	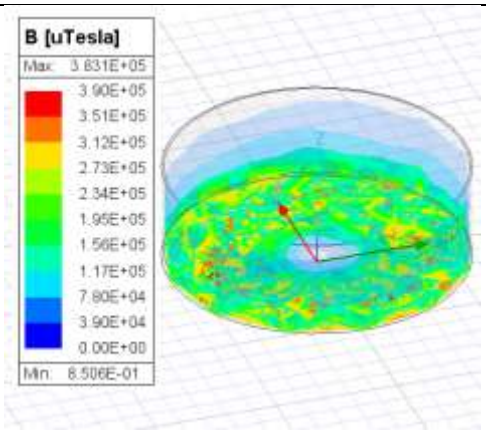

Figure 56 Magnetic flux density (B) comparison for 15A and 30A

It is important to strike a balance between efficient heating and optimal cooking performance based on a design requirement. Based on the simulation outputs the magnetic flux density obtained from the laboratory is less than 0.074569 Tesla, as this value is obtained at 5 Ampere of current at 50 kHz of frequency. This was the reason the system caused a hissing nose other than heating the pan.

In marketable induction stoves, the most common thickness of the mirror, if used, is typically very thin. The mirror-like surface found on induction stoves is usually achieved through a glass or ceramic material that has a reflective coating applied to it. This coating is usually very thin, typically in the range of micrometers. The purpose of this thin reflective coating is to provide a visually appealing and easy-to-clean surface for the induction stove. It is not intended to interfere significantly with the magnetic field generated by the induction coils. In the design, a mirror thickness of 0.25 mm was used, and it was thin enough to minimize interference with the magnetic field in an induction stove.

Mag J (A/m^2): Maximum and minimum values of magnetization current density (Mag J) in amperes per square meter. The maximum value ranges from approximately 3.96E+7 A/m^2 to 7.917E+7 A/m^2, while the minimum value varies from 5.22E+4 A/m^2 to 9.062E+4 A/m^2. The magnetization current density is affected by the current and frequency settings, with higher currents and frequencies resulting in higher values. The flow of current on the coil versus the flow of current and the magnetization current density (Mag J) of the cooking pan is shown in the figure below. It confirms that the two bodies have opposite flow directions.

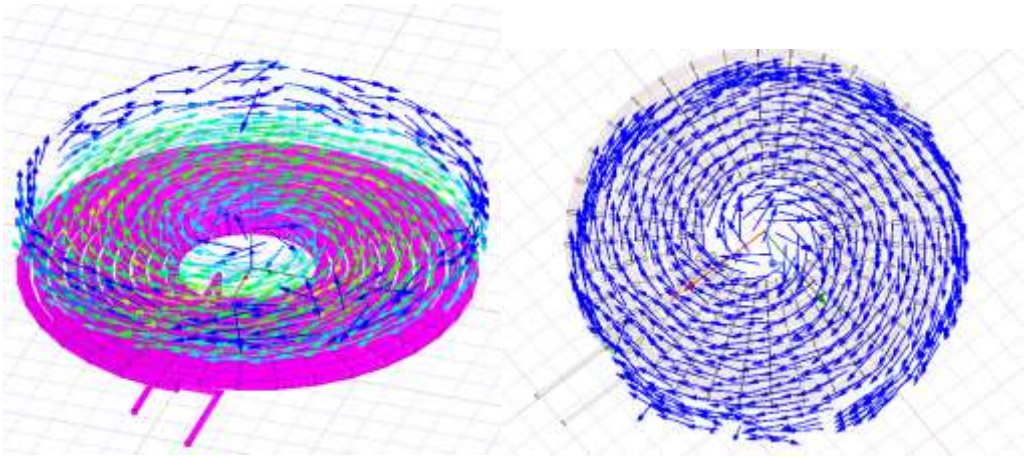

Figure 57 Magnetization current density

To compare the magnetic flux density values of 15A and 30A with different frequencies in the context of induction cooking, higher values of magnetic flux density generally lead to more efficient and faster induction cooking. They can generate more heat within the cookware, allowing for quicker cooking times.

Based on the ideas visually presented through Proteus and Ansys software, along with physical demonstrations, the DC source can be transformed into fluctuating AC using a multivibrator. Subsequently, the half-bridge circuit can help stabilize the output voltage, while the amplification section can boost both the output voltage and operating current. This setup allows for monitoring the magnetic field surrounding the cooking coil, inducing a current flow in the cooking pan due to its metallic resistance, generating the necessary heat for meal preparation. Key considerations include intensity variations with current, direction, and distance from the cookware. The utilization of LED lighting powered by DC for cooking on a larger scale is also a notable aspect of this innovative approach.

Chapter Five

5 Conclusion and Recommendations

1.1 Conclusion

The study focused on researching household electric cooking demand and designing a solar PV system to accommodate the appropriate load. A 500-watt induction stove design was developed for an average family size of five, considering 3.5 daily cooking hours. The PV system design included two parallel-connected 12V, 250W panels and three parallel-connected 12V, 150Ah batteries to power the induction cooker effectively.

Through the use of Proteus software and laboratory simulations, it was demonstrated that an induction cooking system powered by a solar PV system or DC source is achievable, utilizing an astable multidirector with a half-bridge inverter circuit. Testing of wireless electric conduction on the cooking wire was successful, enabling LED lighting without direct contact. The developed induction cook stove design was tested using a 24V panel and voltage divider, yielding similar output characteristics in terms of LED and current flow of 0.37Ampere. With the addition of current through an external inductor, it reaches 1.26 Ampere. The intensity of the light varied with height due to changes in voltage and current caused by magnetic field variations. The induction cook stove design was further enhanced by injecting additional current into the system, resulting in a humming or buzzing noise due to magnetostriction (a phenomenon where certain materials, like iron and nickel, produce audible vibrations and sound waves when subjected to a magnetic field).

Ansys simulation results provided insights into current flow direction, magnetic field density, field intensity, and the impact of the magnetic field on the coil, mirror, and pan. The conduction of energy was found to be influenced by the current and its frequency flowing through the coil, while the magnetic flux density affected the total energy transfer based on the distance between the pan and the coil.

Aim for a magnetic flux density within the typical range of 0.1 to 1.5 T. This range is known to be effective for induction cooking. Through the simulation results a range of B values from 0.06385 – 0.562 Tesla was ordained. The higher the value the better the heating effect it creates on the pan.

The coil loss for the same current value was seen unchanged, but in reality, coil losses can vary with frequency in induction systems. The coil loss is primarily influenced by factors such as the resistance of the coil windings, the skin effect, and the proximity effect. These effects become more significant at higher frequencies. This is observed from the varying output values at 5, 15, and 30Ampes. Focus on designing an induction cooktop that maximizes energy efficiency. This can be achieved by minimizing power losses in both the cooking coil and the cooking pan. Attention must be given to parameters such as coil loss and pan loss.

The findings of the study aligned with previous research and market devices, showcasing similar outputs. The design and manufacturing of DC sourced stoves is achievable. However, further amplification of the design would have allowed for efficiency measurements. In the current stage, the efficiency was evaluated by examining the output through Ansys simulation, considering a conceptual output of the calculated ferrite core transformer design.

Finally, the study has assessed Ethiopian household cooking demand, the required solar PV system design for the induction cooker, the cooker circuit design on proteus, and a 3D model for assessing the relation of current. Frequency and material type for induction cooking system implementation. As induction cooking is developing globally due to its efficiency and safety advantages, this study can be used as a reference for the development of solar/DC-powered cooking alternatives for off-grid cooking designs for remote areas and areas with high power interruption.

5.2 Recommendations

The successful integration of wireless electric conduction and the understanding of the magnetostriction phenomenon further validate the effectiveness and viability of DC-sourced cooking systems. The recommendation is to continue exploring ways to enhance the efficiency of the induction cook stove and measure its performance in real-world settings. Conducting further experiments and tests on the amplification part, as well as evaluating the efficiency using practical measurements, would contribute valuable insights and provide more accurate assessments of the design's performance.

Furthermore, the Ansys simulation results shed light on the current flow direction, magnetic field effects, and energy transfer characteristics. This information can be utilized for future improvements and optimization of the design.

Since the free license was used, it was compelled to reduce the size of the simulation to comply with the licensing restrictions. It would be more favorable if reliable licensed software was used for better results by designing for the actual sizes.

In conclusion, the functionality test showed the potential of generating heat from a DC source, which can be further adapted for sustainable cooking solutions. By leveraging renewable energy sources and understanding the underlying principles of induction heat transfer and wireless electric conduction, furthermore designs can be designed which are environmentally friendly and efficient alternative for households cooking energy. Continued research and practical measurements will further refine and validate the better design's, to making it a viable option for promoting clean energy cooking practices.

Reference

[1] Weber, Daniel J., M. Eng. Massachusetts Institute of Technology. (2015). Design of a battery-powered induction stove. *ResearchGate*. https://www.researchgate.net/publication

/290182173_Design_of_a_battery-powered_induction_stove

[2] B. I. Sibiya, "SCHOOL OF ELECTRICAL, ELECTRONICS, AND COMPUTER ENGINEERING SMART INDUCTION COOKING SYSTEM USING SOLAR By Bandile Innocent Sibiya," 2017.

[3] S. O. E. Thirithandar, C. Saldanah, and W. I. N. K. Moe, "Design and Construction of Power System for Induction Heating (IH) Cooker Using Resonant Converter 2. TYPES OF POWER SYSTEM," pp. 183–192.

[4] R. Hemalatha and J. P. Koujalagi, "Design and Simulation of Induction Heating Equipment using MATLAB / SIMULINK Environment," *Int. J. Sci. Res.*, vol. 2, no. 8, pp. 2319–7064, 2013, [Online]. Available: www.ijsr.net

[5] GH Group, "GH IA Induction Heating Guide," *Induction Atmos.*, pp. 1–12.

[6] S. Stritzke *et al.*, "Benin eCooking Market Assessment," no. February, 2022, [Online]. Available: https://mecs.org.uk/wp-content/uploads/2022/02/MECS-EnDev-Benin-eCooking-Market-Assessment-presentation.pdf

[7] A. Ababa, "Ethiopian Energy Authority Project document On Locally manufactured electric stoves Energy Efficiency Standards and Labeling Consultant: DANAS Electrical Engineering," no. March, 2017.

[8] E. Plumed, J. Acero, I. Lope, and J. M. Burdío, "Design methodology of high-performance domestic induction heating systems under the worktop," *IET Power Electron.*, vol. 13, no. 2, pp. 300–306, 2020, doi: 10.1049/iet-pel.2019.0693.

[9] S. C. Industries, U. States, F. D. A. Class, S. Buyer, E. Opportunity, and A. A. Employer, "AND9166 / D Induction Cooking Everything You Need to Know".

[10] B. Adhikari, J. N. Shrestha, and S. R. Shakya, "Design and Simulation of a Solar Electricity Based Induction Cooker using Quasi Resonant Topology," pp. 1–11, 2016.

[11] B. J. Knauf, D. P. Webb, C. Liu, and P. P. Conway, “Low-Frequency Induction Heating (LFIH) for the Sealing of Plastic Microfluidic Systems,” no. August 2009, doi: 10.1007/s10404-009-0539-x.

[12] L. Koller and B. Novák, “Improving the energy efficiency of induction cooking,” *Electr. Eng.*, vol. 91, no. 3, pp. 153–160, 2009, doi: 10.1007/s00202-009-0127-9.

[13] M. Kayode, L. O. Kazeem, and A. Enock, “Design and Fabrication of a Digital Solar-Powered DC Induction Cooker,” *Int. J. Res. Sci. Innov.*, vol. 09, no. 07, pp. 77–84, 2022, doi: 10.51244/ijrsi.2022.9708.

[14] N. Femia, M. Migliaro, C. Pastore, and D. Toledo, “In-system IGBT power loss behavioral modeling,” *2016 13th Int. Conf. Synth. Model. Anal. Simul. Methods Appl. to Circuit Des. SMACD 2016*, no. June 2016, doi: 10.1109/SMACD.2016.7520723.

[15] B. I. Sibiya and C. Venugopal, “Solar Powered Induction Cooking System,” *Energy Procedia*, vol. 117, pp. 145–156, 2017, doi: 10.1016/j.egypro.2017.05.117.

[16] A. H. A. R. Shaikh and S. K. Akireddy, “Simulation of MOSFET Based Inverter for Induction Heating In MATLAB,” *Int. J. Sci. Res.*, vol. 4, no. 11, pp. 28–31, 2015, doi: 10.21275/v4i11.nov151017.

[17] B. Adhikari, J. N. Shrestha, and S. R. Shakya, “A New Approach to the Design of DC Powered Induction Cooker,” vol. 1, no. 1, pp. 35–42, 2018.

[18] Vaidya, A. (2020). Promoting electric cooking in Nepal: Opportunities and Challenges. *ResearchGate*. https://www.researchgate.net/publication/339237483_Promoting_electric_cooking_in_Nepal_Opportunities_and_Challenges

[19] R. Sabzehgar, R. Ghali, and P. Fajri, “A Novel Combined Control Strategy for a Two-Stage Parallel Full-Wave ZCS Quasi Resonant Boost Converter for PV-Based Battery Charging Systems with Maximum Power Point Tracking,” *Electricity*, vol. 3, no. 1, pp. 145–161, 2022, doi: 10.3390/electricity3010009.

[20] PCIA & Global Alliance, “The Water Boiling Test Version 4.2.3; Cookstove Emissions and Efficiency in a Controlled Laboratory Setting,” *Glob. Alliances clean cookstoves*, vol. 2,

no. January 2013, p. 52, 2013, Available: http://www.aprovecho.org/lab/pubs/testing

[21] L. Ayele and Y. Eneyew, "Experimental investigation on the renovation of locally manufactured electrical cooking stove," *Case Stud. Therm. Eng.*, vol. 30, no. October 2021, p. 101712, 2022, doi: 10.1016/j.csite.2021.101712.

[22] S. I. Annie, K. M. Salim, Z. Tasneem, and M. R. Uddin, "Design and performance analysis of a ZVS parallel quasi-resonant converter for a solar-based induction cooking system," *IEEE Reg. 10 Annu. Int. Conf. Proceedings/TENCON*, no. November, pp. 2638–2641, 2017, doi: 10.1109/TENCON.2016.7848516.

[23] M. Sweeney, J. Dols, B. Fortenbery, and F. Sharp, "Induction Cooking Technology Design and Assessment," *2014 ACEEE Summer Study Energy Effic. Build.*, pp. 370–379, 2014, [Online]. Available: https://aceee.org/files/proceedings/2014/data/papers/9-702.pdf

[24] A. M. Ismail, A. S. Nur, U. Tun, H. Onn, and A. A. Nur, "Case study in Somalia," no. March, pp. 0–11, 2022.

[25] Philip, T. (2021, December 14). Debunking some common Induction Heating myths. - Nymble - Medium. *Medium*. https://medium.com/nymble/induction-heating-myths-debunked-4c9802f527dd

[26] J. Acero *et al.*, "The domestic induction heating appliance : an overview of recent research," 2008."ON Semiconductor".

[28] J. M. Burdío, F. Monterde, J. R. García, L. A. Barragán, and A. Multiple-burner, "A Two-Output Series-Resonant Inverter for Induction-Heating Cooking Appliances," vol. 20, no. 4, pp. 815–822, 2005.

[29] A. K. M. Al-Shaikhli and A. T. Meka, "Design and Implementation of Practical Induction Heating Cooker," *Int. J. Soft Comput. Eng.*, no. 4, pp. 2231–2307, 2014.

[30] E. Engineering, "Induction Cooker Design and Experimental Results With Quasi Resonant Topology and Jitter Method Induction Cooker Design and Experimental Results," no. August, 2012.

[31] V. Crisafulli and C. V. Pastore, "New control method to increase power regulation in an

AC / AC quasi-resonant converter for high-efficiency Induction cooker," pp. 628–635, 2023.

[32] V. Crisafulli, A. Gallivanoni, C. Pastore, and W. Europe, "Model-Based Design Tool for EMC Reduction Using Spread Spectrum Techniques in Induction Heating Platform," pp. 845–852, 2012.

[33] A. Note, "Reverse-conducting IGBTs for induction cooking and resonant applications," pp. 1–29, 2021.

[34] M. B. Wollele, "Quantifying Energy Losses on Electric Cooking Stove," vol. 9, no. 05, pp. 753–756, 2020.

[35] K. A. Rahman, A. M. Leman, F. M. M, M. Z. M. Yusof, H. Azian, and M. N. M. Salleh, "Energy Consumption Analysis Based on Energy Efficiency Approach : A Case of Suburban Area Energy Consumption Analysis Based on Energy Efficiency Approach : A Case of Suburban Area," no. January 2017, doi: 10.1051/matecconf/20178702003.

[36] K. Troncoso and M. Tesfamichael, "Ethiopia eCooking Market Assessment EnDev / MECS eCooking Market Assessments," no. February, 2022.

[38] Solomon Derbie and Mikias Hailu, "Estimation of Greenhouse Gas Emissions and Mitigation Methods in Electrical Power Sector of Dire Dawa City from 2015 to 2025," Journal of Energy and Natural Resources, 7(2). 54-59. 2018.

[39] Mikias Hailu and Solomon Derbie, "Home Appliances Efficiency Improvements for Energy Conservation in Debre Berhan City; Ethiopia," American Journal of Energy Engineering, 6(2). 10-14. 2018.

[40] L. Report, "Clean and Improved Cooking in Sub-Saharan Africa," no. 98664, 2014.

[41] M. Sweeney, J. Dols, B. Fortenbery, and F. Sharp, "Induction Cooking Technology Design and Assessment," *2014 ACEEE Summer Study Energy Effic. Build.*, pp. 370–379, 2014, [Online]. Available: https://aceee.org/files/proceedings/2014/data/papers/9-702.pdf

[42] S. Derbie Gont, “Estimation of Greenhouse Gas Emissions and Mitigation Methods in Electrical Power Sector of Dire Dawa City from 2015 to 2025,” *J. Energy Nat. Resour.*, vol. 7, no. 2, p. 54, 2018, doi: 10.11648/j.jenr.20180702.11.

[43] A. Namadmalan and J. S. Moghani, “Single-phase current source induction heater with improved efficiency and package size,” *J. Power Electron.*, vol. 13, no. 2, pp. 322–328, 2013, doi: 10.6113/JPE.2013.13.2.322.

[44] A. Eid, K. J. Choi, H. W. Lee, and M. Nakaoka, “A novel edge-resonant soft switching PWM controlled high-frequency inverter with minimum circuit components,” *Proc. Int. Conf. Power Electron. Drive Syst.*, vol. 1, pp. 101–106, 2005, doi: 10.1109/peds.2005.1619668.

[45] D. J. Tschirhart, “EFFICIENT CONTROL OF THE SERIES RESONANT by,” 2012.

[46] C. J. E. Sciences and W. Journals, “RESEARCH ARTICLE SIMULATION OF INVERTER CIRCUIT USING MULTISM AND PROTEUS Akhikpemelo, A., Matsunde, P., and Ebenso, F.P. Departmet of Electrical/Electronic Engineering, Maritime Academy of Nigeria, Oron, Nigeria.,” vol. 11, no. 2, pp. 1–11, 2016, doi: 10.5707/cjengsci.2016.11.2.1.11.

[47] R. Haider, R. Alam, N. B. Yousuf, and K. M. Salim, “Design and construction of single-phase pure sine wave inverter for photovoltaic application,” 2012 Int. Conf. Informatics, Electron. Vision, ICIEV 2012, pp. 190–194, 2012, doi: 10.1109/ICIEV.2012.6317332.

[48] Ramalingam, S.R.; Boopthi, C.S.; Ramasamy, S.; Ahsan, M.; Haider, J. Induction Heating for Variably Sized Ferrous and Non-Ferrous Materials through Load Modulation. *Energies* 2021, *14*, 8354. https://doi.org/10.3390/en14248354

[49] Armin Altouni, Shiva Gorjian, Ahmad Banakar,” Development and performance evaluation of a photovoltaic-powered induction cooker (PV-IC): An approach for promoting clean production in rural areas”,Cleaner Engineering and Technology,Volume 6,2022

[50] Han, Wei et al. “All-In-One Induction Heating Using Dual Magnetic Couplings.” *Energies* (2019): n. pag.

[51] Y. Uthman, G. Oletu, and O. Longe, “Practical DC Induction Cooker Design and Implementation.,” pp. 231–238, 2021, doi: 10.22624/aims/teams-2021/v27p19.

[52] Clean cookstoves: Impact and determinants of . https://ifmrlead.org/wp-content/uploads/2021/12/Clean-Cookstoves-2021-Report.pdf

[53] Ethiopia eCooking Market Assessment. https://mecs.org.uk/wp-content/uploads/2022/02/MECS-EnDev-Ethiopia-eCooking-Market-Assessment-presentation.pdf

[54] Carr, J. A., Rowden, B., & Balda, J. C. (2009). A Three-Level Full-Bridge Zero-Voltage Zero-Current switching converter with a simplified switching scheme. *IEEE Transactions on Power Electronics*, *24*(2), 329–338. https://doi.org/10.1109/tpel.2008.2007211

[55] Kimmer, Thomas et al. "Reverse Conducting IGBT - A new Technology to Increase the Energy Efficiency of Induction Cookers." *2008 IEEE Power Electronics Specialists Conference* (2008): 2284-2287.

[56] Ezhilvannan, P., Ramasamy, D., Subramanian, S. K., & Krishnan, S. (2024). Enhancing power conversion efficiency in five-level multilevel inverters using reduced switch topology. *Bulletin of Electrical Engineering and Informatics*, *13*(3), 1495–1503. https://doi.org/10.11591/eei.v13i3.6884

Appendices

1. Datasheets of Electronic components

1.1 IRF740

N - CHANNEL 400V - 0.48 Ω - 10 A - TO-220
PowerMESH™ MOSFET

TYPE	V_{DSS}	$R_{DS(on)}$	I_D
IRF740	400 V	< 0.55 Ω	10 A

- TYPICAL $R_{DS(on)}$ = 0.48 Ω
- EXTREMELY HIGH dv/dt CAPABILITY
- 100% AVALANCHE TESTED
- VERY LOW INTRINSIC CAPACITANCES
- GATE CHARGE MINIMIZED

TO-220

DESCRIPTION

This power MOSFET is designed using the company's consolidated strip layout-based MESH OVERLAY™ process. This technology matches and improves the performances compared with standard parts from various sources.

APPLICATIONS

- HIGH CURRENT SWITCHING
- UNINTERRUPTIBLE POWER SUPPLY (UPS)
- DC/DC COVERTERS FOR TELECOM, INDUSTRIAL, AND LIGHTING EQUIPMENT.

INTERNAL SCHEMATIC DIAGRAM

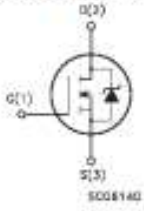

ABSOLUTE MAXIMUM RATINGS

Symbol	Parameter	Value	Unit
V_{DS}	Drain-source Voltage (V_{GS} = 0)	400	V
V_{DGR}	Drain- gate Voltage (R_{GS} = 20 kΩ)	400	V
V_{GS}	Gate-source Voltage	± 20	V
I_D	Drain Current (continuous) at T_c = 25 °C	10	A
I_D	Drain Current (continuous) at T_c = 100 °C	6.3	A
I_{DM}(•)	Drain Current (pulsed)	40	A
P_{tot}	Total Dissipation at T_c = 25 °C	125	W
	Derating Factor	1.0	W/°C
dv/dt(1)	Peak Diode Recovery voltage slope	4.0	V/ns
T_{stg}	Storage Temperature	-65 to 150	°C
T_j	Max. Operating Junction Temperature	150	°C

(•) Pulse width limited by safe operating area (1) I_{SD} ≤10 A, di/dt ≤120 A/µs, V_{DD} ≤ $V_{(BR)DSS}$, T_j ≤ T_{JMAX}

First Digit of the Datecode Being Z or K Identifies Silicon Characterized in this Datasheet

1.2 PN2222A

PN2222, PN2222A

PN2222A is a Preferred Device

General Purpose Transistors

NPN Silicon

ON Semiconductor™

http://onsemi.com

MAXIMUM RATINGS

Rating		Symbol	Value	Unit
Collector-Emitter Voltage	PN2222 PN2222A	V_{CEO}	30 40	Vdc
Collector-Base Voltage	PN2222 PN2222A	V_{CBO}	60 75	Vdc
Emitter-Base Voltage	PN2222 PN2222A	V_{EBO}	5.0 6.0	Vdc
Collector Current – Continuous		I_C	600	mAdc
Total Device Dissipation @ T_A = 25°C Derate above 25°C		P_D	 625 5.0	 mW mW/°C
Total Device Dissipation @ T_C = 25°C Derate above 25°C		P_D	 1.5 12	 Watts mW/°C
Operating and Storage Junction Temperature Range		T_J, T_{stg}	–55 to +150	°C

THERMAL CHARACTERISTICS

Characteristic	Symbol	Max	Unit
Thermal Resistance Junction-to-Ambient	$R_{\theta JA}$	200	°C/W
Thermal Resistance Junction-to-Case	$R_{\theta JC}$	83.3	°C/W

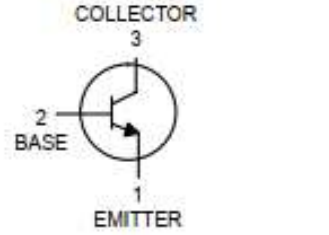

TO–92
CASE 29
STYLE 1

MARKING DIAGRAM

PN222x= Device Code
x = 2 or A
Y = Year
WW = Work Week

ORDERING INFORMATION

Device	Package	Shipping
PN2222	TO–92	5000 Units/Box
PN2222A	TO–92	5000 Units/Box
PN2222ARLRA	TO–92	2000/Tape & Reel
PN2222ARLRM	TO–92	2000/Ammo Pack
PN2222ARLRP	TO–92	2000/Ammo Pack

Preferred devices are recommended choices for future use and best overall value.

1.3 1N4001

1N4001, 1N4002, 1N4003, 1N4004, 1N4005, 1N4006, 1N4007

1N4004 and 1N4007 are Preferred Devices

Axial Lead Standard Recovery Rectifiers

This data sheet provides information on subminiature size, axial lead mounted rectifiers for general−purpose low−power applications.

Features

- Shipped in plastic bags, 1000 per bag
- Available Tape and Reeled, 5000 per reel, by adding a "RL" suffix to the part number
- Available in Fan−Fold Packaging, 3000 per box, by adding a "FF" suffix to the part number
- Pb−Free Packages are Available

Mechanical Characteristics

- Case: Epoxy, Molded
- Weight: 0.4 gram (approximately)
- Finish: All External Surfaces Corrosion Resistant and Terminal Leads are Readily Solderable
- Lead and Mounting Surface Temperature for Soldering Purposes: 260°C Max. for 10 Seconds, 1/16 in. from case
- Polarity: Cathode Indicated by Polarity Band

*For additional information on our Pb−Free strategy and soldering details, please download the ON Semiconductor Soldering and Mounting Techniques Reference Manual, SOLDERRM/D.

ON Semiconductor®

http://onsemi.com

LEAD MOUNTED RECTIFIERS
50−1000 VOLTS
DIFFUSED JUNCTION

CASE 59−10
AXIAL LEAD
PLASTIC

MARKING DIAGRAM

A = Assembly Location
1N400x = Device Number
x = 1, 2, 3, 4, 5, 6 or 7
YY = Year
WW = Work Week
• = Pb−Free Package
(Note: Microdot may be in either location)

ORDERING INFORMATION

See detailed ordering and shipping information on page 4 of this data sheet.

Preferred devices are recommended choices for future use and best overall value.

August, 2005 − Rev. 12

Publication Order Number:
1N4001/D

1N4001, 1N4002, 1N4003, 1N4004, 1N4005, 1N4006, 1N4007

MAXIMUM RATINGS

Rating	Symbol	1N4001	1N4002	1N4003	1N4004	1N4005	1N4006	1N4007	Unit
†Peak Repetitive Reverse Voltage Working Peak Reverse Voltage DC Blocking Voltage	V_{RRM} V_{RWM} V_R	50	100	200	400	600	800	1000	V
†Non−Repetitive Peak Reverse Voltage (halfwave, single phase, 60 Hz)	V_{RSM}	60	120	240	480	720	1000	1200	V
†RMS Reverse Voltage	$V_{R(RMS)}$	35	70	140	280	420	560	700	V
†Average Rectified Forward Current (single phase, resistive load, 60 Hz, T_A = 75°C)	I_O	1.0							A
†Non−Repetitive Peak Surge Current (surge applied at rated load conditions)	I_{FSM}	30 (for 1 cycle)							A
Operating and Storage Junction Temperature Range	T_J T_{stg}	−65 to +175							°C

Maximum ratings are those values beyond which device damage can occur. Maximum ratings applied to the device are individual stress limit values (not normal operating conditions) and are not valid simultaneously. If these limits are exceeded, device functional operation is not implied, damage may occur and reliability may be affected.

ELECTRICAL CHARACTERISTICS†

Rating	Symbol	Typ	Max	Unit
Maximum Instantaneous Forward Voltage Drop, (I_F = 1.0 Amp, T_J = 25°C)	v_F	0.93	1.1	V
Maximum Full−Cycle Average Forward Voltage Drop, (I_O = 1.0 Amp, T_L = 75°C, 1 inch leads)	$V_{F(AV)}$	–	0.8	V
Maximum Reverse Current (rated DC voltage) (T_J = 25°C) (T_J = 100°C)	I_R	 0.05 1.0	 10 50	μA
Maximum Full−Cycle Average Reverse Current, (I_O = 1.0 Amp, T_L = 75°C, 1 inch leads)	$I_{R(AV)}$	–	30	μA

†Indicates JEDEC Registered Data

1N4001, 1N4002, 1N4003, 1N4004, 1N4005, 1N4006, 1N4007

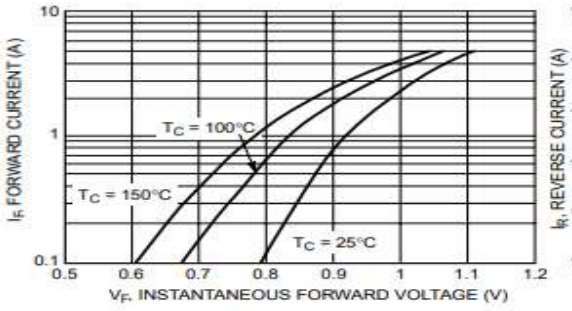

Figure 1. Typical Forward Voltage

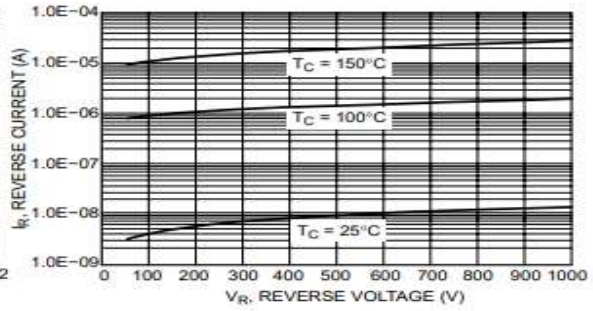

Figure 2. Typical Reverse Current

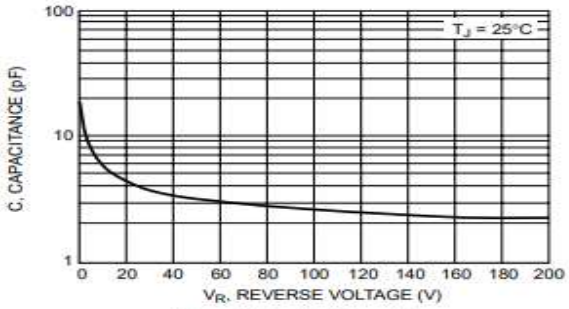

Figure 3. Typical Capacitance

2. Laboratory Setup and used materials

2.1 Laboratory Setup

2.2 Function generator, Oscilloscope, and DC source generator

2.3 Variable Capacitor and Variable resistor

2.4 Copper litz wires uses used as a coil and pan

2.5 Pan, Plastic insulators and Induction coil

2.6 Transformer test in High Voltage lab